W&M ScholarWorks

Dissertations, Theses, and Masters Projects

Theses, Dissertations, & Master Projects

2001

Modeling of Critically-Stratified Gravity Flows: Application to the Eel River Continental Shelf, Northern California

Malcolm E. Scully
College of William and Mary - Virginia Institute of Marine Science

Follow this and additional works at: https://scholarworks.wm.edu/etd

Part of the Geology Commons, Geophysics and Seismology Commons, and the Oceanography Commons

Recommended Citation

Scully, Malcolm E., "Modeling of Critically-Stratified Gravity Flows: Application to the Eel River Continental Shelf, Northern California" (2001). *Dissertations, Theses, and Masters Projects*. Paper 1539617769.
https://dx.doi.org/doi:10.25773/v5-9qh6-2c38

This Thesis is brought to you for free and open access by the Theses, Dissertations, & Master Projects at W&M ScholarWorks. It has been accepted for inclusion in Dissertations, Theses, and Masters Projects by an authorized administrator of W&M ScholarWorks. For more information, please contact scholarworks@wm.edu.

MODELING OF CRITICALLY-STRATIFIED GRAVITY FLOWS: APPLICATION TO THE EEL RIVER CONTINENTAL SHELF, NORTHERN CALIFORNIA

A Thesis
Presented to
The Faculty of the School of Marine Science
The College of William and Mary

In Partial Fulfillment
Of the Requirements for the Degree of
Master of Science

---

by
Malcolm E. Scully
2001

APPROVAL SHEET

This thesis is submitted in partial fulfillment of

the requirements for the degree of

Master of Science

Malcolm E. Scully

Approved, December 2001

Carl T. Friedrichs, Ph.D.
Committee Co-Chairman/Co-Advisor

L. Donelson. Wright, Ph.D.
Committee Co-Chairman/Co-Advisor

John D. Milliman, Ph.D.

Mark R. Patterson, Ph.D.

Peter Traykovski, Ph.D.
Woods Hole Oceanographic Institute
Woods Hole, Massachusetts

TABLE OF CONTENTS

Page

ACKNOWLEDGMENTS v

LIST OF TABLES vi

LIST OF FIGURES vii

ABSTRACT xii

1. INTRODUCTION 2

2. ANALYTICAL MODELING 8

2.1. THEORETICAL DEVELOPMENT 8

2.2. ANALYTIC PREDICTIONS OF GRAVITY-DRIVEN VELOCITY 14

2.2.1. 1996-97 Flood Season—S60 14

2.2.2. 1997-98 Flood Season—K60 17

2.2.3. 1996-97 Flood Season—S60 20

2.3. ANALYTIC PREDICTIONS OF GRAVITY-DRIVEN DEPOSITION 21

2.3.1. K60 Tripod 21

2.4. FLOOD DELIVERY OF SEDIMENT VS. POTENTIAL FLUX VIA GRAVITY FLOWS 23

2.4.1. 1996-97 Flood Season—S60 25

2.4.2. 1997-98 Flood Season—K60 26

2.4.3. 1996-97 Flood Season—S60 28

2.5. COMPARISON OF MODEL RESULTS WITH CORE DATA 29

2.6. ALONG-SHELF BATHYMETRIC CONTROL OF GRAVITY-DRIVEN DEPOSITION 35

2.7. LIMITATIONS OF THE APPROACH 41

3. NUMERICAL MODELING 44

3.1. THE MODEL 44

3.2. RESULTS 49

3.2.1. Mid-Shelf Deposition 56

3.2.2. Inner-shelf Deposition 63

3.2.3. Off-Shelf and Canyon Delivery 65

3.3. MODEL SENSITIVITY 68

3.3.1. Delivery of River Sediment 68

3.3.1.1. Amount of Sediment Delivery 68

3.3.1.2. Along-Shelf Distribution of Sediment 72

3.3.2. Along-Shelf Currents 74

3.3.3. Resuspension/Erosion 79

3.3.4. Consolidation 81

3.3.5. Along-Shelf Slope 83

3.3.6. Richardson Number & Drag Coefficient 86

4. CONCLUSIONS 89

4.1. CONCLUSIONS FROM ANALYTICAL MODELING 89

4.2. CONCLUSIONS FROM NUMERICAL MODELING 91

LITERATURE CITED 96

ACKNOWLEDGEMENTS

The research presented in this thesis would not have been possible without the guidance and insight provided by my advisor Carl Friedrichs. I am grateful for his support, encouragement, and patience throughout the course of this project. I also would like to acknowlege my other advisor, Don Wright, for his thoughtful input and comments. I also would like to thank the other members of my advisory committee. In particular, I am extremely grateful to Peter Traykovski for sharing both his thoughts and his data. This work builds directly upon Peter's observations and would not have been possible without his previous findings. Andrea Ogston provided data from the S-60 tripod which was used extensively in my analysis and Courtney Harris provided wave data and assistance in calculating bottom orbital velocities. Funding for this research was provided by the Office of Naval Research as part of the STRATAFORM program under the supervision of Joe Kravitz. I feel fortunate to have had the opportunity to participate in this project and I am extremely greatful for the generous funding that was provided.

LIST OF TABLES

Table Page

Table 3-1 Table acounting for relative fate of sediment for all model runs conducted and the thickness and along-shelf location of maximum deposition along the 60-m isobath.....52

LIST OF FIGURES

Figure | Page

Figure 1-1 Site map of the STRATAFORM study area including the locations of tripod deployments and general location of the 1995 and 1997 flood deposits (shaded area) based on Wheatcroft *et al.,* 1996 and Wheatcroft and Borgeld, 2000 4

Figure 2-1 Conceptual diagram illustrating transport by gravity-driven flows trapped within the wave boundary layer and the relative contributions to the near-bed velocity scale (u_{max}) 10

Figure 2-2 Time series observations and predicted gravity-driven velocity for S-60 1996-97; (a) Eel River discharge at Scotia; (b) bottom wave orbital velocity calculated from NDBC buoy 46022 for 60-m depth; (c) across-shelf current 30 cmab (dotted line) and 100 cmab (solid line) from EMCM @ S-60; (d) gravity-driven velocity predicted by Equation 2-9 (dotted line) and S-60 across-shelf current linearly extrapolated to top of the wave boundary layer (solid line) 17

Figure 2-3 Time series observations and predicted gravity-driven velocity for S-60 and K-60 1997-98; (a) Eel River discharge at Scotia; (b) bottom wave orbital velocity calculated from NDBC buoy 46022 for 60-m depth; (c) across-shelf current 50 cmab (dotted line) and 100 cmab (solid line) from EMCM @ K-60; (d) across-shelf current 30 cmab (dotted line) and 100 cmab (solid line) from EMCM @ S-60 (e) gravity-driven velocity predicted by Equation 2-9 (dotted line) and K-60 across-shelf current linearly extrapolated to top of the wave boundary layer (solid line); (f) gravity-driven velocity predicted by equation 2-9 (dotted line) and S-60 across-shelf current linearly extrapolated to top of the wave boundary layer (solid line) 19

Figure 2-4 Time series observations and predicted deposition for K-60 1997-98; (a) bottom wave orbital velocity calculated from NDBC buoy 46022 for 60-m depth; (b) ABS image from K-60 tripod with deposition predicted by Equation 2-13 assuming a porosity of 0.90 22

Figure 2-5 (a) Estimated along-shelf delivery of river sediment assuming exponential decay moving north away from the river mouth; (b) comparison of estimated sediment delivery to K and S transects with maximum potential down-slope flux at 60-m depth (Equation 2-12) for 1996-97; (c) comparison of estimated sediment delivery to K and S transects with maximum potential down-slope flux at 60-m depth (Equation 2-12) for 1997-98 24

Figure 2-6 (a) Comparison of estimated sediment delivery to S transect with maximum potential down-slope flux at S-60 for 1996-97 flood events; (b) comparison of cumulative sediment delivery to S transect with the cumulative down-slope flux capacity at S-60 26

Figure 2-7 (a) Comparison of estimated sediment delivery to K and S transects with maximum potential down-slope flux at 60-meters for 1997-98 flood events; (b) comparison of cumulative sediment delivery to K and S transects with the cumulative down-slope flux capacity at 60-meters 28

Figure 2-8 Predicted deposition at S-60 for three largest flood events observed during the STRATAFORM program (January 1995, March 1995 and January 1997). Deposition was predicted by applying Equation 2-13 for 20 days beginning with on-set of elevated river discharge and assuming a porosity of 0.75. Dotted vertical line represents 7 days from peak river discharge and is representative of approximate time for fine sediment consolidation 31

Figure 2-9 Predicted across-shelf distribution of deposition for S-transect for January 1995, March 1995 and January 1997 floods. Deposition was predicted by applying Equation 2-13 for 14 days and assuming a porosity of 0.75. Deposition was assumed to begin at depth where the cumulative delivery of sediment first exceeds the cumulative flux capacity of the boundary layer for the 14-day period 33

Figure 2-10 (a) Predicted deposition at 60-meter depth for 1996-97 New Year's flood. Deposition was predicted by applying Equation 2-13 for a 14-day period beginning with on-set of flooding and assuming a porosity of 0.75. Orbital velocities were calculated from spectral energy density from NDBC buoy 46022 for appropriate depth; (b) across-shelf slope at 60-m isobath inferred from smoothed N.O.S. bathymetry; (c) across-shelf slope gradient at 60-m isobath calculated from smoothed N.O.S. bathymetry 37

Figure 2-11 Across-shelf depth profile for S and K transects. Profiles were obtained by smoothing N.O.S. bathymetry data 39

Figure 2-12 Comparison of estimated along-shelf delivery of sediment with cumulative down-slope flux capacity for the periods associated with the largest floods of a) 1995; b) 1997; c) 1998. Arrow indicates region where cumulative down-flux capacity at 60-m exceeds the estimated delivery of sediment 40

Figure 3-1 Modeled along-shelf sediment distribution with exponentially decaying sediment delivery north of the river mouth (efolding length = 20 km) 46

Figure 3-2 River discharge measured at Scotia and Bridgeville gauging stations and bottom wave energy calculated at 60-meter depth from NDBC buoy 46022 spectral wave energy density for the four periods to which the model was applied 50

Figure 3-3 Across-shelf profiles of predicted deposition along the K and S transects for the a) 1994-95; b) 1995-96; c) 1996-97; d) 1997-98 flood seasons. Deposition was calculated assuming a porosity of 0.75. 51

Figure 3-4 Predicted gravity-driven deposition for four flood seasons. Deposition was calculated assuming a porosity of 0.75 and only deposition deeper than 50 meters is shown 52

Figure 3-5 Time-series of predicted deposition at S-60 assuming porosity of 0.75 for four flood seasons 59

Figure 3-6 Comparison of wave orbital velocity, modeled drag coefficient, and gravity-driven velocity at S-60 during 1996-97 and 1997-98 flood season 61

Figure 3-7 Along-shelf distribution of cumulative (a) mid-shelf gravity-driven deposition; (b) inner-shelf deposition; (c) off-shelf gravity-driven flux predicted by the model for the four flood seasons 63

Figure 3-8 Time series of cumulative gravity-driven sediment flux into Eel Canyon for four flood seasons 67

Figure 3-9 ABS image of bed elevation change and predicted deposition at K-60 in 1997-98 assuming normal sediment delivery (red line) and a 2-fold increase in sediment delivery (black line). Wave orbital velocities calculated from NDBC buoy 46022 are shown in blue 70

Figure 3-10 Observations and model predictions for K-60 during 1997-98. (a) Observed across-shelf velocity from EMCM 50 cmab (dashed line) and 110 cmab (solid line); (b) Predicted gravity-driven velocity at K-60 for normal sediment input (dashed line) and doubled sediment input (solid line). (c) Predicted Richardson number at K-60 for normal sediment input and (d) doubled sediment input 71

Figure 3-11 Predicted gravity-driven velocity at S-60 and G-60 for 1996-97 using uniform along-shelf sediment with no sediment input south of the river mouth (a) not including influence of observed along-shelf currents, and (b) including the influence of the observed along-shelf currents. Arrows indicate on-set of inferred gravity-driven transport from tripod observations @ G-60 and S-60 77

Figure 3-12 Change in predicted deposition along 60-meter isobath due to including effect of along-shelf slope for 1994-95 (solid line) and 1996-97 (dashed line). The predicted deposition along the 60-meter isobath without including the influence of the along-shelf slope was subtracted from the predicted deposition including the influence of the along-shelf slope 84

Figure 3-13 Predicted deposition along the 60-meter isobath for model run using uniform along-shelf sediment delivery and neglecting the effect of the along-shelf slope for the four years modeled 86

ABSTRACT

An analytical and numerical model are presented and applied to predict gravity-driven transport and deposition of fluid mud layers that form within the wave boundary layer on the continental shelf off the Eel River in northern California. Observations indicate that following floods of the Eel River down-slope transport of fluid mud trapped within the wave boundary layer is the dominant across-shelf transport mechanism. The models are based upon the assumption that following significant floods, an abundant supply of easily suspended fine sediment is delivered to the coastal ocean, allowing a negative feedback mechanism to maintain the near-bed Richardson number at its critical value. Thus, sediment-induced stratification effectively limits the amount of fine sediment that can be maintained in suspension, allowing the calculation of down-slope transport and deposition knowing only the appropriate near-bed velocity scale.

Analytic predictions of mid-shelf mud transport and deposition are spatially and temporally consistent with field observations and provide strong evidence that gravity-driven processes control the emplacement and location of the Eel margin flood deposit. Analytic predictions of deposition suggest that the magnitude of wave energy is more important than the magnitude of the flood event in controlling the thickness of mid-shelf gravity-driven deposition following floods. Higher wave energy increases the capacity for critically-stratified gravity flows to transport sediment to the mid-shelf and results in greater deposition. The bathymetry of the Eel margin plays a critical role in gravity-driven transport and deposition. Analytic predictions indicate that gravity-driven deposition on the mid-shelf begins roughly 7-8 km north of the river mouth. Closer to the river mouth, the seaward increasing mid-shelf slope associated with the concave downward subaqueous delta causes gravity-driven flux divergence, preventing significant mid-shelf gravity-driven deposition and favoring sediment bypassing. Seaward decreases in shelf slope in the vicinity of the observed flood depo-center leads to greater flux convergence by gravity-driven flows, and hence greater deposition.

The numerical model predicts gravity-driven deposition on the continental shelf for four consecutive flood seasons of the Eel River using realistic bathymetry, waves and river forcing. Results from the numerical model are consistent with observations of deposition on the mid-self and support the results of the analytical model that suggest wave intensity and bathymetry are the dominant factors controlling the location and magnitude of observed deposition. Despite significantly greater sediment input near the river mouth, little mid-shelf deposition is predicted in this region due to the increasing off-shelf slope. The numeric results suggest that gradients in the along-shelf components of bed-slope also favor gravity-driven deposition 10-30 km north of the river mouth. Including the influence of along-shelf currents had little impact on the location of mid-shelf deposition, providing further support for bathymetric control of flood sedimentation on the Eel margin. A significant fraction of sediment from the Eel River was predicted to leave the shelf as a gravity-driven flow during floods with large wave energy. However, in extremely large floods, gravity-driven processes were not capable of removing river-derived fine sediment from the inner-shelf.

MODELING OF CRITICALLY-STRATIFIED GRAVITY FLOWS: APPLICATION TO THE EEL RIVER CONTINENTAL SHELF, NORTHERN CALIFORNIA

1. INTRODUCTION

There is considerable evidence documenting the role of gravity-driven down-slope transport of river-derived sediment across continental shelves (Eisma and Kalf, 1984; Wright *et al.*, 1988; Mathew and Baba, 1995; Mulder and Syvitski, 1995; Kineke *et al.*, 1996; Ogston *et al.*, 2000; Traykovski *et al.*, 2000). The high-suspended sediment concentrations necessary to initiate this process make it an extremely effective mechanism for transporting sediment. Direct observations of gravity-driven transport have been associated with large rivers that more-or-less continually discharge a significant sediment load into the ocean (Wright *et al.*, 1988, 1990; Kineke *et al.*, 1996). While these large rivers contribute a significant input of sediment into the world's oceans, recent work has illuminated the important contribution to the global input by rivers with small, mountainous basins on active continental margins (Milliman and Syvitski, 1992; Mulder and Syvitski, 1995; Wheatcroft, 2000).

Mid-shelf mud-belts are a common depositional feature found off rivers on mountainous margins exposed to energetic waves (Nittrouer and Sternberg, 1981; Foster and Carter, 1997; Lopez-Galino *et al.*, 1999; Wheatcroft and Borgeld, 2000). Thus mid-shelf mud-belts play an important role in modulating the dispersal of fine sediment to the world's oceans. Classically, mid-shelf mud-belts have been assumed to be regions of diffusive, low energy, low concentration deposition (McCave, 1972). However, recent observations off northern California indicate that mud from the Eel River is primarily deposited on the mid-shelf by gravity currents of fluid mud trapped within the wave boundary layer during storms (Traykovski *et al.*, 2000). These important observations suggest a new paradigm for the formation of mid-shelf mud-belts on energetic,

depositional coasts. Similar to the classical model for energetic, near-shore deposition of mud (McCave, 1972), energetic mid-shelf deposition also must involve extremely high sediment concentrations. Wave-induced gravity currents may provide the transport mechanism necessary for the formation of mid-shelf mud-belts on energetic shelves. Whether in the near-shore or the mid-shelf, rapid deposition of mud requires the suspension capacity of the bottom boundary layer to be exceeded (McCave, 1972). Under high-energy conditions, suppression of turbulence by sediment induced stratification is necessary to exceed the capacity of the bottom boundary layer to carry fine sediment (Trowbridge and Kineke, 1994; Friedrichs *et al.*, 2000). Under high-energy, depositional conditions, a negative feedback cycle is induced, where the total load in suspension keeps the gradient Richardson number near the critical value marking the initial suppression of shear-induced instabilities by stratification (Kineke *et al.*, 1996; Wright *et al.*, 2001).

The Eel River shelf combines large sediment input, high wave energy, and mid-shelf deposition of mud, making it an ideal location for testing a model for critically-stratified, gravity-driven sediment transport and deposition. Investigation of the continental margin adjacent to the Eel River as part of the Office of Naval Research (ONR) STRATAFORM program (Nittrouer, 1999) reveals that following significant floods, fine-grained sediment accumulates in a distinct flood deposit centered near the 70-m isobath and extends over 30 km along-shelf and 8 km across-shelf (Wheatcroft *et al.*, 1997; Borgeld *et al.*, 1999; Drake, 1999; Sommerfield and Nittrouer, 1999; and Wheatcroft and Borgeld, 2000) (Figure 1-1). Distinct fine-grained flood deposits from

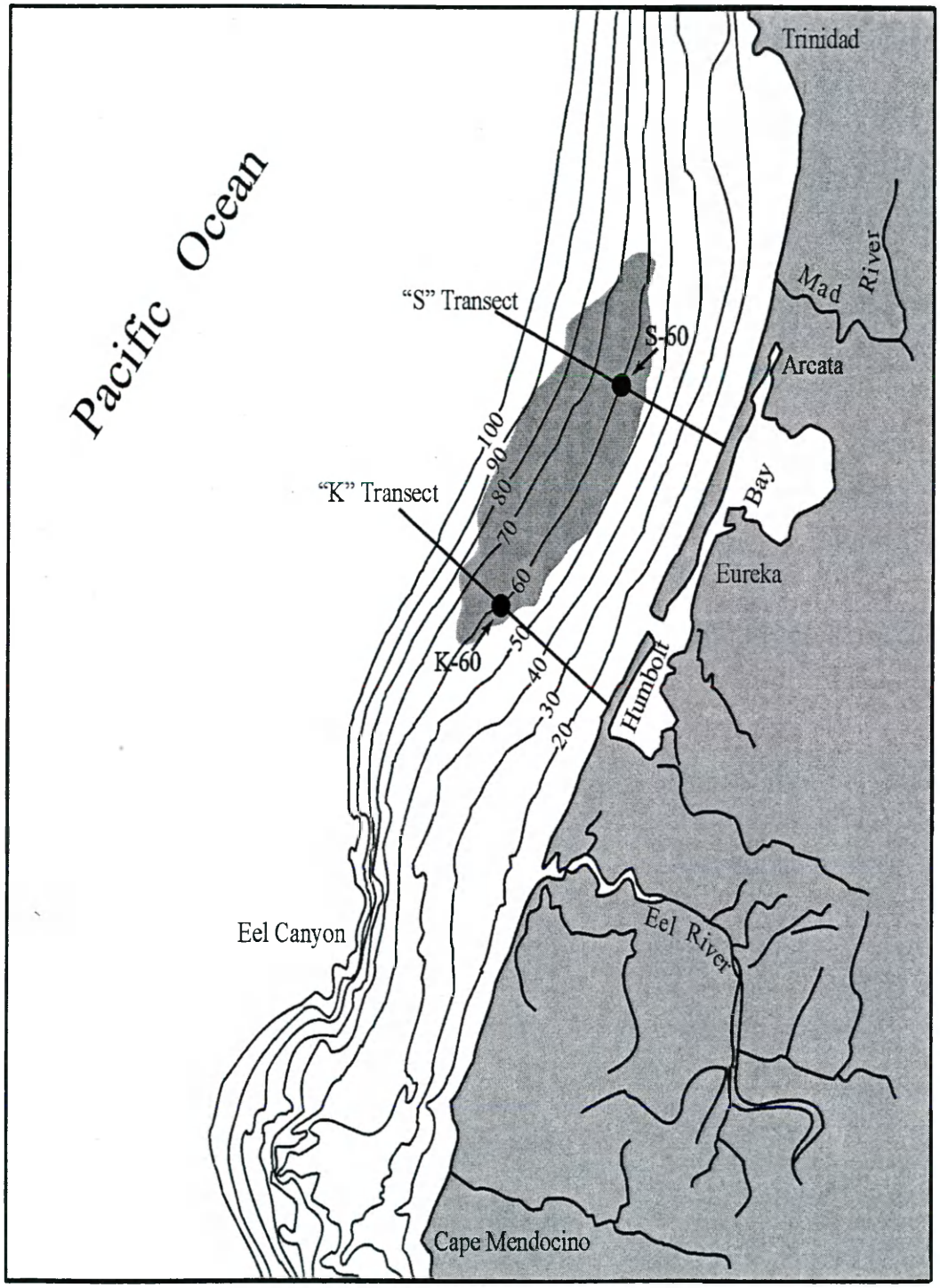

Figure 1-1 Site map of the STRATAFORM study area including the locations of tripod deployments and general location of the 1995 and 1997 flood deposits (shaded area) based on Wheatcroft *et al.,* 1996 and Wheatcroft and Borgeld, 2000.

both the winter of 1994-95 and 1996-97 appear in cores taken as part of the STRATAFORM program, while no significant flood deposits from the 1995-96 and 1997-98 seasons were preserved (Wheatcroft *et al.*, 1997; Borgeld *et al.*, 1999; Drake, 1999; Sommerfield and Nittrouer, 1999; Wheatcroft and Borgeld, 2000; Drake *et al.*, 2000).

Floods of the Eel River are often associated with large storm systems with high wave energy and strong winds. During the early portion of many storms, winds are often from the south causing the river plume to travel north, hugging the coast. Helicopter surveys during flood conditions indicate that the Eel River plume exits the mouth and travels north, staying inshore of the 40-m isobath (Geyer *et al.*, 2000). It has been proposed that much of the sediment from the plume is initially deposited near-shore where it is temporarily stored before moving offshore to the region of the flood deposit (Geyer *et al.*, 2000; Ogston *et al.,* 2000; Traykovski *et al.*, 2000). Instrumented tripods deployed as part of the STRATAFORM program provide strong evidence that across-shelf gravity-driven transport plays an important role in the dispersal and deposition of flood sediment from the Eel River (Ogston *et al.*, 2000; Traykovski *et al.,* 2000). Traykovski *et al.* (2000) observed highly turbid near-bed layers (>> 10 g/L) with a strong lutocline that appeared to scale with the wave boundary layer. They propose that these turbid layers are trapped within the wave boundary layer and are dependent upon wave-induced turbulence and propagate across-shelf under the influence of gravity (Traykovski *et al.*, 2000). They further propose that the offshore flow of fluid mud is the dominant depositional mechanism on the Eel River mid-shelf.

There are still several intriguing patterns regarding the geometry of mid-shelf flood deposits off the Eel River that have yet to be adequately addressed by hydrodynamic modeling. Both ^{210}Pb geochronology applied to century time-scales (Sommerfield and Nittrouer, 1999) and shallow coring of the 1994-95 and 1996-97 flood layers (Wheatcroft and Borgeld, 2000) indicate that less than 25% of fluvial mud discharge is deposited on the mid-shelf. Sommerfield and Nittrouer (1999) conclude that a major fraction of fine-grained flood sediment bypasses the narrow shelf, while Wheatcroft and Borgeld (2000) suggest a substantial fraction may be temporarily sequestered in the inner-shelf sands. The mud that does make it to the mid-shelf is not thickest offshore of the river mouth where initial settlement from the river plume is most intense (Geyer *et al.*, 2000). Rather, the center of the flood deposit is displaced 15 to 20 km to the north (Wheatcroft and Borgeld, 2000). Wheatcroft and Borgeld (2000) further note that larger floods do not always produce larger flood deposits. In terms of total sediment discharge, the January 1997 flood was larger than the January 1995 flood, yet the total volume of the two mid-shelf flood deposits were similar (Wheatcroft and Borgeld, 2000). Finally, a three-fold increase in mid-shelf sediment accumulation since 1955 has been documented without a similarly large increase in river discharge (Sommerfield and Nittrouer, 1999; Sommerfield *et al.,* 2000).

We apply both an analytical and numerical model for critically-stratified, gravity-driven sediment transport and deposition to the Eel shelf in order to understand the above geological patterns, as well as the formation of energetic mid-shelf mud-belts in general. Analytic predictions of near-bed velocity and deposition are compared with observations collected by benthic boundary layer tripods deployed during the STRATAFORM

program. To understand better when gravity-driven processes will occur, we use the analytic formulation to compare the ability of gravity-driven processes to transport sediment to the mid-shelf relative to the ability of the river to supply sediment to the inner-shelf. We use the analytic solution to help explain the large-scale geometry of flood deposition as observed in the cores collected from the Eel River continental shelf.

To provide a more realistic representation of the large-scale processes controlling deposition on the Eel shelf, we developed a two-dimensional numerical model to predict transport and deposition of fine sediment derived from the Eel River. The numerical model is intended to realistically represent the first order forcings in order to predict large scale deposition of fine-grained sediment on the continental shelf following floods of the Eel River. Application of the model is intended to build upon the analytic results by more realistically predicting deposition on the shelf in a manner that is computationally efficient. By accounting only for gravity-driven transport and deposition, the model is relatively simple and allows us to focus on the importance of this mechanism. The numerical approach allows us to more thoroughly examine the role that gravity-driven processes play in the fate of flood-derived fine sediment, further constraining the overall sediment budget for the Eel River system. Sensitivity analysis highlights the importance of processes that influence gravity-driven transport and deposition and provides further insight into the formation and preservation of flood deposition on the Eel margin.

2. ANALYTICAL MODEL

2.1. THEORETICAL DEVELOPMENT

The classic understanding of the forces governing gravity-driven flows is the balance between a down-slope pressure gradient driven by the negative buoyancy associated with suspended sediment and frictional drag forces (*e.g.*, Komar, 1976). In its simplest form, the Chezy equation quadratic drag law can represent this balance:

$$\alpha B = C_d u_{grav}^2 \qquad (2\text{-}1)$$

where α is the sine of bottom slope, u_{grav} is the velocity of the gravity-driven flow, C_d is the frictional drag coefficient at the bottom of the layer, and B is the depth-integrated buoyancy of the hyperpycnal layer:

$$B = g\ s \int_0^{\delta} c' dz \qquad (2\text{-}2)$$

where g is the acceleration of gravity, s is the submerged weight of siliceous sediment relative to sea water, δ is the layer thickness, and c' is the sediment volume concentration. At first order, this relation ignores interfacial friction at the top of the layer, advective acceleration, large-scale pressure gradients, and the Coriolis force. In general, advective acceleration is negligible and the bottom drag coefficient is often much larger than that of the top, allowing interfacial drag to be ignored (for thin layers). The entrainment of less dense fluid from above can play an important role controlling the buoyancy and hence the governing forces. However, Ellison and Turner (1959) found that turbulent entrainment of surrounding fluid into the layer is negligible when the top of the layer is significantly stratified. Coriolis also will be secondary for gravity flows that are on the order of the wave boundary layer in thickness (Traykovski *et al.,* 2000).

The negative buoyancy force can only be maintained as long as sediment is maintained in suspension. In order for this to occur, sufficient turbulence must exist such that upward turbulent diffusion can balance particle settling. Turbidity currents can become auto-suspending if they reach a velocity at which sediment can be entrained into the flow, increasing the negative buoyancy and leading to acceleration (Parker *et al.*, 1986). Such flows are not likely to be observed on the continental shelf because the slope is generally not sufficient to generate currents with sufficient velocity to reach the auto-suspending criteria (Wright *et al.*, 2001). On the shelf, both wave and current energy can supply the turbulence necessary to maintain a gravity flow in suspension. At the same time, turbulence also will increase the drag, resisting down-slope motion. To describe this process, the linearized form of the Chezy equation then can be expanded to a more general case as (Wright *et al.*, 2001):

$$\alpha\ B \approx C_d u_{\max} u_{grav} \tag{2-3}$$

where u_{max} is the magnitude of the velocity at the top of the near-bed layer (Figure 2-1). The u_{max} term includes wave orbital velocity amplitude (u_{wave}), along-shelf current magnitude (v_{curr}), and the across-shelf gravity current speed (u_{grav}), and is approximated by:

$$u_{\max} = \sqrt{u_{wave}^2 + v_{curr}^2 + u_{grav}^2} \tag{2-4}$$

When significant suspended sediment is present, the gradient Richardson number can be represented simply as the ratio of the buoyancy to the shear produced by the maximum velocity scale (Trowbridge and Kineke, 1994), or

$$Ri_g = gs\frac{(\partial c'/\partial z)}{(\partial u/\partial z)^2} = \frac{(B/\delta^2)}{(u_{\max}/\delta)^2} = \frac{B}{u_{\max}^2} \tag{2-5}$$

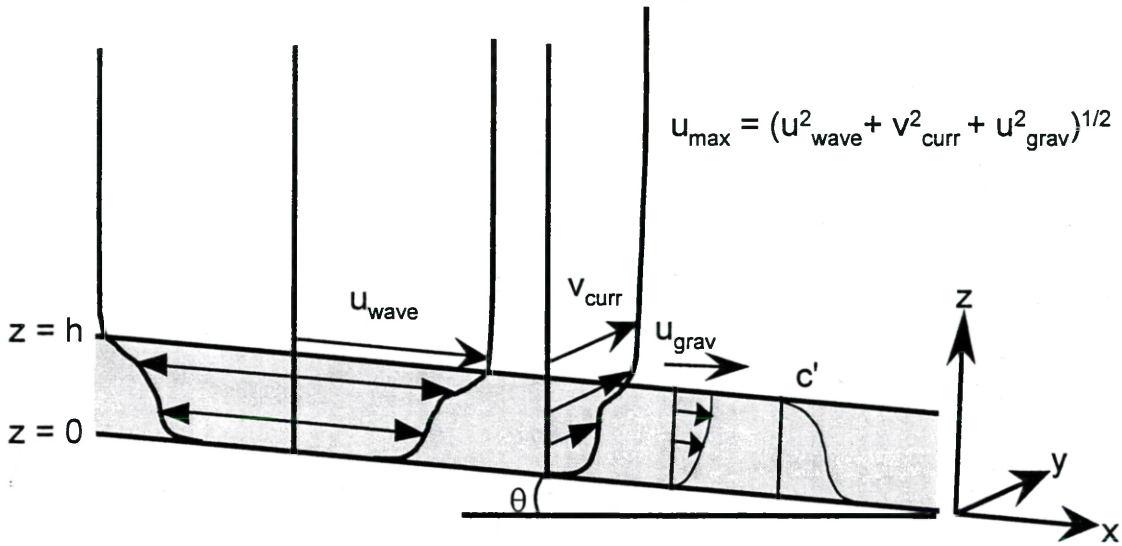

Figure 2-1 Conceptual diagram illustrating transport by gravity-driven flows trapped within the wave boundary layer and the relative contributions to the near-bed velocity scale (u_{max}).

For tidal boundary layers on the continental shelf off the Amazon River, Trowbridge and Kinke (1994) found that vertical transport was controlled by the suppression of turbulent mixing when Ri_g is maintained near its critical value of 0.25 due to the presence of high concentration fluid mud layers. They presented a one-dimensional model that assumed that Ri_g was maintained at its critical value everywhere within the boundary layer. Although their solution is unrealistic at both the top and bottom of the boundary layer, their results suggest that the structure in the majority of the flow is controlled by the suppression of turbulent mixing and $Ri_g \sim 0.25$. Building upon these results, we assume that following floods of the Eel River, sufficient easily suspended sediment is available to maintain the bulk Richardson number (Ri_b) for the wave boundary layer at a critical value given as:

$$Ri_b = \frac{B}{u_{\max}^2} = 0.25 \qquad (2\text{-}6)$$

Kundu (1981) showed that a constant bulk Richardson number is consistent with the maintenance of the gradient Richardson number at its critical value throughout the layer. Interpretation of laboratory experiments indicates that Ri_b maintains a relatively constant value of unity for turbulent flows with stable stratification (Price, 1979 and Thompson, 1979). In the bulk scaling, the velocity shear is represented by the average velocity scale. We do not attempt to resolve the velocity profile within the wave boundary layer. However, by assuming that the velocity profile within the wave boundary layer is approximately linear, the scaling for Ri_b in Equation 2-6 is equivalent to:

$$Ri_b = \frac{B}{\bar{u}_{\max}^2} \approx 1 \qquad (2\text{-}7)$$

where the overbar indicates the vertically averaged velocity scale for the wave boundary layer. It is unlikely that the velocity profile in the wave boundary layer is linear, so this scaling relationship represents a maximum value of B that can be maintained.

Assuming that the Richardson number is maintained at its critical value as defined in Equation (2-6), Equations (2-2) and (2-6) can be solved for the maximum turbulent load that the gravity-driven current can hold (Wright *et al.*, 2001):

$$\int_0^{\delta} c' \, dz = \frac{Ri_{cr} u^2{}_{\max}}{s \; g} \qquad (2\text{-}8)$$

The velocity at which the current will move down-slope can be obtained from Equations (2-3) and (2-6) to give (Wright *et al.*, 2001):

$$u_{grav} = \frac{\alpha\ Ri_{cr} u_{\max}}{C_d} = \beta\ u_{\max} \tag{2-9}$$

where:

$$\beta = \frac{\alpha\ Ri_{cr}}{C_d} \tag{2-10}$$

Here we extend the analysis of Wright *et al.* (2001) by further considering the case for which u_{grav} approaches u_{max}. Combining Equations (2-4) and (2-9) and solving for u_{max} gives:

$$u_{\max} = \sqrt{\frac{u_{wave}^2 + v_{curr}^2}{1-\beta^2}} \tag{2-11}$$

As β approaches one, more and more turbulence is provided by the gravity flow itself, increasing the capacity of the gravity current to carry sediment. The asymptote of $\beta = 1$ represents the transition to autosuspension, where stratification no longer can limit the suspended sediment capacity of the gravity current. Clearly the assumption behind maintenance of $Ri_b = Ri_{cr}$ breaks down somewhat before β reaches one. Nonetheless, the qualitative trend toward enhanced gravity currents is sensible, with no limiting role for stratification on shelves with slopes greater than $\alpha = C_d/Ri_{cr}$.

Knowing both the maximum turbulent load and velocity of the gravity current gives the across-shelf flux of sediment:

$$Flux = Q_{grav} = u_{grav} \int_0^{\delta} c'\,dz = \frac{\alpha\ Ri_{cr}^2 \rho_{sed} u_{\max}^3}{C_d s\ g} \tag{2-12}$$

Assuming that C_d remains constant with depth, net deposition or erosion associated with the gravity current is determined by across-shelf gradients in sediment flux:

$$deposition = -\partial \frac{Q_{grav}}{\partial x} = -\frac{Ri^2_{cr}\rho_{sed}}{C_d s\, g}\partial \frac{\alpha\, u^3_{max}}{\partial x} \qquad (2\text{-}13)$$

Assuming monochromatic waves and that u_{wave} ($\partial u_{wave}/\partial x$) >> v_{curr} ($\partial v_{curr}/\partial x$), Equation (2-13) can be re-expressed as:

$$deposition = \frac{Ri^2_{cr}\rho_{sed}}{C_d s\, g}\frac{\alpha^2 u^3_{max}}{h}\left\{\frac{3kh}{\tanh kh} - \frac{h}{\alpha^2}\frac{\partial \alpha}{\partial x}\frac{(2\beta^2+1)}{(1-\beta^2)}\right\} \qquad (2\text{-}14)$$

where k is the orbital wave number and h is depth. If Equation (2-14) is negative, erosion (or at least a lack of deposition) will occur.

The first term in bracketed expression in Equation (2-14) always favors deposition and originates from the offshore decay in wave orbital velocity with increased depth. As wave orbital decays offshore, the capacity of the gravity flow decreases, and sediment is deposited. When u_{max} is dominated by u_{wave}, the rate of deposition decreases dramatically offshore because of the equation's overall dependence on u^3_{max}. The second term in the bracketed expression favors erosion if the shelf is concave downward and deposition if the shelf is concave upward. It originates from the direct dependence of the sediment transport capacity on bed slope, α. If bed slope increases offshore ($\partial\alpha/\partial x > 0$), gravity flow capacity increases and flux divergence occurs; if bed slope decreases ($\partial\alpha/\partial x < 0$), capacity decreases and the result is flux convergence. This second term also incorporates the turbulence provided by the gravity flow itself and it dominates toward the autosuspending limit of $\beta = 1$.

2.2. ANALYTIC PREDICTIONS OF GRAVITY-DRIVEN VELOCITY

2.2.1. 1996-97 Flood Season—S-60

The 1996-97 New Year's flood of the Eel River, with an estimated return interval of approximately 80 years (Syvitski and Morehead, 1999), was the largest flood event to occur during the ONR STRATAFORM program. Peak discharge exceeded 12,000 m^3/s and a conservative estimate of roughly 29 million metric tons of sediment were discharged into the adjacent coastal waters (Wheatcroft and Borgeld, 2000). During the 1996-97 winter, an instrumented tripod with electromagnetic current meters (EMCMs) at 30 and 100 cm above bed (cmab) was maintained along the S-transect (Figure 1-1) in approximately 60 m water depth (S-60) (Ogston *et al.*, 2000). The EMCM data show an extended period where the current 30 cmab is directed offshore with a greater velocity than the current measured 100 cmab (Figure 2-2c). Consistent with the observations of Traykovski *et al.* (2000), we infer that these periods occur when high concentration fluid mud suspensions trapped within the wave boundary layer move down-slope under the force of gravity, exerting a frictional drag on the overlying water column that causes the magnitude of off-shelf directed flows to increase as the top of the wave boundary layer is approached.

To predict the down-slope velocity from Equation (2-9) all that is needed is the bed-slope, drag coefficient, and appropriate near-bed velocity scale (u_{max}). A bed slope of 0.0043 was estimated from the N.O.S. bathymetry data for the S-60 site. The results of Wright *et al.* (2001), as well as laboratory flume experiments by van Kessel and Kranenburg (1996), indicate that the drag coefficient for O(10 cm) thick critically-stratified flows is approximately 0.003. On an energetic shelf, such as that off the Eel

River, wave orbital velocity often dominates the near-bed velocity, although ambient along-shelf currents and the velocity generated by the gravity-flow also can contribute. Wave orbital velocity at a given depth can be reasonably inferred from observations of wave height and period for a general area, while accurate knowledge of near-bed current velocity on the mid-shelf during storms requires in situ observations due to complex time-dependent pressure gradients. In order to apply the model in areas where in situ current data were not available and to avoid complications of potential Ekman forcing by along-shelf currents, v_{curr} was not included in the calculation of u_{max}.

In calculating u_{max} via Equation (2-11), u_{wave} was determined from spectral wave density data collected by the National Data Buoy Center (NDBC) buoy 40622, including the frequency-based decay for the appropriate depth following the methods of Sherwood *et al.* (1994). Comparison of orbital velocities calculated from the offshore buoy with tripod observations indicates that this method slightly over-predicts bottom orbital velocity at the 60-m depth, so a correction coefficient of 0.79 was applied to maximize agreement with tripod data. The correction coefficient was determined by calculating the ratio of the calculated orbital velocity to the observed rms wave orbital velocity for all data collected at both the S-60 and K-60 tripod during the 1997-98 season. Figure 2-2d compares predicted gravity-driven down-slope velocity with observations collected from the S-60 tripod during fall/winter 1996-97. No direct observations of velocity were available from within the wave boundary layer, thus the across-shelf velocity component of the EMCM data was linearly extrapolated down to the top of the wave boundary layer. Based on the observations of Traykovski et al. (2000), the thickness of the wave boundary layer (δ_w) was estimated as:

$$\delta_w = 0.08(u_{wave}/\omega). \qquad (2\text{-}15)$$

A theoretically predicted scaling factor is not used here because no appropriate theory has been put forward for accurately predicting critically-stratified wave boundary layer thickness based on first principles. The evaluation of observed u_{grav} here is relatively insensitive to δ_w, and theoretical estimates of u_{grav} and associated deposition are independent of δ_w.

Consistent with our assumptions, the predicted gravity-flow velocity does not appear to be correlated with the observed across-shelf velocity outside of the periods of significant river discharge. Between Julian Day 1996 (JD96) 300 and 320 the correlation coefficient, r, is -0.09. Before the on-set of flooding, sufficient easily suspended fine sediment was presumably not present to maintain near-bed critical stratification. The predicted velocity does a much better job reproducing the observed near-bed velocity for the extended period coinciding with the offset in the across-shelf EMCM data. In fact, for the twenty-day period beginning on JD96 350, r=0.59. For the ten-day period beginning with onset of the New Year's flood, the correlation coefficient between the observed and predicted velocities improves to 0.76. Consistent with the observations of Geyer *et al.* (2000) and other STRATAFORM investigators, we hypothesize that following the New Year's flood, significant quantities of river sediment initially settled out of the river plume into the bottom boundary layer of the inner-shelf north of the river mouth. Enough of this in-shore supply of fine-grained sediment was suspended by the energetic waves and currents to maintain critical near-bed stratification as it moved down-slope across the mid-shelf. This process continued until the supply of sediment was exhausted, or significant consolidation or dispersion occurred.

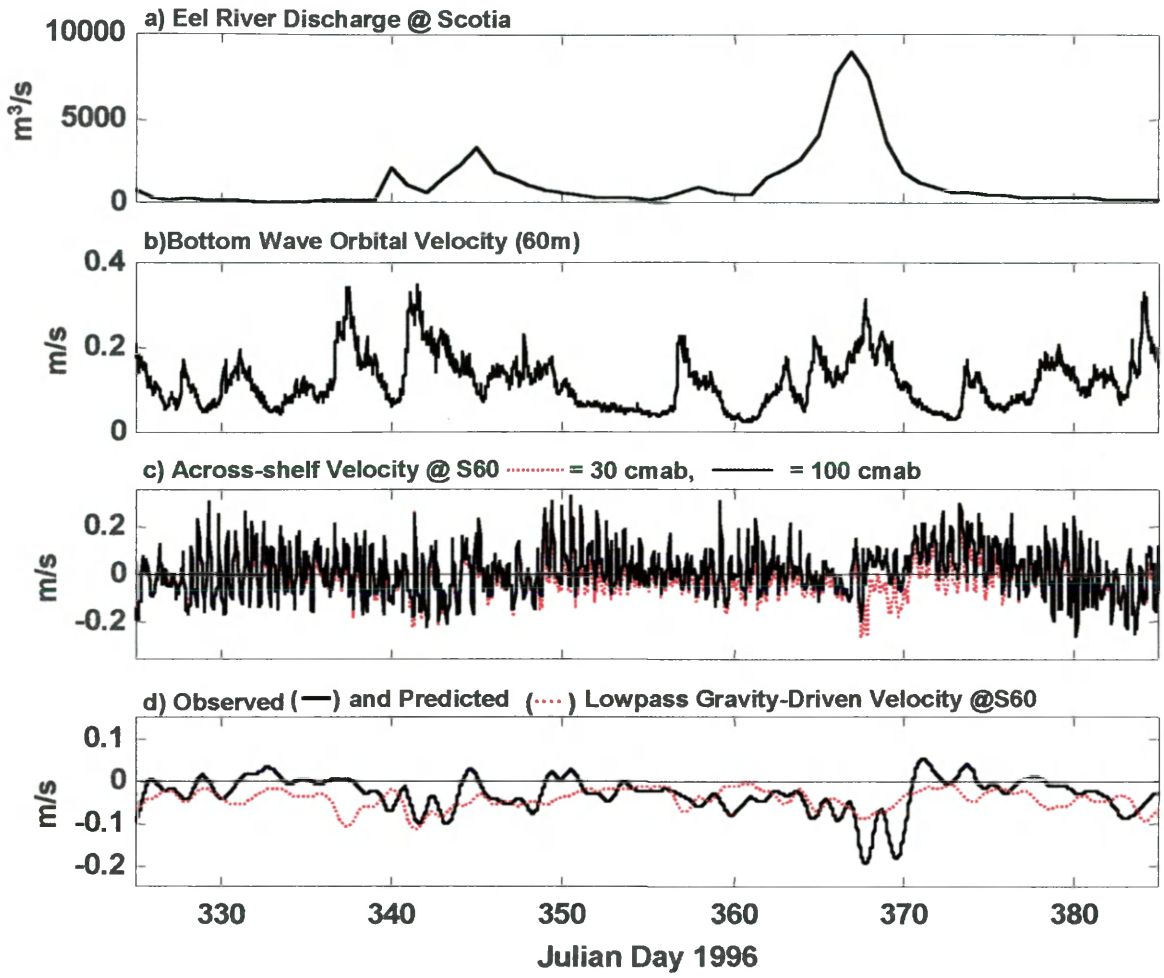

Figure 2-2 Time series observations and predicted gravity-driven velocity for S-60 1996-97; (a) Eel River discharge at Scotia; (b) bottom wave orbital velocity calculated from NDBC buoy 46022 for 60-m depth; (c) across-shelf current 30 cmab (dotted line) and 100 cmab (solid line) from EMCM @ S-60; (d) gravity-driven velocity predicted by Equation 2-9 (dotted line) and S-60 across-shelf current linearly extrapolated to top of the wave boundary layer (solid line).

2.2.2. 1997-98 Flood Season—K-60

The 1997-98 flood season consisted of several modest flood events, all of which were significantly smaller in magnitude than the New Year's flood the previous winter. Beginning on Julian Day 1997 (JD97) 375, the Eel River experienced four consecutive flood events over the course of approximately 10 days, each with a peak discharge

exceeding 3,000 m^3/s (Figure 2-3a). During this time, a tripod with EMCMs at 50 and 110 cmab as well as a downward looking Acoustic Backscattering Sensor (ABS) was deployed on the K-transect at a depth of 60 m (K-60). During the ten-day period of increased river discharge, Traykovski *et al.* (2000) report periods of increasing off-shore flow (Figure 2-3c) closer to the bed associated with ABS images of a thin (~10 cm), high concentration (>10g/L) near-bed layer, providing the most conclusive evidence to date of significant gravity-driven sediment transport on the Eel Shelf.

Near-bed orbital velocities again were calculated from NDBC buoy 46022, and v_{curr} was excluded from the calculation of u_{max}. Equation (2-9) was applied to K-60 with $C_d = 0.003$ and a bed slope of 0.004 based on N.O.S. bathymetry. Again, the across-shelf velocity from the lowest two EMCMs was linearly extrapolated down to the top of the predicted wave boundary layer. Similar to the results from 1996-97, there is relatively little correlation between the observed and predicted velocities prior to significant river discharge ($r = -0.30$ for JD97 360-375) and much better correlation during the period of elevated river discharge ($r = 0.80$ for JD97 380-390).

The success of the analytic prediction of near-bed velocity during the 1997-98 flood season is limited to the period associated with the four consecutive floods of the Eel River (Figure 2-3e). While other floods of comparable, albeit slightly smaller magnitude occurred during this winter, little evidence of gravity-driven transport is seen in the EMCM data. This suggests that for a given wave energy, only floods exceeding a particular magnitude are capable of supplying enough sediment to critically stratify the wave boundary layer. The cumulative delivery of sediment associated with the rapid succession of relatively modest flood events over the ten-day period beginning on JD97

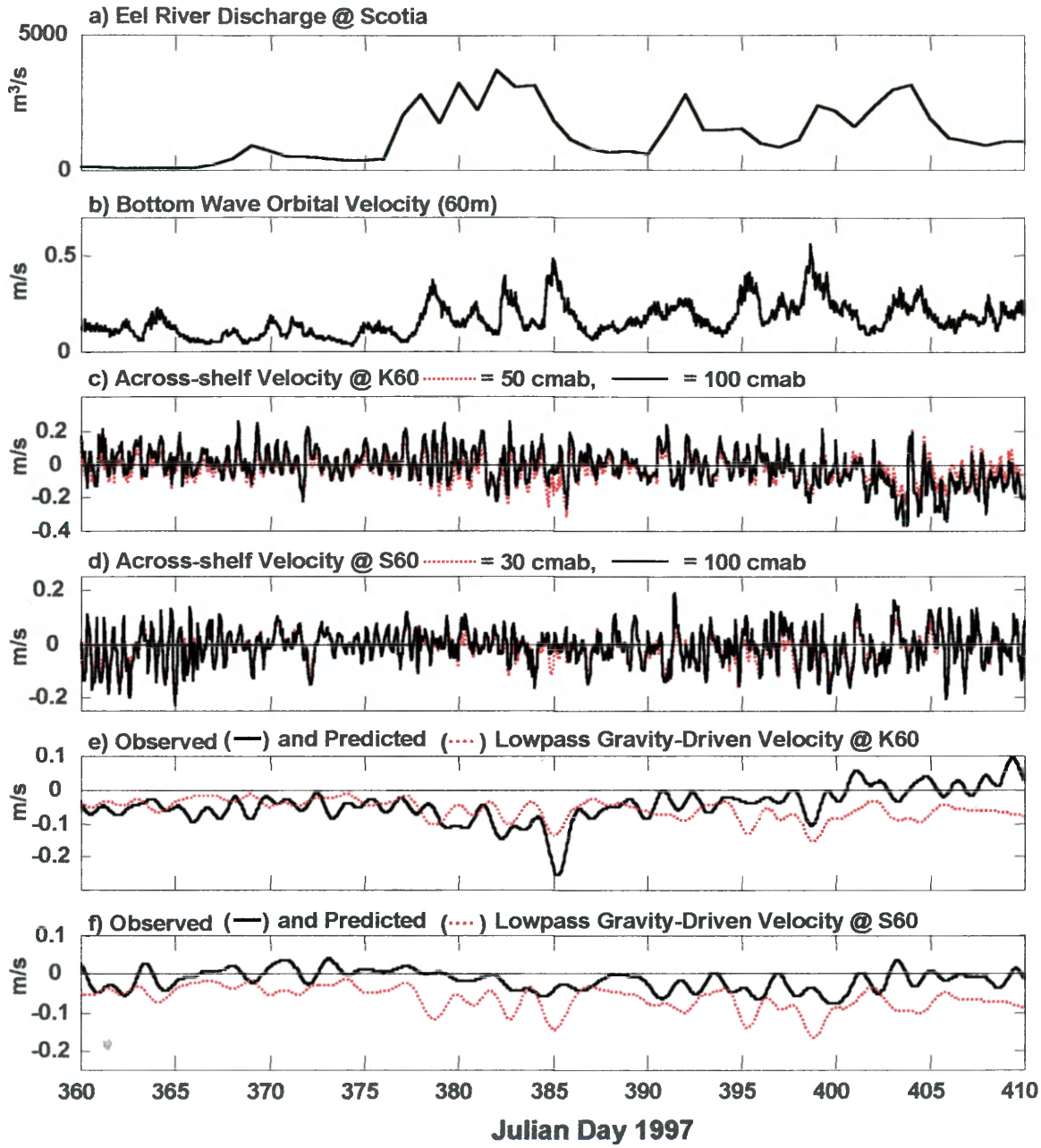

Figure 2-3 Time series observations and predicted gravity-driven velocity for S-60 and K-60 1997-98; (a) Eel River discharge at Scotia; (b) bottom wave orbital velocity calculated from NDBC buoy 46022 for 60-m depth; (c) across-shelf current 50 cmab (dotted line) and 100 cmab (solid line) from EMCM @ K-60; (d) across-shelf current 30 cmab (dotted line) and 100 cmab (solid line) from EMCM @ S-60 (e) gravity-driven velocity predicted by Equation 2-9 (dotted line) and K-60 across-shelf current linearly extrapolated to top of the wave boundary layer (solid line); (f) gravity-driven velocity predicted by Equation 2-9 (dotted line) and S-60 across-shelf current linearly extrapolated to top of the wave boundary layer (solid line).

375 may have been necessary to trigger the critically-stratified gravity-driven transport mechanism. During single flood events that occurred later in January and in February, the energetic coastal environment was probably capable of dispersing much of the fine sediment, preventing critical stratification from dominating the near-bed dynamics.

2.2.3 1997-98 Flood Season—S-60

Examination of the current meter data collected at S-60 during the 1997-98 flood season provides additional, albeit weaker, evidence of gravity driven transport. There are a few occasions associated with elevated wave energy where the current at 30 cmab had stronger off-shelf velocities than the current 100 cmab (Figure 2-3d). Specifically, the current meter data suggest potential gravity-driven transport on JD97 385 corresponding in time with the strongest evidence for gravity-driven flow from the K-60 tripod. There is also some evidence for gravity-driven transport in the current meter data on JD97 395 and 397, well after the observed deposition at K-60.

The predicted down-slope velocity for S-60 was calculated in the same manner as for K-60. While the predicted velocity for K-60 in 1997-98 and S-60 in 1996-97 slightly under-predicts the velocity observed during greatest down-slope flow, the prediction for S-60 in 1997-98 consistently over-predicts the observed velocity (Figure 2-3f). This is consistent with the idea that insufficient sediment was supplied by the river plume to critically stratify the boundary layer at S-60 during 1996-97 (see following discussion of flux). Because the boundary layer was not critically-stratified, increased drag caused by the waves and currents retarded down-slope transport. There is only a weak correlation between the observed and predicted velocities ($r = 0.41$ for JD97 380-390), indicating

that while gravity-driven transport may have occurred sporadically, the sediment-induced down-slope pressure gradient was not a dominant term in the near-bed force balance.

2.3. ANALYTIC PREDICTIONS OF GRAVITY-DRIVEN DEPOSITION

From our results, it appears that following a significant flood of the Eel River one can reasonably predict the down-slope velocity of wave-induced gravity currents knowing only the bed slope and near-bed orbital velocity. Because the near-bed orbital velocity decreases seaward with increased depth, a gradient in flux will exist causing a predictable rate of deposition via Equation (2-13).

2.3.1. K-60 Tripod

Coinciding with the periods of strong off-shore directed near-bed flow, Traykovski *et al.* (2000) show two rapid depositional events at K-60 that are the result of down-slope gravity-driven transport. Both depositional events occurred during a period of elevated near-bed wave velocity (Figure 2-4a). Both wave events lasted approximately 2 days, with peak orbital velocities exceeding 0.50 m/s. During the first wave event beginning on JD97 378, approximately 6 cm of deposition were seen in the ABS data. The second event beginning JD97 385 resulted in 13 cm of deposition (Figure 2-4b). Although there were two periods of elevated wave energy in the intervening period, there is little evidence for gravity-driven transport or deposition during this time.

Using the calculated gradient in wave orbital velocities and bed slope for the K-60 site, Equation (2-13) was applied to predict deposition for the period from JD97 377-387. The resulting prediction for deposition is shown in Figure 2-4b assuming a porosity of 0.90, consistent with the initial water content of the flood layers found in cores reported by Drake (1999). Both the timing and magnitude of the predicted deposition are consistent with those observed in the ABS data with the exception of the predicted

deposition close to JD97 383. During this period of higher waves, the model predicts roughly 4 cm of deposition while the ABS data indicate little deposition or erosion during this period. It seems plausible that sufficient sediment was not available to critically stratify the boundary layer during this brief period. In fact, estimates of sediment delivery discussed in the next section support this possibility.

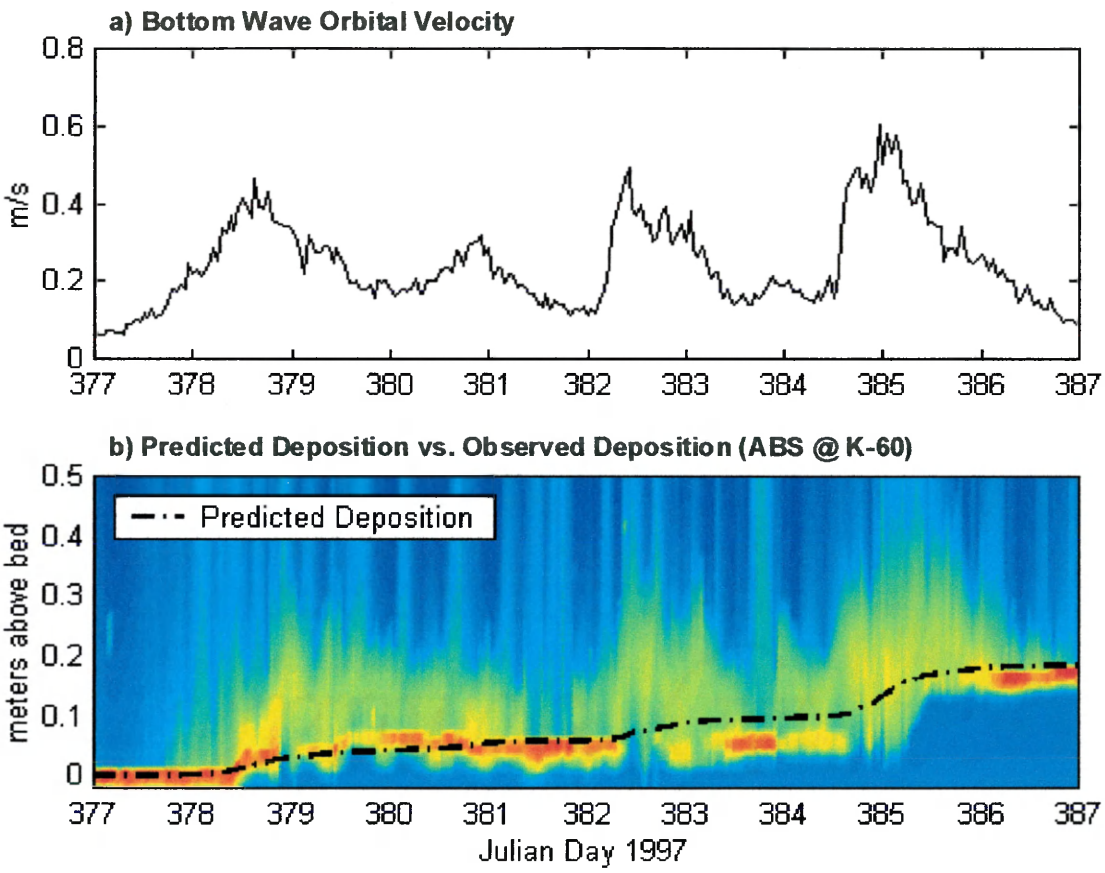

Figure 2-4 Time series observations and predicted deposition for K-60 1997-98; (a) bottom wave orbital velocity calculated from NDBC buoy 46022 for 60-m depth; (b) ABS image from K-60 tripod with deposition predicted by Equation 2-13 assuming a porosity of 0.90.

Because the predicted deposition depends on gradients in the cube of u_{max}, rapid deposition is predicted to coincide with the short periods of highest wave energy associated with the storm events. So, despite wave orbitals in excess of 0.50 m/s, no erosion is seen or predicted and significant deposition occurs. The predicted deposition is very sensitive to bed slope because ultimately it is the local bathymetry that governs the gradient in wave energy. Because the gravity-driven velocity also contributes to u_{max}, across-shelf gradients in slope will have additional influence on the deposition rate as indicated by Equation (2-14). The large-scale implications of this will be discussed below.

2.4 FLOOD DELIVERY OF SEDIMENT VS. POTENTIAL FLUX VIA GRAVITY FLOWS

The model described here demonstrates an ability to capture the timing and magnitude of depositional events observed in the tripod data. However, successful application is dependent upon knowing when sufficient sediment is available to critically stratify the boundary layer. Figure 2-5 compares the predicted maximum capacity for gravity-driven flux of sediment past K-60 and S-60 with the estimated along-shelf delivery of sediment by the river plume for both 1996-97 and 1997-98. The gravity-driven sediment flux calculations for K-60 and S-60 are assumed to be the same (using $\alpha = 0.004$), although slight differences in slope would result in minor differences that are ignored for the purpose of this comparison. The along-shelf delivery of sediment to the inner-shelf by the river plume (Figure 2-5a), expressed as percent of the Eel River sediment load per kilometer, was calculated by applying the rating curve of Syvitski and Morehead (1999) to the Eel River discharge and assuming an exponential decay of sediment delivery north of the river mouth with an e-folding length of 20 km, roughly

consistent with the observations of Geyer *et al.* (2000). During peak wave events, the capacity of the boundary layer to transport sediment down-slope was almost an order of magnitude larger during the 1997-98 flood season (Figure 2-5c), despite the fact that peak sediment input by the flood was over three times greater in 1996-97 (Figure 2-5b).

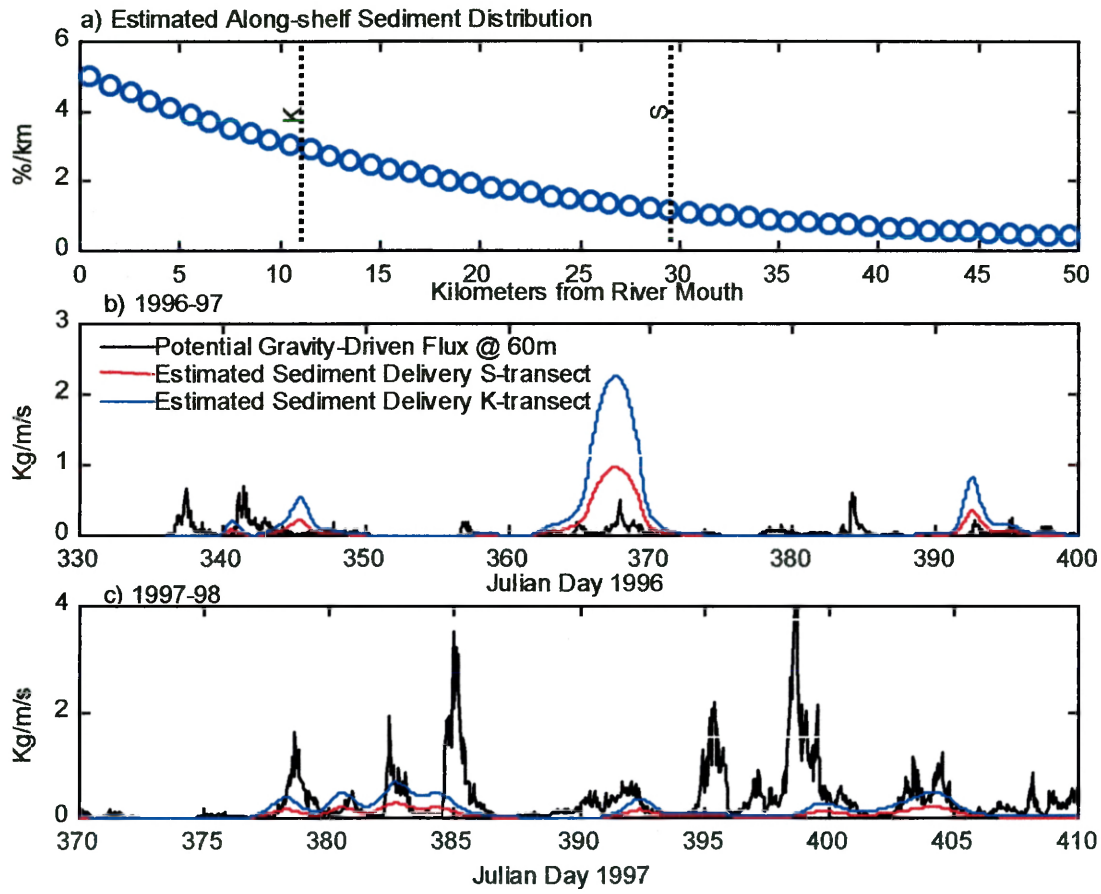

Figure 2-5 (a) Estimated along-shelf delivery of river sediment assuming exponential decay moving north away from the river mouth; (b) comparison of estimated sediment delivery to K and S transects with maximum potential down-slope flux at 60-m depth (Equation 2-12) for 1996-97; (c) comparison of estimated sediment delivery to K and S transects with maximum potential down-slope flux at 60-m depth (Equation 2-12) for 1997-98.

2.4.1. 1996-97 Flood Season—S-60

We estimate that approximately 370 t/m of sediment were delivered to the S-transect by the river plume between JD96 340 and 375, with 55 t/m coming during the modest flood beginning on JD96 340. Despite the comparatively modest discharge of this early event, the analytical model suggests that low wave energy only allowed a limited amount of sediment to be transported by gravity-driven flows. This allowed critical stratification to occur for a significant period of time following the input of sediment. During this early flood event, the majority of the river discharge occurred after the peak wave energy (see Figure 2-2). Thus, it is unlikely that gravity-driven processes immediately removed this sediment. The across-shelf shear in the EMCM data (Figure 2-2c) suggests that a prolonged period of persistent off-shelf near-bed flow began around JD96 350. This supports the idea that sediment was stored on the inner-shelf prior to moving off-shore as a gravity flow. Figure 2-6 displays cumulative sediment delivery to the inner-shelf region on the S-transect starting JD96 343 compared with the cumulative ability of the boundary layer at S-60 to transport sediment down-slope under the influence of gravity. The comparison begins on JD96 343 because this is when the delivery of sediment first exceeds the down-slope capacity and represents the time when the wave boundary layer is expected to become critically-stratified. As shown in Figure 2-6, the estimate of cumulative sediment input equals or exceeds the potential for gravity-driven flux for nearly the entire period.

According to the analytic calculations of flux, only a portion of sediment discharged during the New Year's flood could have been transported off-shore beyond S-60. However, from the observations of velocity shear, it appears that significant gravity-

driven transport ceased near JD96 376. Thus, we infer that either bed consolidation limited resuspension and resulted in significant inshore deposition of mud, or other oceanic forces effectively dispersed the sediment along and across-shelf. In all likelihood a combination of factors resulted in the cessation of gravity flows at S-60.

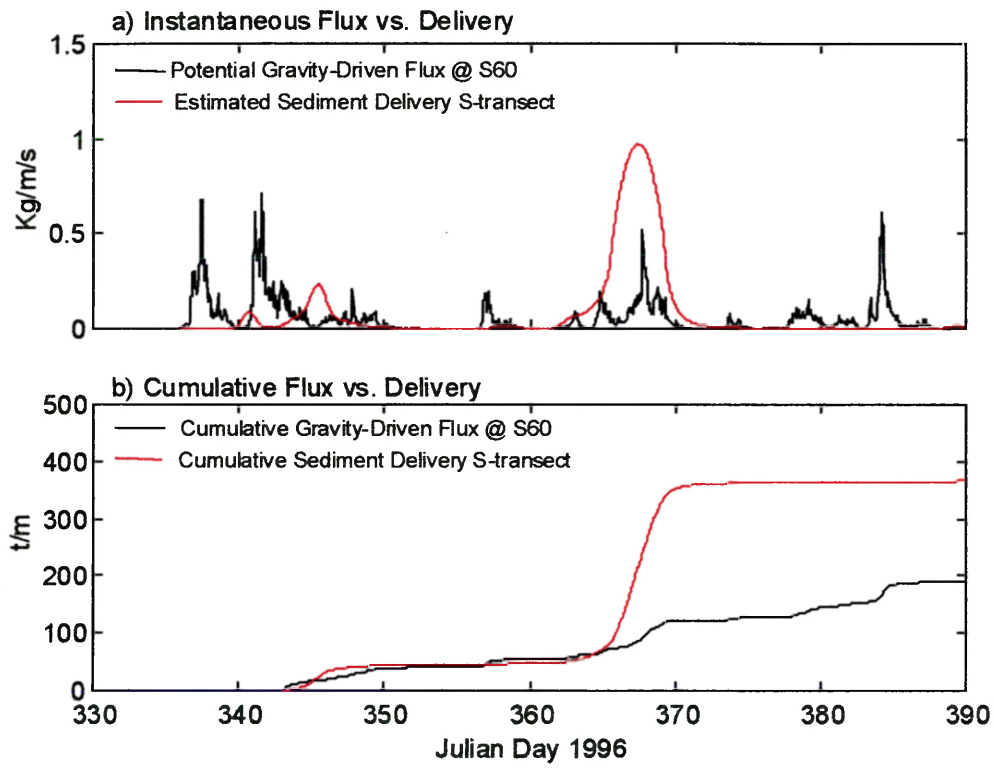

Figure 2-6 (a) Comparison of estimated sediment delivery to S transect with maximum potential down-slope flux at S-60 for 1996-97 flood events; (b) comparison of cumulative sediment delivery to S transect with the cumulative down-slope flux capacity at S-60.

2.4.2. 1997-98 Flood Season—K-60

Figure 2-5c demonstrates why prolonged periods of gravity-driven transport were not observed during the 1997-98 flood season. In contrast to the previous year, the resuspension capacity of the wave boundary layer at the 60-m isobath exceeded the input of sediment for nearly the entire record. However, closer examination provides some

insight into both the timing and duration of the observed down-slope flow. Figure 2-7a compares sediment delivery by the river flood in-shore of K-60 and S-60 to the gravity-driven boundary layer flux capacity for the twelve-day period during which the two significant depositional events occur. Although the delivery of sediment to the inner-shelf does not exceed the flux capacity of the boundary layer at K-60 during any of the wave events, delivery does exceed flux capacity during the intervals in between events. If we assume that this sediment remains inshore of K-60 during the period of low wave energy, this sediment would then be available to be resuspended and transported down-slope.

Figure 2-7b integrates the instantaneous delivery and flux in Figure 2-7a in order to compare the cumulative values. The two periods during which the cumulative delivery of river sediment inshore of K-60 most significantly exceeds the cumulative down-slope flux potential immediately precede the observations of gravity-driven deposition in the ABS data. Based on our calculation of river plume sediment delivery and gravity-induced flux, one would conclude that sufficient sediment was delivered for the boundary layer to remain critically-stratified only during the beginning of these two wave events. When the boundary layer is not critically-stratified, the wave orbitals will act to increase drag and retard down-slope flux (Equation 2-3). Therefore, it is likely that much of the sediment input between the two depositional events remained in-shore of K-60 and was available for transport when wave energy increased on JD97 385. A rough estimate of gravity-induced sediment flux during the second depositional event indicates that during the 48-hour period beginning on JD97 384, 160 t/m were transported down-slope past K-60. If the sediment delivered to the K-transect by the river in between these two events

did in fact remain inshore of K-60 prior to the onset of energetic waves on JD97 384, then 200 t/m would have been available during the second event.

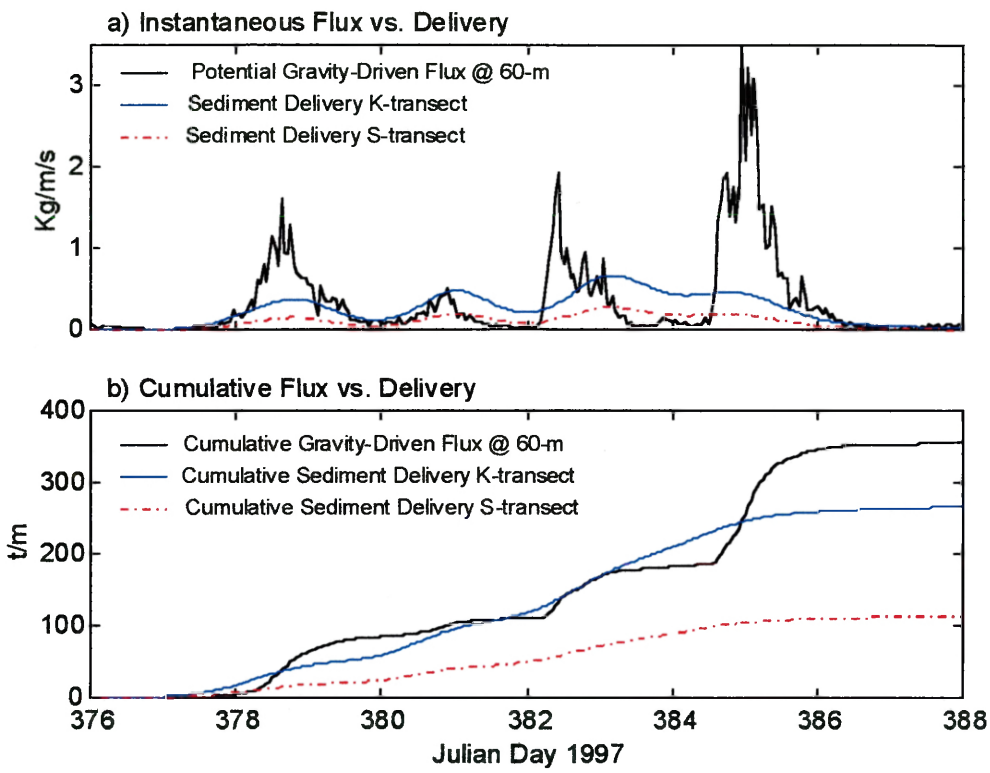

Figure 2-7 (a) Comparison of estimated sediment delivery to K and S transects with maximum potential down-slope flux at 60-m for 1997-98 flood events; (b) comparison of cumulative sediment delivery to K and S transects with the cumulative down-slope flux capacity at 60-m.

2.4.3. 1997-98 Flood Season—S-60

The analytic solution for continual gravity flows over-predicts the down-slope velocity observed at S-60 in 1997-98. Therefore, one would speculate that the down-slope flux capacity of the boundary layer exceeded the delivery of flood sediment to the S-transect. Consistent with expectations, the instantaneous down-slope sediment flux exceeded the rate of sediment delivery to the S-transect by almost an order of magnitude (Figure 2-7a), and the cumulative delivery of flood sediment never exceeded the

cumulative capacity for down-slope transport (Figure 2-7b). Therefore, we logically conclude that critically-stratified conditions did not control the wave boundary layer at S-60 during 1997-98 and significant gravity-driven deposition was unlikely.

2.5. COMPARISON OF MODEL RESULTS WITH CORE DATA

Extensive coring of the flood deposit on the Eel margin following major flood events reveals the preservation of several distinct layers of fine-grained sediment on the mid-shelf (Wheatcroft *et al.*, 1997; Borgeld *et al.*, 1999; Drake, 1999; Sommerfield and Nittrouer, 1999; Wheatcroft and Borgeld, 2000). Specifically, efforts have focused on characterizing the deposits from the January 1995, March 1995, and January 1997 floods—the three largest during the STRATAFORM program. Examination of cores reveal that the deposits from all three floods were areally extensive and remarkably similar in distribution, with the center of mass for all three floods located within 8 km (Wheatcroft and Borgeld, 2000). Maximum thickness of the preserved layers seen in mid-shelf cores along the 70-m isobath were roughly 8 cm, 4 cm, and 5 cm for the January 1995, March 1995, and January 1997 respectively (Wheatcroft and Borgeld, 2000).

Although the 1997 New Year's flood was the largest event observed, the January 1995 flood produced the locally thickest deposit (Wheatcroft and Borgeld, 2000). This is not counter-intuitive if one assumes that deposition was dominated by gravity-driven flows because the analytic solution predicts wave energy to control the deposition rate. Therefore, if enough sediment was supplied to critically stratify the boundary layer following the floods of 1995 and 1997, the event with the greatest wave energy should result in the thickest mid-shelf deposits. This is in fact what the data show. The mean rms orbital velocity for the 15-day period beginning with the on-set of flooding was 20.3

cm/s at 60-m depth for the January 1995 flood, while mean values for the 15-day period coinciding with the March 1995 and January 1997 floods were only 15.7 cm/s and 11.7 cm/s, respectively.

Figure 2-8 shows the predicted deposition at S-60 for the January 1995, March 1995, and January 1997 flood events assuming a porosity of 0.75, consistent with the partially de-watered flood layers observed in cores by Wheatcroft and Borgeld (2000). Deposition was predicted following Equation (2-13) for a twenty-day period beginning with the onset of elevated river discharge. The largest predicted deposition was associated with the January 1995 flood, followed by the March 1995 and January 1997 floods. These values are probably an over-prediction of actual deposition because it is likely that significant consolidation or dispersion of fine sediment occurred before the end of the twenty-day period. The dashed line in Figure 2-8 corresponds to the period roughly 7 days after the end of elevated river discharge for all of the flood events and represents an estimate of when significant bed consolidation may have occurred. A period of 7 days is consistent with the findings of Metha and McAnally (2001), who report that many estuarine mud deposits largely consolidate within one to two weeks. They report that within the first week following deposition, fluid mud layers rapidly de-water and compact, resulting in increased shear strength of the bed. Additionally, the 7-day period is consistent with the cessation of increased across-shelf near-bed flow observed in the velocity data at S-60 following the major flood in 1996-97. Assuming that either consolidation or sediment dispersal prevented significant gravity-driven transport from occurring 7 days after the peak river discharge gives values of predicted deposition of 11cm, 5 cm, and 4 cm for the floods of January 1995, March 1995, and

January 1997, respectively. These values agree favorably with the maximum values reported by Wheatcroft and Borgeld (2000).

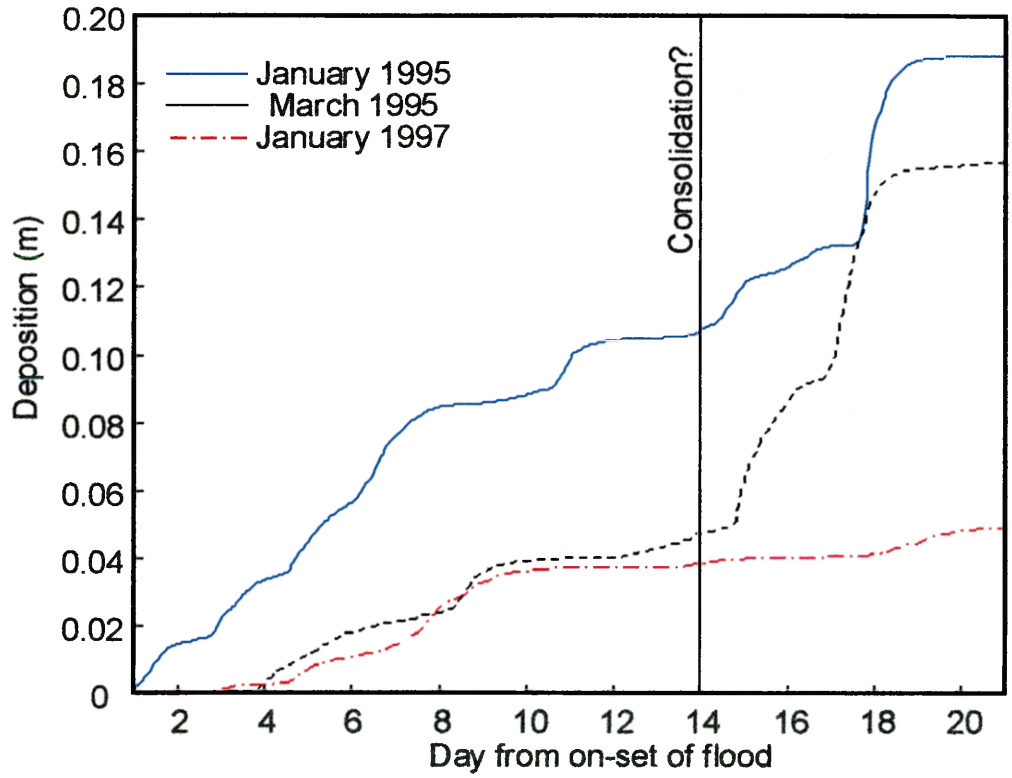

Figure 2-8 Predicted deposition at S-60 for three largest flood events observed during the STRATAFORM program (January 1995, March 1995 and January 1997). Deposition was predicted by applying Equation 2-13 for 20 days beginning with on-set of elevated river discharge and assuming a porosity of 0.75. Dotted vertical line represents 7 days from peak river discharge and is representative of approximate time for fine sediment consolidation.

To examine the across-shelf distribution of mud deposition predicted by gravity-driven flows, Equation (2-13) was used to predict deposition across the S-transect for the three largest floods during the STRATAFORM program. In applying Equation (2-13), bed slope varied as a function of depth as indicated by N.O.S. bathymetry data. Figure 2-9 shows the cumulative deposition predicted for a 14-day period at each depth across the

S-transect. Deposition was assumed to take place only at depths where the cumulative down-slope flux capacity of the boundary layer for the 14-day period was exceeded by the estimated cumulative delivery of sediment to the S-transect by the river plume. During large flood events with relatively small wave energy, such as the January 1997 flood, this approach predicts the deposition of mud beginning closer to shore. Conversely, during floods with larger wave energy or more moderate discharge, deposition will not begin until farther offshore. So, floods with extremely high sediment input and/or relatively low wave energy have a much greater potential to preserve fine sediment on the inner-shelf. This result is consistent with Wheatcroft and Borgeld (2000), who concluded that a substantial fraction of fine sediment discharged during large floods may be temporarily sequestered among inner-shelf sands. Although the inner-shelf boundary of the flood deposit in Figure 2-9 is predicted to be an abrupt transition, in reality, this transition would be more gradual. As one moves offshore and the boundary layer begins to approach its capacity, deposition may increase across a finite transition zone. Additionally, as the wave energy rises and falls and the supply of fine sediment changes, the region where the boundary layer begins carrying its maximum load will migrate back and forth, smoothing the transition.

The predicted deposition in Figure 2-9 approaches zero at depths between 80 and 90 m. This outer edge of mud deposition is roughly consistent with the distribution of flood layers observed in cores collected during STRATAFORM (Wheatcroft *et al.*, 1997; Borgeld *et al.*, 1999; Drake, 1999; Sommerfield and Nittrouer, 1999; and Wheatcroft and Borgeld, 2000). At depths greater than approximately 90 m, the effect of increasing off-shelf slope overwhelms the effect of decreasing orbital velocity, resulting in flux

divergence and causing the analytic solution to predict erosion (or lack of deposition—see Equation 2-14).

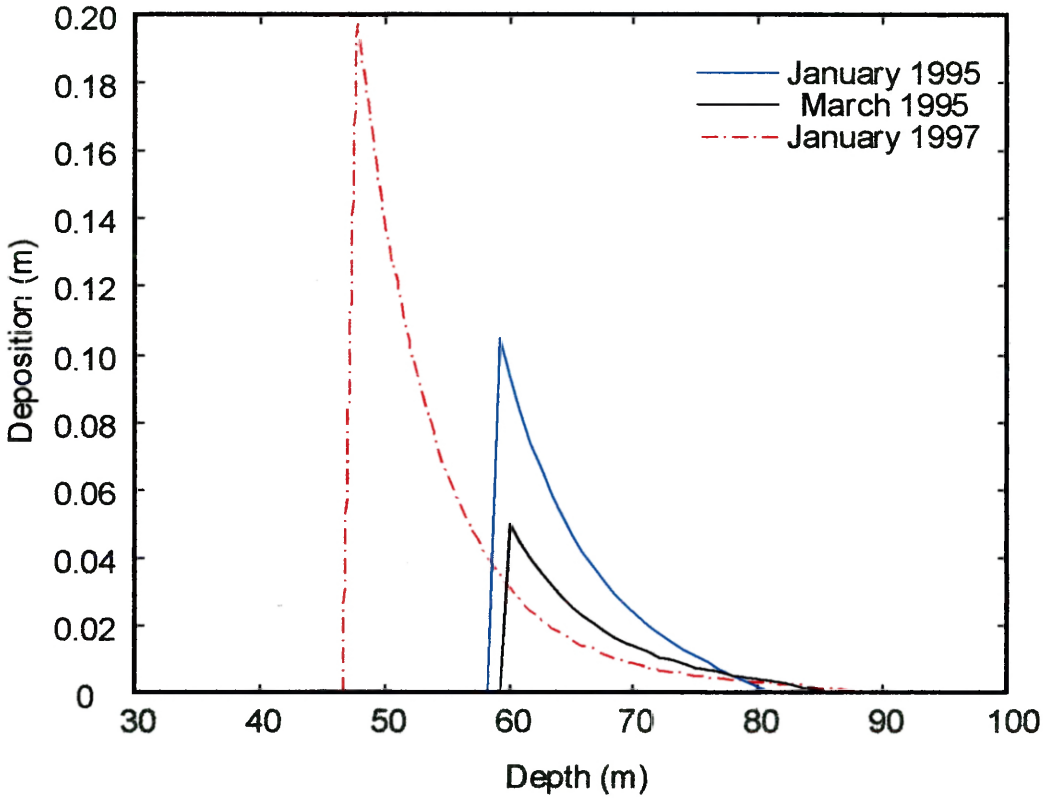

Figure 2-9 Predicted across-shelf distribution of deposition for S-transect for January 1995, March 1995 and January 1997 floods. Deposition was predicted by applying Equation 2-13 for 14 days and assuming a porosity of 0.75. Deposition was assumed to begin at depth where the cumulative delivery of sediment first exceeds the cumulative flux capacity of the boundary layer for the 14-day period.

It is interesting to note that the offshore edge of the predicted deposit is not the same for the three events modeled. The January 1995 flood event had the largest waves and hence the greatest mid-shelf deposition. However, predicted deposition does not extend offshore as far as the January 1997 or March 1995 deposits. While the magnitude of the wave energy ultimately governs the amount of deposition on the mid-shelf, with α

unchanged between years, it is actually the wave period that controls the offshore extent of deposition. The waves during the January 1995 flood produced greater near-bed orbital velocities, but they also had a longer period. Longer period waves result in a smaller gradient in bottom wave orbital velocity. Because gradients in u_{wave} favor deposition, deposition pinches out at a shallower depth under longer period waves. The importance of period can be seen in Equation (2-14): increased period (smaller kh) will decrease the first term in the bracketed expression, allowing the increase in off-shelf slope to dominate.

Our results indicate that the wave energy associated with a flood event plays a key role in governing gravity-driven deposition. Floods with large waves will have greater deposition at mid-shelf depths, while floods with smaller wave energy may favor greater inner-shelf preservation of fine sediment. The importance of wave energy provides a possible explanation for the three-fold increase in accumulation rates for the Eel mid-shelf since 1955 as reported by Sommerfield *et al.* (2000). While Sommerfield and Nittrouer (1999) also report a doubling of the Eel River sediment load over the same period, our theory suggests the magnitude of wave energy is ultimately more important in controlling deposition on the mid-shelf. A study of the Eastern North Pacific wave climate indicates a trend of increasing wave height over the past 25 years (Allan and Komar, 2000). Specifically, Allan and Komar (2000) report an increase in average winter wave height of 3.1 cm/yr since the installation of a NOAA wave buoy off the southern Oregon coast in the mid-1970s and an increase of 3.5 m in maximum annual wave height off Washington over the same period. Ward and Hoskins (1996) further document a long-term trend of increasing wind speeds between 1949 and 1988 for the

North Pacific in general. Because our analytic prediction of gravity-driven deposition is governed by the wave energy associated with these winter storm/flood events, the documented increase in wave energy off the Pacific northwest coast of the U.S. provides a possible explanation for the trend of increased mid-shelf deposition.

While the 1964 flood of the Eel River is the largest flood on record, it has been difficult to identify a distinct flood layer on the mid-shelf associated with this large flood (Sommerfield and Nittrouer, 1999). However, it is consistent with our modeling results that the wave energy during and immediately after the flood would have governed the magnitude of the associated flood layer preserved on the mid-shelf more directly than would the overall river discharge. As illustrated in Figure 2-9, extremely large discharge should specifically favor thick deposition of mud closer to shore, because the wave-boundary layer would become critically-stratified closer to shore. Indeed, mud layers have recently been found interbedded with sand on the inner-shelf off the Eel River (Crockett *et al.*, 2000; Borgeld and O'Shea, 2000) and have been speculatively associated with the 1964 flood (J. Crockett, personal comm.; J. Borgeld, personal comm.).

2.6. ALONG-SHELF BATHYMETRIC CONTROL OF GRAVITY-DRIVEN DEPOSITION

One of the most intriguing aspects of the Eel shelf flood deposit is the spatial consistency in the observed patterns of deposition given the highly variable and dispersive oceanic forcing conditions that exist during flood events. Both short-term rapid-response coring efforts (Wheatcroft and Borgeld, 2000) and long-term accumulation rates determined from ^{210}Pb-geochronology (Sommerfield and Nittrouer, 1999) place the center of flood deposition well north of the river mouth. These observations seem to conflict with those made by Geyer *et al.* (2000) which indicate that

a significant portion of the Eel River sediment load settles out of the plume before reaching the K-transect. While Traykovski *et al.* (2000), demonstrate the effectiveness and importance of gravity-driven transport and deposition on the mid-shelf, there appears to be no clear explanation for the disconnect between proximal input of sediment near the river mouth and its preferential preservation 15 to 25 km to the north.

To examine the influence of bathymetry on the along-shelf variability in gravity-driven deposition, the analytic solution was used to predict deposition along the 60-m isobath from 5 km south of the river mouth to roughly 50 km north of the river mouth, allowing the slope to vary as indicated by N.O.S. bathymetry data. Figure 2-10a shows the predicted deposition along the 60-m depth contour as a function of distance from the river mouth for the January 1997 flood. The model was applied for a period of 15 days beginning with the on-set of elevated river discharge, and it was assumed that sufficient sediment was delivered to critically stratify the boundary layer at all points on along the shelf. Porosity was set to 0.75 as in Figures 2-8 and 2-9. The model results indicate erosion (or at least lack of deposition) close to the river mouth, deposition beginning in the vicinity of the K-line, and deposition thickness increasing towards the north. Both the lack of deposition predicted near the river mouth and along-shelf increase in deposition northward to the S-line are due primarily to along-shelf variation in the across-shelf gradient in shelf slope (Figure 2-10c).

The effect of the slope gradient on deposition is indicated clearly by the bracket terms in Equation (2-14). If shelf slope increases rapidly offshore, the second term containing the slope gradient will overcome the first term representing the offshore decrease in u_{wave}, and erosion (or lack of deposition) will result. Deposition along the 60-m

isobath is not predicted until approximately 7-8 km to north of the river mouth at a point where the gradient in slope of the shelf has become significantly smaller (Figure 2-10c).

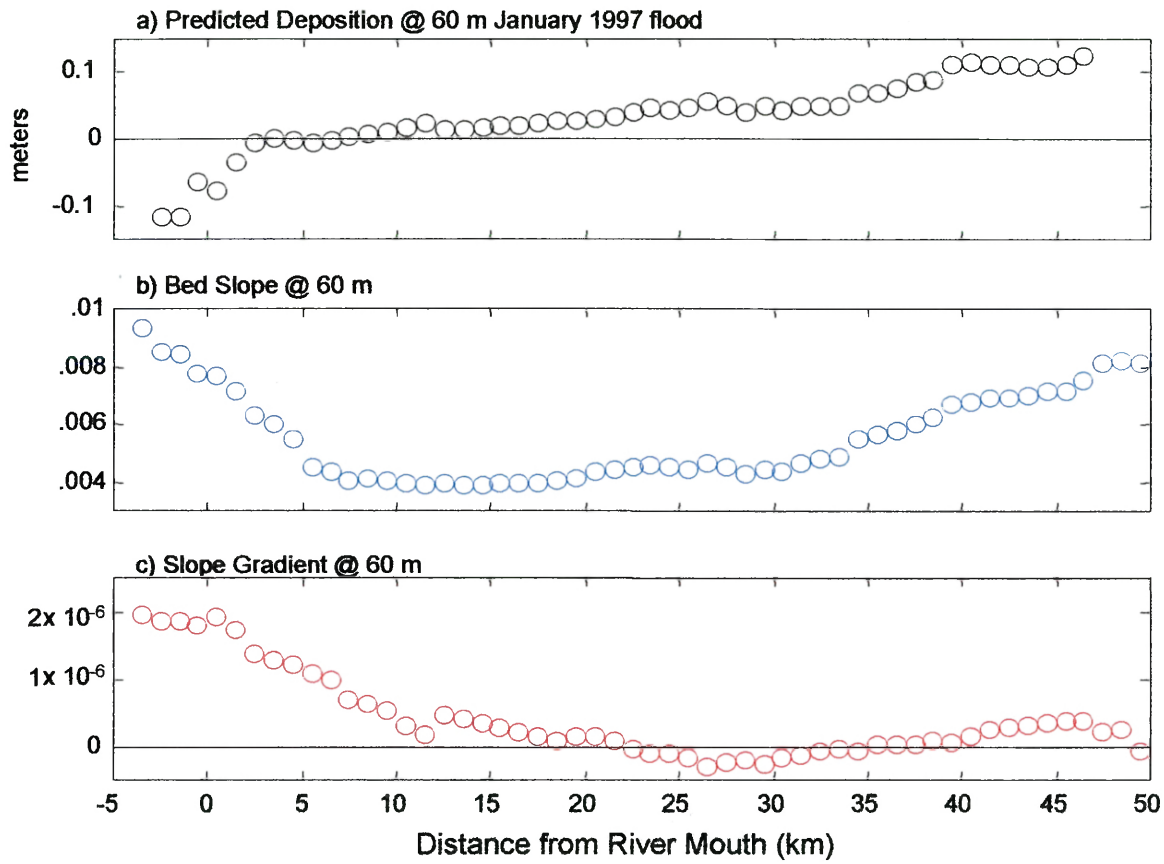

Figure 2-10 (a) Predicted deposition at 60-m depth for 1996-97 New Year's flood. Deposition was predicted by applying Equation 2-13 for a 14-day period beginning with on-set of flooding and assuming a porosity of 0.75. Orbital velocities were calculated from spectral energy density from NDBC buoy 46022 for appropriate depth; (b) across-shelf slope at 60-m isobath inferred from smoothed N.O.S. bathymetry; (c) across-shelf slope gradient at 60-m isobath calculated from smoothed N.O.S. bathymetry.

This agrees favorably with the observed southern extent of the mid-shelf flood deposit (Wheatcroft *et al.*, 1997; Sommerfield and Nittrouer, 1999; Wheatcroft and Borgeld, 2000). Our results suggest that the convex-upward bathymetry associated with the Eel River subaqueous delta prevents gravity-driven deposition on the mid-shelf, thus favoring off-

shelf sediment bypassing. A significant amount of sediment discharged from the Eel River may escape the shelf as gravity-driven flows offshore of the subaqueous delta and potentially enter Eel Canyon. This result is consistent with Sommerfield and Nittrouer (1999), who conclude that a major fraction of flood sediment bypasses deposition on the shelf.

Examination of the bathymetry for the K and S transects illustrates the important constraint that bathymetry has on gravity-driven deposition in the vicinity of the mid-shelf depo-center (Figure 2-11). Because of subtle changes in slope with distance offshore, the predicted deposition for S-60 is nearly twice that predicted for K-60, despite the two sites having similar local values of bed slope. The across-shelf profile in the mid-shelf region on the K-transect shows an increasing slope in the off-shelf direction ($\partial\alpha/\partial x > 0$). Conversely, the mid-shelf slope in the vicinity of S-60 decreases slightly offshore ($\partial\alpha/\partial x < 0$), allowing greater gravity-driven flux convergence. These relatively subtle bathymetric changes appear to strongly influence gravity-driven deposition, favoring greater flux convergence and deposition north of the river mouth in the region near the mid-shelf depo-center documented by Sommerfield and Nittrouer (1999) and Wheatcroft and Borgeld (2000). Despite the highly variable and seemingly dispersive conditions associated with floods of the Eel River, gravity-driven processes provide a mechanism that can explain the consistency in the along-shelf distribution of observed deposition.

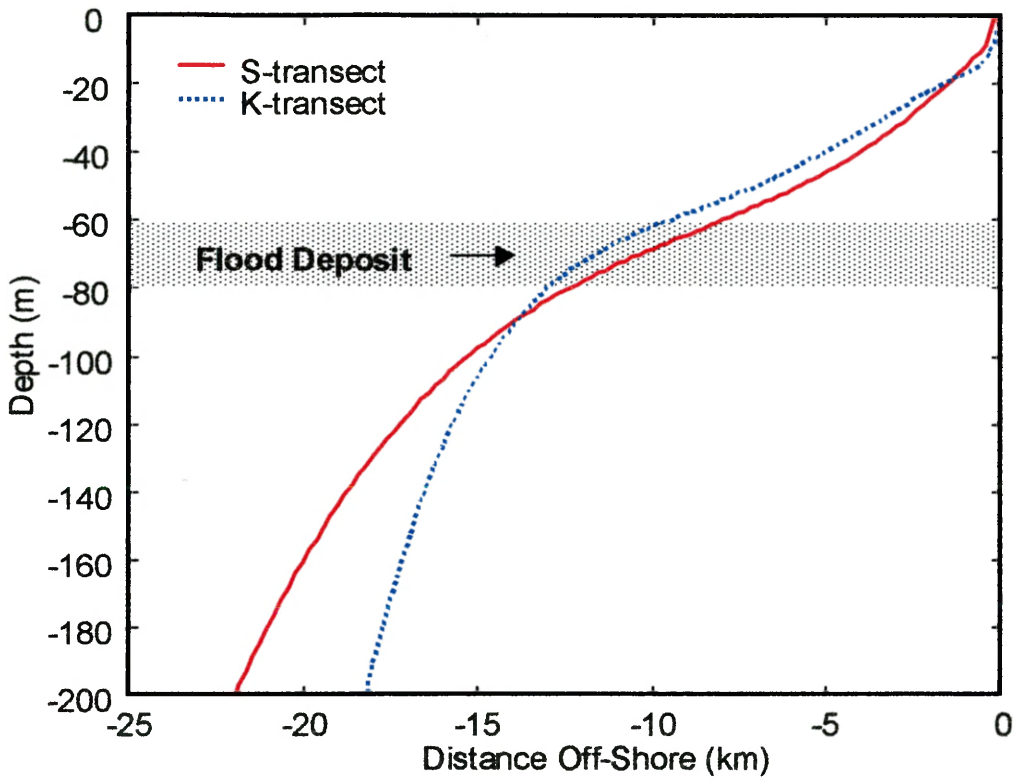

Figure 2-11 Across-shelf depth profile for S and K transects. Profiles were obtained by smoothing N.O.S. bathymetry data.

Far enough from the river mouth, sediment delivery from the river plume eventually will diminish, resulting in an insufficient supply to initiate gravity-driven transport. The evidence of gravity-driven transport from the tripod at S-60 in 1996-97 (Ogston *et al.*, 2000), together with our modeling results suggest that during large flood events sufficient sediment is available to cause critical stratification of the boundary layer as far north as the S-transect. Although Figure 2-10a predicts deposition to continue to increase north of the S-transect, it is likely that sufficient sediment is not available to induce critical stratification much beyond this region. In an attempt to estimate where this will occur, we have calculated the potential cumulative down-slope flux across the 60-m isobath as a function of distance along-shelf from the river mouth for the fourteen-day period beginning with the onset of flooding for the largest flood event of 1995, 1997

and 1998 (Figure 2-12). We then compared the cumulative flux to the cumulative sediment delivery from the river plume for the same periods, also as a function of distance along-shelf. The analytic theory suggests that the along-shelf location where potential cumulative flux exceeds cumulative sediment delivery represents a rough estimate of where critically-stratified gravity-driven deposition is expected to end.

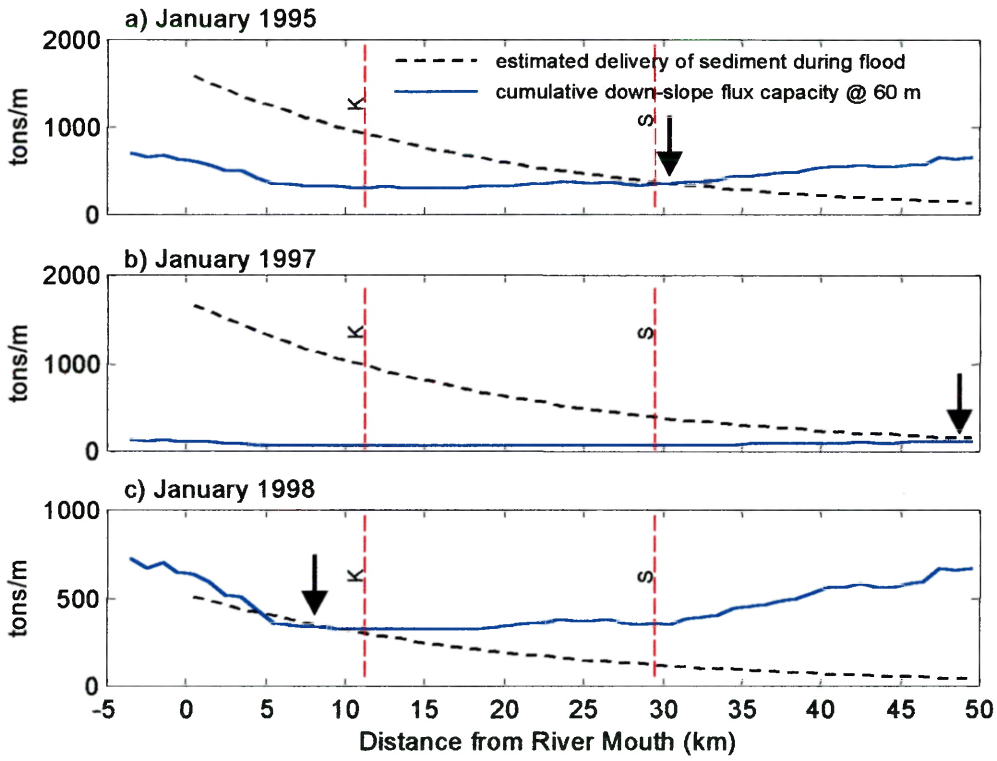

Figure 2-12 Comparison of estimated along-shelf delivery of sediment with cumulative down-slope flux capacity for the periods associated with the largest floods of a) 1995; b) 1997; c) 1998. Arrow indicates region where cumulative down-flux capacity at 60 m exceeds the estimated delivery of sediment.

For the January 1995 and 1997 floods, our estimate for where the cumulative gravity-driven flux exceeds the cumulative supply of sediment is approximately 30 and 50 km north of the river mouth, respectively. While this estimate clearly neglects some important processes associated with the delivery of sediment from the river plume, it

qualitatively agrees with the region where flood deposition begins to diminish (Wheatcroft *et al.*, 1997; Sommerfield and Nittrouer, 1999; Wheatcroft and Borgeld, 2000). This estimate is intended only as a rough indication as to where gravity-driven transport will begin to diminish and not an exact location where gravity-driven deposition will cease. The evidence of gravity-driven transport at S-60 in 1998 demonstrates that gravity-driven transport can occur in the absence of critical stratification. However, it is reasonable to assume that this region represents the area where gravity-driven deposition will begin to decrease. Comparison of cumulative sediment delivery with cumulative sediment flux for the winter of 1997-98 (Figure 2-12c) puts the observations collected at K-60 in an interesting context. From this comparison, it appears that only a relatively small region near the K-transect may have had sufficient sediment delivered during the largest flood events of 1997-98 to critically stratify the boundary layer. So, while this data set from Traykovski *et al.* (2000) provided some of the most dramatic examples of gravity-driven transport and deposition, the K-transect may also have been one of the only locations where these processes could have been observed on the mid-shelf during the 1997-98 flood season.

2.7. LIMITATIONS OF THE APPROACH

It should be noted that several assumptions of the present approach deserve additional examination. For example, we have assumed that the northward directed along-shelf currents that play an essential role in keeping the river plume near the coast (Geyer *et al.*, 2000) do not vary from year-to-year and that the settlement rate into the bottom boundary layer of the inner-shelf is similarly invariant. In reality, settlement onto the inner-shelf from the plume is strongly dependent on plume speed and the settling rate

of suspended particles (Geyer *et al.*, 2000; Hill *et al.*, 2000). Furthermore, if the along-shelf current penetrates to the bottom boundary layer during floods, it may also influence gravity currents. Along-shelf currents on the mid-shelf within a meter of the bed were directed northward during the majority of the January 1997 flood (Ogston *et al.*, 2000). This may explain why gravity flows were not observed within the boundary layer during that flood at a mid-shelf tripod located directly seaward of the Eel River mouth (Friedrichs *et al.*, 2000; Ogston *et al.* 2000). It is therefore likely that along shelf currents, which are typically directed up-coast at the beginning of floods and down-coast at the end of floods, play some role in displacing the center of mass of the flood deposit by laterally advecting down-slope gravity currents. We also have neglected the role of along-shelf currents in contributing to the total velocity that determines the flux capacity of the bottom boundary layer. The contribution of along-shelf velocity to total velocity may help explain why gravity currents were so persistent at S-60 during winter 1996-1997, despite the moderate levels of wave energy.

Periodic tidal currents and waves also can act to disperse sediment on the shelf through processes unrelated to gravity flows. Harris *et al.* (1999) simulated suspension by tides and waves during floods on the Eel River shelf without considering gravity flows and showed that periodic currents alone also tend to move flood sediment toward the mid-shelf. Processes occurring in the absence of floods also affect mid-shelf deposit thickness and permanence. Across-shelf mean currents in the absence of floods have been shown to favor additional deposition on the Eel mid-shelf, both based on observations (Wright *et al.*, 1999; Ogston *et al.*, 2000) and numerical model simulations (Reed *et al.*, 1999; Zhang *et al.*, 1999; Harris and Wiberg, in press). Drake (1999)

demonstrated that flood layers coarsen and even thicken as bioturbation adds material over time. Event layers derived from offshore transport during storms can also contribute significantly to the overall deposition rate on the mid-shelf (Drake *et al.*, 2000).

3. NUMERICAL MODEL

3.1 THE MODEL

Our numerical model is based upon the analytical theory for gravity-driven flows trapped within the wave boundary presented in Section 2. It predicts deposition on the Eel margin by realistically estimating the along-shelf delivery of flood sediment to the boundary layer from river discharge data and calculating the down-slope gravity-driven flux. Deposition is predicted when gravity-driven flux convergence causes the capacity of the wave boundary layer to be exceeded. The model assumes that the sediment carrying capacity of the wave boundary layer is limited by sediment induced stratification as represented by Equation 2-6. Using this relationship, the capacity of the boundary layer to hold suspended sediment can be calculated by knowing only the appropriate near-bed velocity scale.

The model domain consists of a 72 by 64 element grid rotated to conform to the dominant along-shelf direction. Each point in the grid represents an area 1000 m in the along-shelf direction and 400 m in the across-shelf direction. The grid covers roughly the region from 10 km south of the river mouth to approximately 50 km north of the river mouth from the coastline to out beyond the 200-m isobath. The bathymetry for the model was obtained by fitting a fourth-order polynomial to across-shelf transects of N.O.S. bathymetry data followed by along-shelf smoothing using a third-order polynomial and interpolating to obtain the depth and slope for each grid point. Bathymetry must be smoothed somewhat because frictionally-dominated gravity flows will unrealistically pool behind small irregularities in bathymetry.

Wave orbital velocities are calculated for each point in the model grid based on an interpolation of hourly observations of wave energy density made at NDBC buoy 46022. Following the methods of Sherwood *et al.* (1994), the bottom orbital velocity for each model grid-point is calculated from the energy density spectrum knowing the local depth and accounting for the frequency-based decay. Comparison of this method with observations of near-bed velocity collected at various tripods showed good agreement, but with a slight over-prediction. To correct for this over-prediction, a coefficient of 0.79 is applied to the predicted velocity, consistent with the mean ratio between tripod observations and the prediction (see Section 2). On the Eel River continental shelf, it is reasonable to assume that wave orbital velocities will dominate the near-bed velocity scale. However, the gravity-driven velocity also will make a significant contribution at times when high concentrations of suspended sediment are present. Therefore, the near-bed velocity scale that governs the capacity of the boundary layer to hold sediment is calculated using Equation 2-11, to include the influence of u_{grav} on u_{max}. If the relatively minor influence of the along-shelf current is ignored, the carrying capacity of the wave boundary layer for a large region of the shelf can be calculated knowing only the relevant surface wave height and period.

Fine-grained sediment input is calculated by applying the Syvitski and Morehead (1999) rating curve to the discharge data from the USGS gauging stations at Scotia on the main stem of the Eel River and the Bridgeville station on the van Duzen River. The discharge at Bridgeville is doubled to account for downstream inputs and an upper limit of 7 g/L is established for river concentration consistent with the methods of Wheatcroft *et al.* (1997). The predicted sediment load is reduced by 25% to remove the estimated

percentage of sand (Brown and Ritter, 1971; Geyer *et al.,* 2000). The remaining sediment represents our best estimate of fine-grained sediment input to the ocean. Only fine-grained sediment that is input during floods is transported and deposited by the model. Neither coarse-grained sediment nor pre-existing sediment is accounted for in the model.

Using a 30-minute time step, the calculated sediment load is spread along the coast north of the river mouth to create an inshore deposit. The inshore deposit is defined as the region extending from the river mouth to 50 km north of the river mouth and between the 15-m and 35-m isobaths. The along-shelf distribution of river sediment is determined by spreading 80% of the fine-grain sediment discharged along the coast to the north of the river mouth with an e-folding length of 20 km. The remaining 20% of the sediment is spread over a 7-km region south of the river mouth with a linear decrease (Figure 3-1). The existence and along-shelf distribution of the inshore deposit are

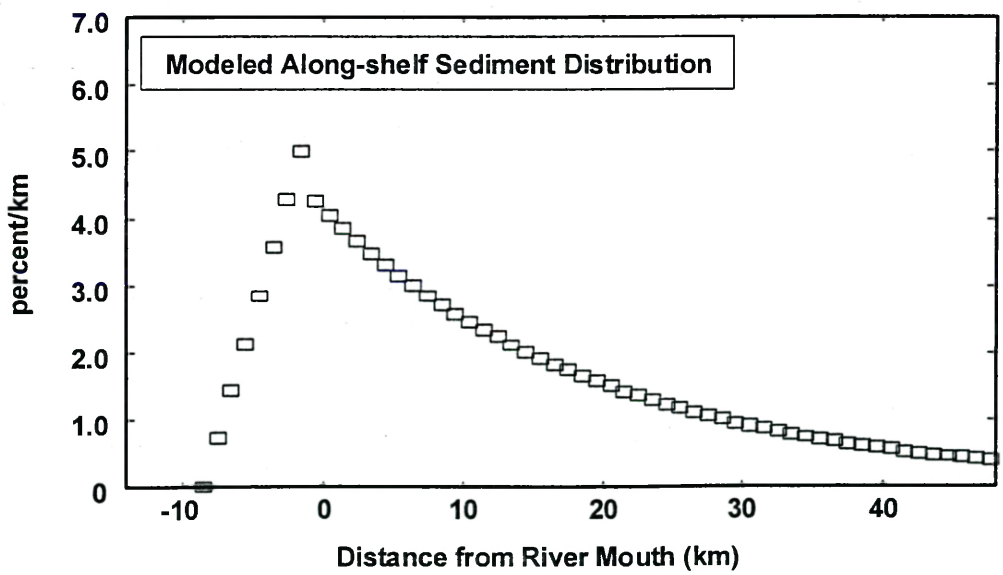

Figure 3-1 Modeled along-shelf sediment distribution with exponentially decaying sediment delivery north of the river mouth (efolding length = 20 km).

consistent with the along-shelf delivery of sediment reported by Geyer *et al.* (2000), as well as observations of temporary and significant inshore deposition of flood derived sediment reported by Traykovski *et al.* (2000). The region inshore of the 15-m isobath was neglected in an attempt to avoid the complicated dynamics associated with the surf-zone.

The in-shore deposit is used as the source of sediment for gravity-driven transport. With each time step, sediment is added to the in-shore deposit and resuspended into the wave boundary layer when the resuspension threshold is exceeded. The down-slope flux of suspended sediment in the boundary layer is calculated knowing the integrated buoyancy and iteratively solving Equations 2-3 and 2-4 for the gravity-driven velocity. When the boundary layer is carrying its maximum capacity, the solution to Equations 2-4 and 2-11 converge. For many grid-points, the bed slope consisted of both an across-shelf and along-shelf component. For each grid-point, the gravity-driven flux was partitioned into an across-shelf and along-shelf component based on the relative strength of the bed slope. Deposition is predicted when flux convergence causes the capacity of the wave boundary layer as given by Equation 2-6 to be exceeded. Both erosion and deposition are governed by the capacity of the wave boundary layer, given as:

$$Deposition / Erosion = \frac{\rho_{sed}}{g\ s}\left[B - \left(u_{\max}^{2} Ri_{cr}\right)\right] \qquad (3\text{-}1)$$

where positive values indicate deposition and negative values indicate erosion. Thus, erosion can only occur when the wave boundary layer is not carrying its maximum load. Erosion of deposited sediment is only predicted to occur when the calculated orbital

velocity exceeded an established threshold value and the sediment at a particular grid point has not consolidated. Sediment that has not been resuspended for a specified period of time is assumed to have consolidated and is no longer available to be transported by the model. For the base model run, a critical resuspension threshold of 0.35 m/s and a consolidation time of 7 days were used. The justification and implications of these parameters will be discussed later. Both deposition and erosion are assumed to occur rapidly enough to bring the amount of suspended sediment in the wave boundary layer to the maximum capacity in one time step. If sufficient unconsolidated sediment is not available to meet the capacity of the wave boundary layer and the critical resuspension criteria is exceeded, only the available sediment in the bed is resuspended.

Consistent with the results of Wright *et al.* (2001) the value of C_d in Equation 2-3 varies inversely Ri. Ri is calculated knowing the integrated buoyancy (B) and u_{max} at all points within the model domain. The drag coefficient is then calculated from the following linear relationship based on the results of Wright *et al.* (2001) for both the wave and current boundary layer:

$$C_d = -0.028*Ri + 0.01 \qquad (3\text{-}2)$$

This relationship establishes a lower limit on C_d of 0.003 for critically-stratified conditions and an upper limit of 0.01 when sediment-induced stratification is absent.

Using this relatively simple approach, we simulated gravity-driven sediment transport and deposition. The model's base run was designed to account only for transport and deposition by gravity-driven processes. While the ambient currents clearly will play some role, they are not accounted for in the base run of the model. However, the ability of the analytic solutions to predict near bed velocity and deposition gives us

confidence that when density-driven processes are active, they represent the dominant mode of sediment transport. The model only accounts for fine-sediment and does not include sand or coarser grained material whose transport may be governed by other mechanisms.

3.2. RESULTS

The model was run for four consecutive flood seasons beginning in 1994-95. These four winter seasons represent a wide range of observed river discharge and wave energy. The time period for the model runs was selected to encompass the significant river discharge events for each year. Figure 3-2 shows the estimated river discharge and bottom wave orbital velocity calculated at the 60-m depth for the four periods of time to which the model was applied. The parameters used in the base model run and predicted fate of sediment input into the model for the four years are shown in Table 3-1. Figure 3-3 shows the across-shelf profiles of predicted deposition predicted along the K and S transects for the four years. The net mid-shelf deposition predicted is shown in Figure 3-4. Because our primary focus is to assess the importance of gravity-driven sediment transport to deposition on the mid-shelf, deposition in Figure 3-4 is only shown for depths greater than 50-m. However, in both 1994-95 and 1996-97, significant deposition was predicted in-shore or the 50-m contour and is not shown in Figure 3-4.

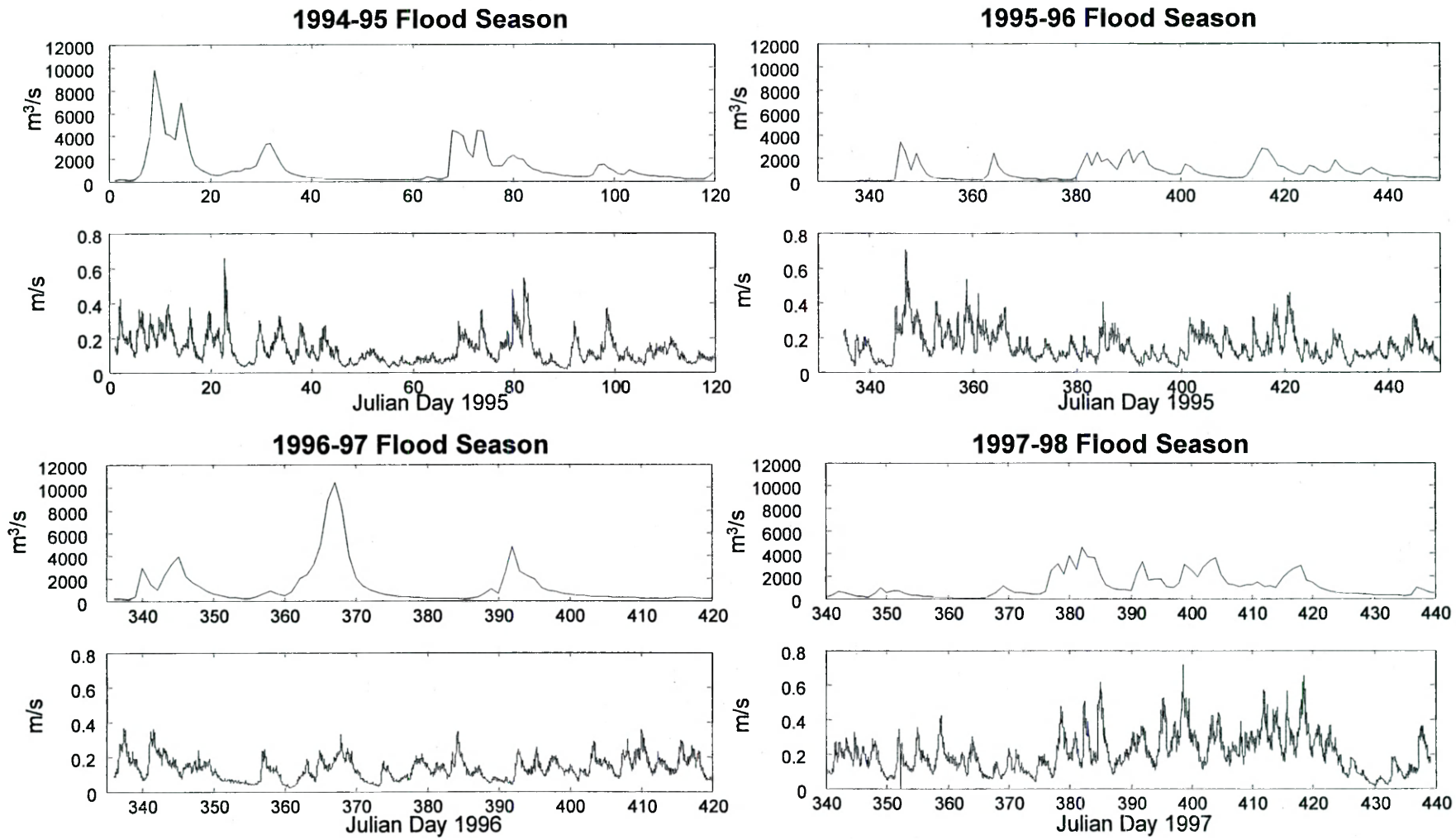

Figure 3-2 River discharge measured at Scotia and Bridgeville gauging stations and bottom wave orbital velocity calculated at 60-m depth from NDBC buoy 46022 spectral wave energy density for the four periods to which the model was applied.

The 50-m contour is generally the location of the sand-mud transition on the Eel shelf, and it is reasonable to assume that the energetic waves off northern California would prevent long-term preservation of fine sediment inshore of this depth unless rapidly burial by coarser sediment occurs. The predicted flood deposit thickness was calculated assuming a porosity of 0.75, consistent with the partially de-watered flood layers observed in cores by Wheatcroft and Borgeld (2000).

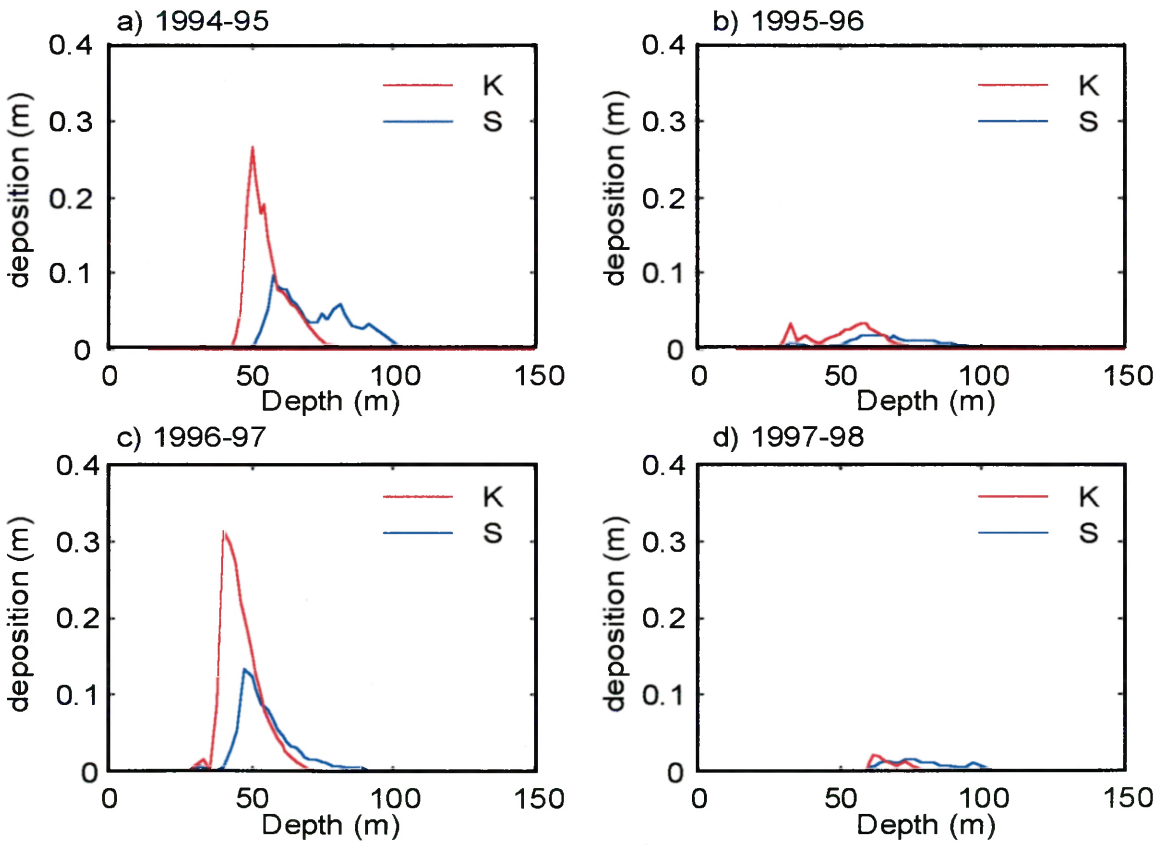

Figure 3-3 Across-shelf profiles of predicted deposition along the K and S transects for the a) 1994-94, b) 1995-96, c) 1996-97, d) 1997-98 flood seasons. Deposition was calculated assuming a porosity of 0.75.

Base Model Run							
Sediment Input = 100%, see Figure 2 C_d = -.28Ri + .01 (Ri_{cr} = 0.25) Resuspension Threshold = 0.35 m/s Consolidation Time = 7 days							
Year	Sediment Input (10^{10} kg)	Inner-Shelf Deposition	Mid-Shelf Deposition	Canyon Flux	Off-Shelf Flux	Max. Deposition (@60m) thickness (cm)	Max. Deposition (@60m) distance from river mouth (km)
1994-95	3.1	12%	33%	11%	44%	11.9	23.5
1995-96	1.0	15%	26%	10%	49%	2.9	15.5
1996-97	2.5	55%	25%	6%	14%	5.7	26.5
1997-98	1.6	<1%	8%	12%	79%	2.0	9.5
Sediment Input Doubled							
1994-95	6.2	30%	30%	9%	30%	18.3	26.5
1995-96	2.0	18%	25%	10%	47%	4.1	22.5
1996-97	5.0	68%	18%	4%	9%	7.9	26.5
1997-98	3.2	<1%	14%	11%	74%	9.7	11.5
50% Sediment Input							
1994-95	1.6	2%	28%	11%	59%	5.3	17.5
1995-96	0.5	13%	28%	10%	49%	1.5	11.5
1996-97	1.3	36%	35%	8%	21%	4.4	23.5
1997-98	0.8	<1%	8%	11%	80%	0.8	9.5
Uniform Along-Shelf Sediment Distribution							
1994-95	3.1	3%	48%	9%	41%	16.4	29.5
1995-96	1.0	14%	35%	8%	44%	3.1	27.5
1996-97	2.5	45%	35%	6%	13%	8.5	36.5
1997-98	1.6	<1%	15%	9%	75%	1.9	27.5
Uniform Along-Shelf Sediment Distribution and No Sediment South of the River Mouth							
1994-95	3.1	5%	56%	0%	39%	18.1	29.5
1995-96	1.0	14%	40%	0%	41%	3.8	27.5
1996-97	2.5	52%	37%	0%	12%	9.1	36.5
1997-98	1.6	<1%	19%	0%	80%	2.3	27.5
No Along-Shelf Current							
1995-96	0.4	28%	33%	8%	30%	2.0	13.5
1996-97	1.8	61%	24%	5%	10%	3.7	26.5
1997-98	1.6	<1%	8%	11%	80%	2.1	9.5

Table 3-1 (cont.)

Year	Sediment Input (10^{10} kg)	Inner-Shelf Deposition	Mid-Shelf Deposition	Canyon Flux	Off-Shelf Flux	Max. Deposition (@60m)	
						thickness (cm)	distance from river mouth (km)
Including Along-Shelf Current							
1995-96	0.4	29%	27%	18%	27%	1.8	17.5
1996-97	1.8	62%	25%	4%	9%	3.8	26.5
1997-98	1.6	<1%	4%	17%	79%	0.5	9.5
Including v_{curr} in u_{max}							
1995-96	0.4	22%	27%	9%	41%	1.7	13.5
1996-97	1.8	51%	24%	7%	18%	4.7	26.5
1997-98	1.6	<1%	3%	11%	85%	0.4	9.5
Resuspension Threshold = 0.15 m/s							
1994-95	3.1	7%	16%	11%	66%	12.0	23.5
1995-96	1.0	3%	12%	11%	73%	1.0	17.5
1996-97	2.5	36%	26%	8%	30%	7.7	26.5
1997-98	1.6	0%	<1%	11%	88%	0	NA
Resuspension Threshold = 0.25 m/s							
1994-95	3.1	8%	23%	11%	58%	12.1	23.5
1995-96	1.0	8%	20%	10%	61%	1.9	10.5
1996-97	2.5	42%	31%	7%	19%	8.1	26.5
1997-98	1.6	<1%	3%	11%	85%	0.3	11.5
Resuspension Threshold = 0.45 m/s							
1994-95	3.1	24%	33%	9%	34%	9.7	13.5
1995-96	1.0	24%	30%	9%	38%	4.0	10.5
1996-97	2.5	67%	18%	5%	11%	4.1	26.5
1997-98	1.6	1%	17%	11%	70%	3.6	11.5
Resuspension Threshold = 0.55 m/s							
1994-95	3.1	38%	31%	8%	24%	10.8	23.5
1995-96	1.0	36%	28%	7%	29%	2.9	11.5
1996-97	2.5	78%	11%	3%	8%	2.4	26.5
1997-98	1.6	4%	26%	11%	59%	5.6	10.5

Table 3-1 (cont.)

Year	Sediment Input (10^{10} kg)	Inner-Shelf Deposition	Mid-Shelf Deposition	Canyon Flux	Off-Shelf Flux	Max. Deposition (@60m)	
						thickness (cm)	distance from river mouth (km)
Consolidation = 1 day							
1994-95	3.1	37%	33%	8%	22%	10.6	23.5
1995-96	1.0	33%	29%	8%	30%	2.8	11.5
1996-97	2.5	59%	24%	5%	12%	5.4	26.5
1997-98	1.6	10%	30%	10%	49%	5.7	11.5
Consolidation = 4 days							
1994-95	3.1	20%	38%	10%	32%	14.0	23.5
1995-96	1.0	19%	27%	9%	46%	2.9	12.5
1996-97	2.5	55%	26%	6%	13%	5.7	26.5
1997-98	1.6	<1%	13%	11%	75%	2.3	9.5
Consolidation = 10 days							
1994-95	3.1	10%	31%	11%	48%	9.7	13.5
1995-96	1.0	8%	27%	10%	54%	3.1	13.5
1996-97	2.5	51%	27%	6%	16%	5.9	26.5
1997-98	1.6	<1%	5%	11%	84%	1.1	9.5
Consolidation = 14 days							
1994-95	3.1	4%	31%	11%	55%	13.5	11.5
1995-96	1.0	2%	26%	11%	60%	3.2	11.5
1996-97	2.5	47%	29%	7%	17%	6.4	23.5
1997-98	1.6	<1%	3%	11%	85%	1.1	9.5
No Along-Shelf Slope (Sediment Distribution = Figure 2)							
1994-95	3.1	12%	33%	11%	45%	8.1	22.5
1995-96	1.0	15%	24%	9%	52%	2.6	11.5
1996-97	2.5	56%	25%	5%	14%	4.9	26.5
1997-98	1.6	<1%	7%	11%	81%	1.8	9.5
No Along-Shelf Slope (Uniform Along-Shelf Sediment Distribution)							
1994-95	3.1	3%	44%	8%	45%	12.1	26.5
1995-96	1.0	15%	33%	7%	45%	2.6	26.5
1996-97	2.5	49%	32%	5%	14%	8.7	46.5
1997-98	1.6	<1%	12%	9%	78%	1.4	9.5

Table 3-1 (cont.)

Year	Sediment Input (10^{10} kg)	Inner-Shelf Deposition	Mid-Shelf Deposition	Canyon Flux	Off-Shelf Flux	Max. Deposition (@60m)	
						thickness (cm)	distance from river mouth (km)
Constant C_d = 0.003 and Constant Ri_{cr} = 0.25							
1994-95	3.1	10%	30%	11%	49%	11.3	23.5
1995-96	1.0	11%	21%	10%	58%	2.5	11.5
1996-97	2.5	50%	27%	7%	16%	6.8	26.5
1997-98	1.6	<1%	5%	11%	84%	1.4	23.5
Constant C_d = 0.006 and Constant Ri_{cr} = 0.25							
1994-95	3.1	34%	42%	8%	17%	11.4	23.5
1995-96	1.0	19%	40%	9%	32%	3.3	10.5
1996-97	2.5	72%	21%	3%	4%	3.5	26.5
1997-98	1.6	<1%	28%	11%	60%	5.7	23.5
Constant C_d = 0.003 and Constant Ri_{cr} = 0.15							
1994-95	3.1	42%	36%	7%	15%	9.6	26.5
1995-96	1.0	21%	37%	9%	34%	3.1	11.5
1996-97	2.5	76%	17%	3%	4%	3.0	26.5
1997-98	1.6	<1%	30%	11%	58%	4.6	23.5

Table 3-1 Table acounting for relative fate of sediment for all model runs conducted and the thickness and along-shelf location of maximum deposition along the 60-m isobath

3.2.1. Mid-Shelf Deposition

As expected and observed, significant mid-shelf deposition was predicted during the 1994-95 and 1996-97 periods when historically large floods of the Eel River occurred. The model predicts that roughly 33% and 25% of the fine sediment discharged from the Eel River was deposited on the mid-shelf (between 50 m and the shelf break) during 1994-95 and 1996-97 respectively (Table 3-1). This agrees favorably with estimates extrapolated from core data that indicate approximately 25% of the fine sediment was preserved in the flood deposit following the January flood of 1995 (Wheatcroft *et al.*, 1997). The thickness of predicted mid-shelf deposition of river-derived fine sediment also is consistent with the thickness observed in mid-shelf cores. Wheatcroft and Borgeld (2000) report maximum mid-shelf flood layer thickness of 8, 5, and 5 cm along the 70-m isobath for the January 1995, March 1995, and January 1997 floods, respectively. This agrees favorably with our model results that indicate maximum deposition along the 60-m isobath of 12 cm for the combined floods of 1995 and 6 cm following the 1997 flood season. It is worth noting that Wheatcroft and Borgeld (2000) report maximum thickness near the 70-m isobath, and our model results somewhat under predict deposition at this depth.

No significant flood layers associated with the 1995-96 and 1997-98 flood seasons were observed in cores collected from the mid-shelf (Wheatcroft and Borgeld, 2000; Drake *et al.*, 2000). Model results predict minor deposition during these years with 26% and 8% of the sediment discharge remaining on the mid-shelf during 1995-96 and 1997-98, respectively. Maximum predicted deposition at 60 m was less than 3 cm for both 1995-96 and 1997-98. However, there was evidence for gravity-driven transport at

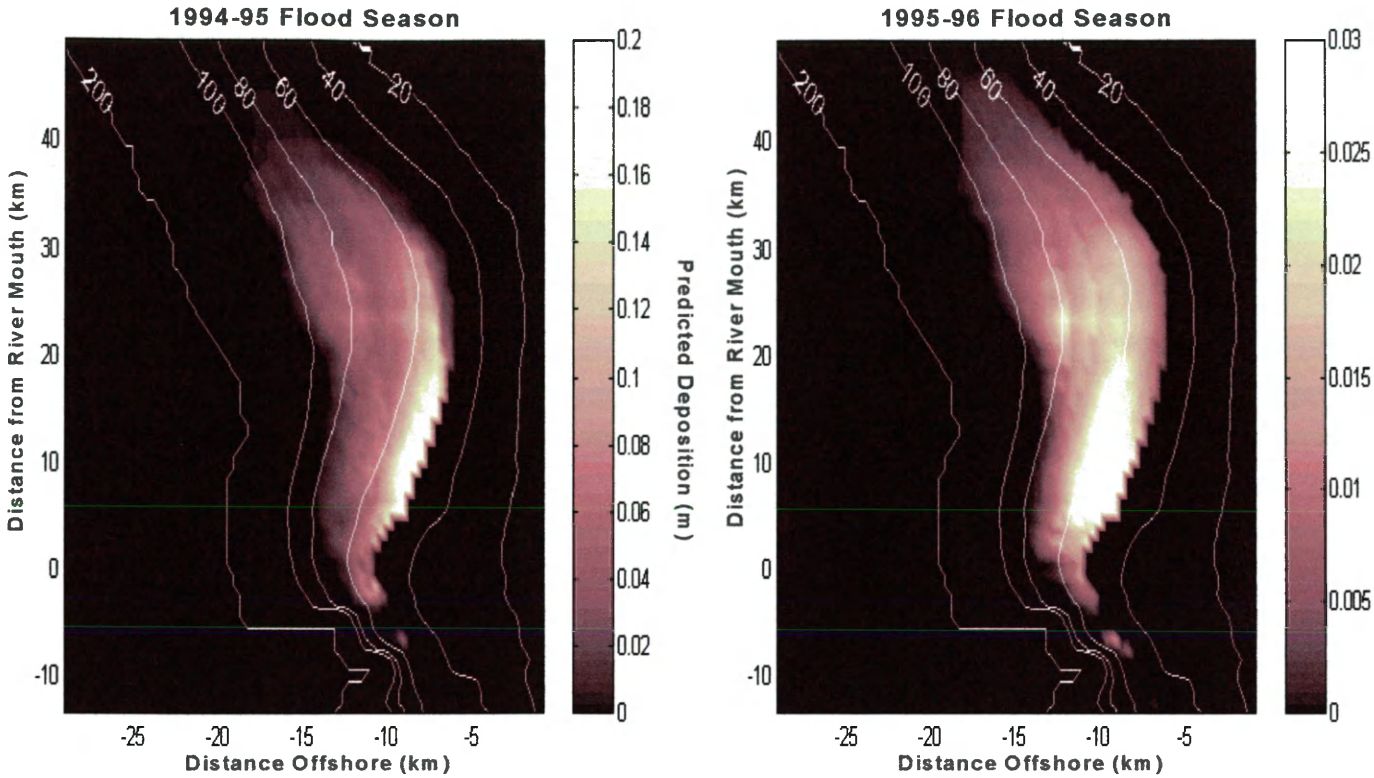

Figure 3-4 Predicted gravity-driven deposition for four flood seasons. Deposition was calculated assuming a porosity of 0.75 and only deposition deeper than 50 m is shown.

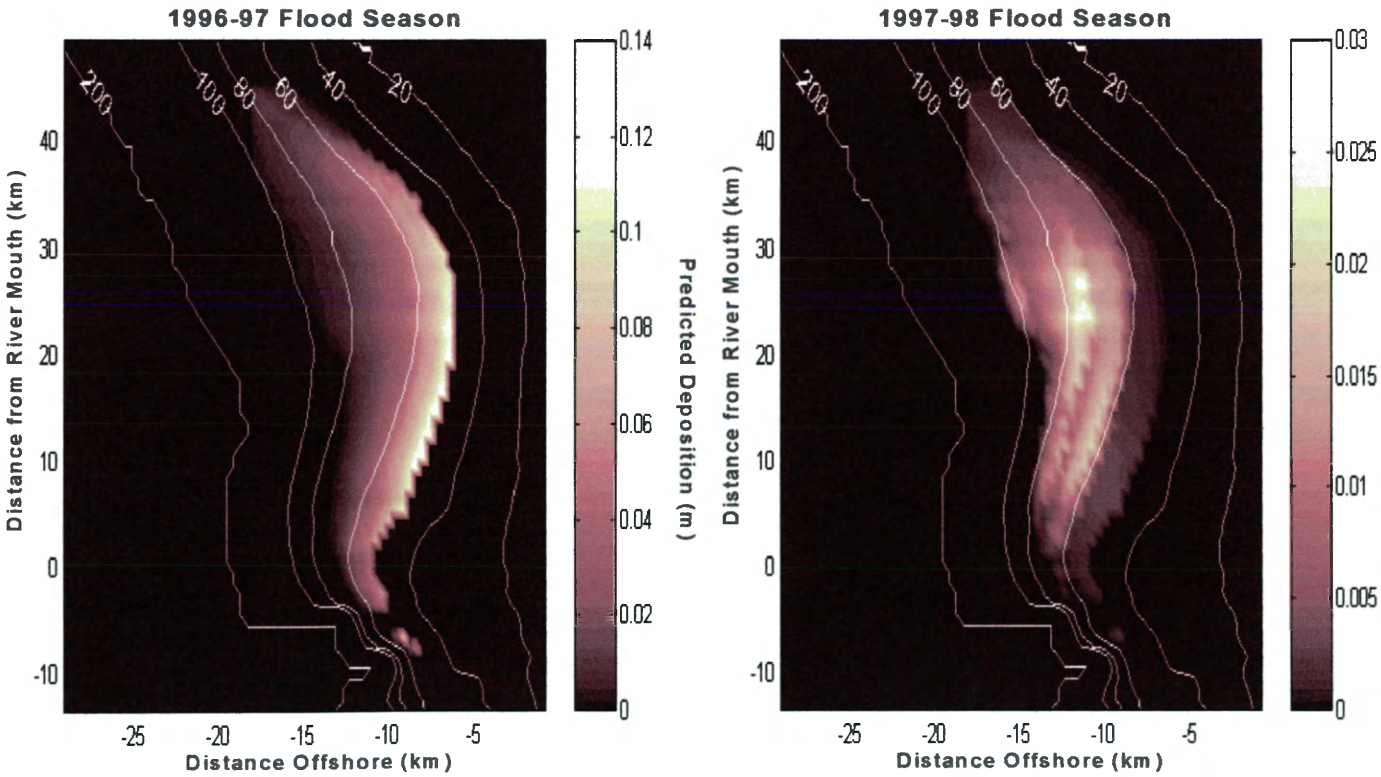

the mid-shelf during these years. Wright *et al.* (2001) provide evidence for weak gravity-driven transport at S-60 during 1995-96. The results of Traykovski *et al.* (2000) demonstrate significant gravity-driven deposition at K-60 during 1997-98. Two gravity-driven depositional events were observed to result in approximately 7 and 11 cm of bed accretion, respectively, with a net deposition of nearly 10 cm for the tripod deployment (Traykovski *et al.,* 2000). The analytic results presented in Section 2.3.1. demonstrated an ability to reproduce the timing and magnitude of this observed deposition at K-60, assuming that sufficient sediment was supplied to critically stratify the wave boundary layer. However their results also suggested that during the 1997-98 flood season, gravity-driven deposition may have only occurred over a very limited region of the shelf near the K-transect. The numerical modeling was unable to reproduce the magnitude of observed deposition at K-60 without significantly increasing the predicted sediment delivery to this area. This suggests that in 1997-98 gravity-driven deposition may have only occurred over a relatively small region of the shelf, where delivery of sediment from the plume was enhanced.

The sediment input during the 1994-95 flood season was greater than the input during any other of the three seasons because of the two large flood events in January and March of 1995. Therefore, it is not unexpected that the greatest mid-shelf deposition was predicted for this year. However, a closer examination of the predicted deposition supports the analytical modeling results presented in Section 2 that suggest that the magnitude of wave energy plays a crucial role in controlling mid-shelf gravity-driven deposition. Figure 3-5 shows the time-series of predicted deposition at S-60 for the four flood seasons. Although the January 1997 flood was larger than the January 1995 flood,

greater deposition was predicted in association with the January 1995 flood. Nearly nine cm of deposition was predicted following the January 1995 flood at S-60. An erosive event removed approximately 3 cm on roughly the 23rd day of the model run (Julian Day 23 of 1995), resulting in a net deposition of 6 cm. The larger January 1997 flood (beginning on model day 30) only resulted in about 4 cm of deposition at S-60. This is roughly equal to the predicted deposition associated with the much smaller March 1995 flood, prior to erosion on day 80 of the model run.

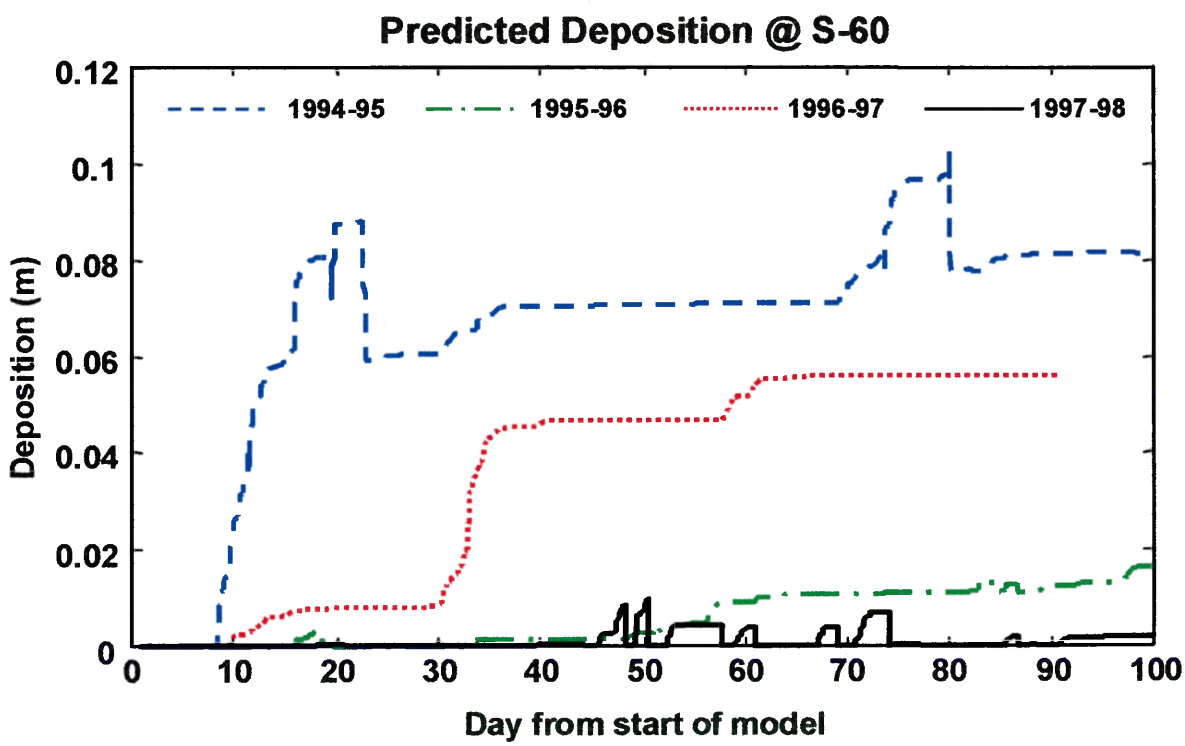

Figure 3-5 Time-series of predicted deposition at S-60 assuming porosity of 0.75 for four flood seasons.

Greater wave energy will lead to greater gravity-driven deposition only if sufficient sediment is delivered to critically stratify the wave boundary layer (see Section 2). In the absence of critical stratification, higher wave energy may erode deposited sediment reducing the overall deposition. A comparison of the predicted deposition for 1995-96 and 1997-98 illustrates the important relationship between sediment supply and wave energy. The observed wave energy during the 1997-98 flood season was the greatest of the four winters to which the model was applied (Figure 3-2). However, the predicted deposition was not largest. Apparently, sufficient sediment was not delivered to critically stratify the boundary layer for significant periods of time. Even though sediment input was roughly 60% greater in 1997-98 than 1995-96, greater deposition is predicted in 1995-96. The energetic waves and modest riverine sediment input not only prevented extended periods of critical stratification of the wave boundary layer, but also resulted in significant erosion of sediment at mid-shelf depths.

The important relationship between sediment supply and wave energy is demonstrated in Figure 3-6. Model predictions at S-60 are compared for the periods when the greatest river discharge was observed in 1996-97 and 1997-98. The large flood in early 1997 supplied more sediment to the wave boundary layer than could be transported by gravity-driven processes. Thus, the wave boundary layer was predicted to remain critically-stratified for a prolonged period. As a result, increases in wave energy did not increase drag and prolonged down-slope transport was predicted with greatest velocities associated with the highest wave orbital velocities. In contrast, in 1997-98, insufficient sediment was supplied to critically stratify the wave boundary layer for prolonged periods of time. In this case, increases in wave energy decreased Ri and

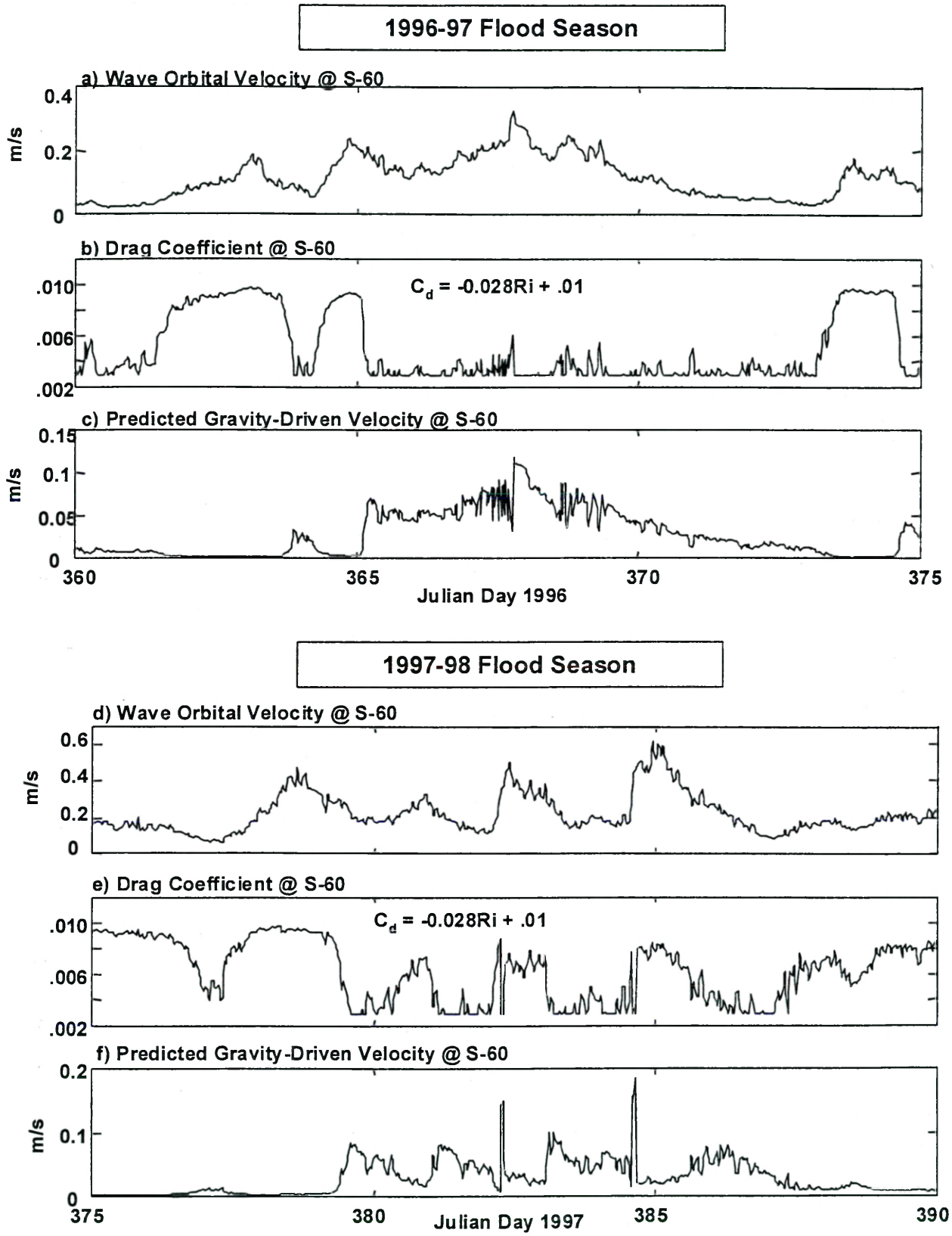

Figure 3-6 Comparison of wave orbital velocity, modeled drag coefficient, and gravity-driven velocity at S-60 during 1996-97 and 1997-98 flood season.

increased the drag, reducing downslope transport (following Equation 2-3). In Figure 3-6 this can be clearly seen by the increase in the predicted drag coefficient associated with increased in bottom wave energy. In 1997-98, only very brief periods of rapid down-slope transport were predicted during elevated wave energy conditions when critical stratification temporarily reduced bottom drag.

Figure 3-7a shows the total predicted mid-shelf deposition for the four modeled flood seasons. Despite significantly larger sediment input near the river mouth (Figure 3-1), maximum mid-shelf deposition was predicted to occur roughly 10 to 30 km north of the river mouth during all four flood seasons. Minimal mid-shelf deposition was predicted in the region offshore from the river mouth despite this region having the highest inshore sediment input. This is consistent with the analytic results in Section 2, which suggest that concave downward bathymetry associated with Eel River subaqueous delta (increasing off-shelf slope) prevents significant mid-shelf gravity-driven deposition in this region. The mid-shelf region north of the subaqueous delta, where greatest deposition was predicted and observed, has constant and even decreasing off-shelf slopes which favors gravity-driven flux convergence. Further north, predicted deposition begins to diminish with no predicted deposition extending further than 45 km north of the river mouth. The predicted northern limit of flood deposition is also consistent with observations (Wheatcroft *et al.*, 1997; Borgeld *et al.*, 1999; Drake, 1999; Sommerfield and Nittrouer, 1999; and Wheatcroft and Borgeld, 2000). The decrease of deposition in this region appears to be the result of diminishing sediment delivery by the Eel River plume. Presumably, sufficient sediment was not delivered to critical stratify the wave boundary layer, preventing gravity-driven sediment transport and deposition.

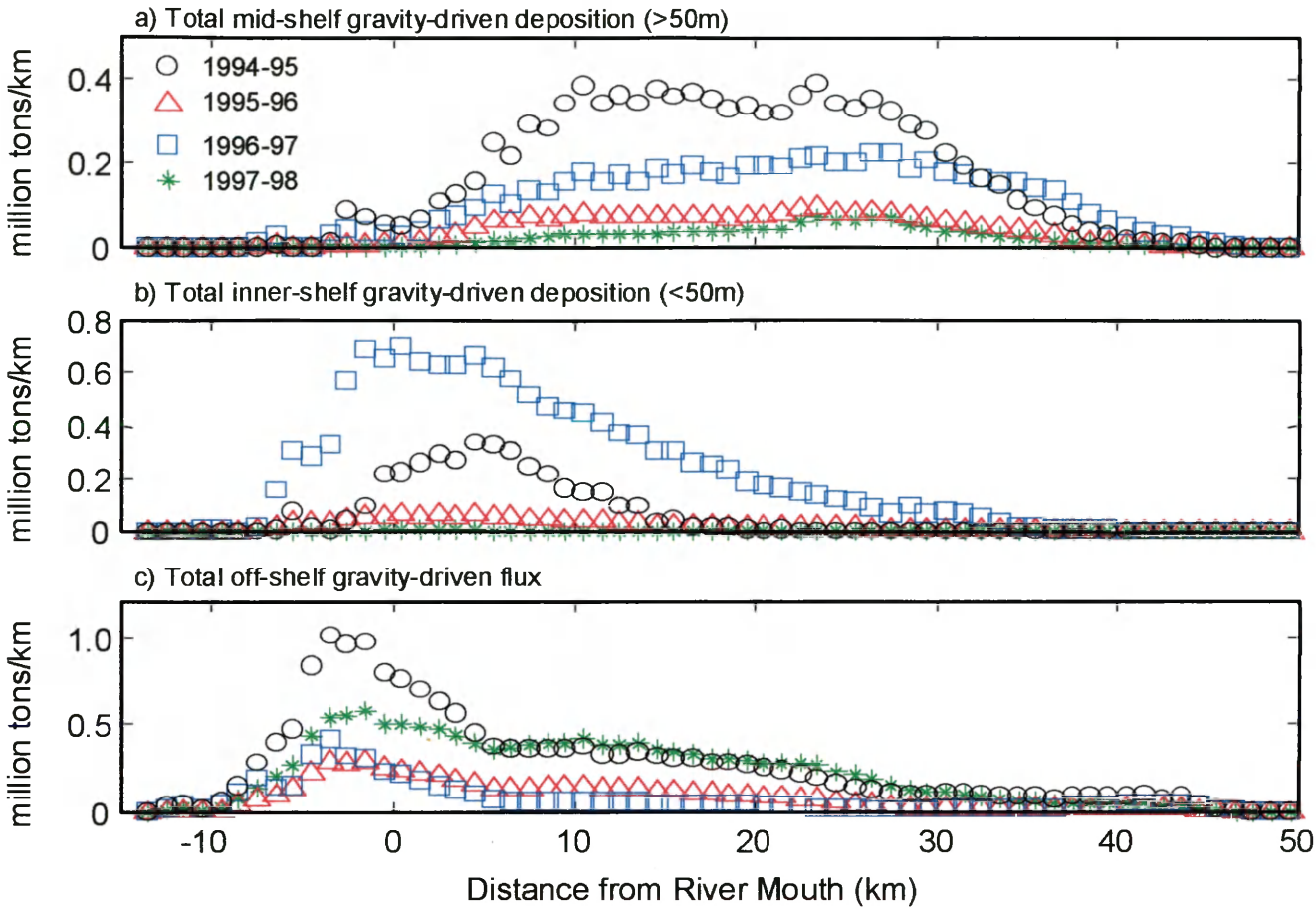

Figure 3-7 Along-shelf distribution of cumulative (a) mid-shelf gravity-driven deposition; (b) inner-shelf deposition; (c) off-shelf gravity-driven flux predicted by the model for the four flood seasons.

3.2.2. Inner-Shelf Deposition

Following the large floods of 1995 and 1997, significant deposition is predicted on the inner-shelf. Predicted inner-shelf deposition was highest in the region near the river mouth where the largest along-shelf input of sediment was supplied (Figure 3-7b). During 1996-97, approximately 55% of the fine sediment discharged by the Eel River was predicted to be deposited in-shore of the 50-m isobath. In contrast, only 12%, 15% and <1% of the fine sediment discharged was predicted to remain in-shore of the 50-m

isobath during the 1994-95, 1995-96 and 1997-98 seasons respectively. The January 1997 flood was the largest flood event that was modeled (with presumably the greatest sediment input), but the associated wave energy was relatively low. As a result significantly greater sediment was supplied by the river plume than could be transported offshore by gravity-driven processes. The more energetic waves associated with the large floods of 1995 allowed greater transport of sediment offshore and resulted in less predicted inner-shelf deposition. Because of the energetic waves and modest input of sediment during 1997-98, no inner-shelf deposition was predicted.

Observations have not documented widespread deposition of fine sediment on the inner-shelf after floods. However, cores collected from the inner-shelf reveal that fine-grained sediment layers are preserved within the inner-shelf sands (Borgeld and O'Shea, 2000; Crockett *et al.,* 2000). While energetic waves and currents may subsequently disperse much of the predicted inner-shelf deposition, the potential for preservation exists. Additionally, there is evidence for rapid deposition of fine sediment on the inner-shelf following floods of the Eel River. Traykovski *et al.* (2000) report that a bottom mounted acoustic doppler current profiler (ADCP) deployed at K-20 was buried under an estimated 1 m of mud following a flood early in 1998. Although such extreme deposition was not predicted by our numerical model, these observations suggest nonetheless that the rapid delivery of sediment from the Eel River plume may have been capable of overwhelming the capacity of the boundary layer resulting in the observed deposition at K-20.

While our results suggest that gravity-driven processes alone are not capable of removing all of the sediment delivered to the inner shelf following large floods, the

processes governing the delivery and potential preservation of fine sediment on the inner-shelf represents a gap in the understanding of this system. The surf zone, which during large storms may comprise a significant percentage of the inner shelf region, may play a key role in sediment delivery and preservation. Our model does not account for the complex interactions that occur within the surf zone. Preservation of fine material on an energetic inner-shelf such as the Eel River is probably unlikely unless it is rapidly covered by coarser grained material. Again, because our model does not account for sand, such processes cannot be addressed. Lastly, our parameterization of consolidation is basic and a more complex representation of time and depth-dependent consolidation is necessary to successful model inner-shelf deposition.

3.2.3. Off-Shelf and Canyon Delivery

The model predicts that significant sediment may be capable of leaving the shelf as gravity-driven flows that enter Eel Canyon or traverse the shelf to the shelf break. Wright *et al* (2001) found that the slope of the continental shelf was generally too gentle to allow significant gravity-driven transport in the absence of an external source of turbulence. On an energetic margin such as that off northern California, waves play a key role in allowing gravity-driven flows to propagate across-shelf (Traykovski *et al.*, 2000). It follows that greater wave energy allows greater gravity-driven flux, increasing the likelihood that sediment may leave the shelf as a gravity flow. The 1996-97 season had the lowest amount of sediment predicted to leave the shelf despite having the second highest total sediment input (Table 3-1). This is a direct consequence of the relatively low wave energy that occurred during this year. As a result only 6% of the sediment discharge was predicted to enter Eel canyon with 14% escaping past the shelf break. In

contrast, the energetic waves in 1997-98 allowed significantly more sediment to escape the shelf. Nearly 90% of the discharge was predicted to leave the shelf during 1997-98. Over half of the sediment input was predicted to leave the shelf in 1994-95 as the result of relatively high wave energy.

Recent investigations reveal that flood sediment is entering Eel Canyon (Mullenbach and Nittrouer, 2000). Cores collected from the head of the canyon in January 1998 before any significant river discharge for the season reveal little ^{7}Be evidence for river derived sediment. However, later in March following a period of elevated river discharge and energetic waves, cores revealed a 30-fold increase of ^{7}Be inventories, with elevated ^{7}Be extending down nearly 10 cm (Mullenbach and Nittrouer, 2000). Model results indicate that there was significant flux of river-derived sediment by gravity flows that can account for the observations collected at the head of Eel Canyon. Figure 3-8 shows the time series of cumulative flux into Eel Canyon for the four modeled years. Prior to day 40 of the model run (which corresponds to JD98 375), no sediment flux into the canyon was predicted. However, nearly 0.2×10^{6} t of sediment was predicted to enter the canyon due to gravity-driven transport during the flood events of January and February of 1998.

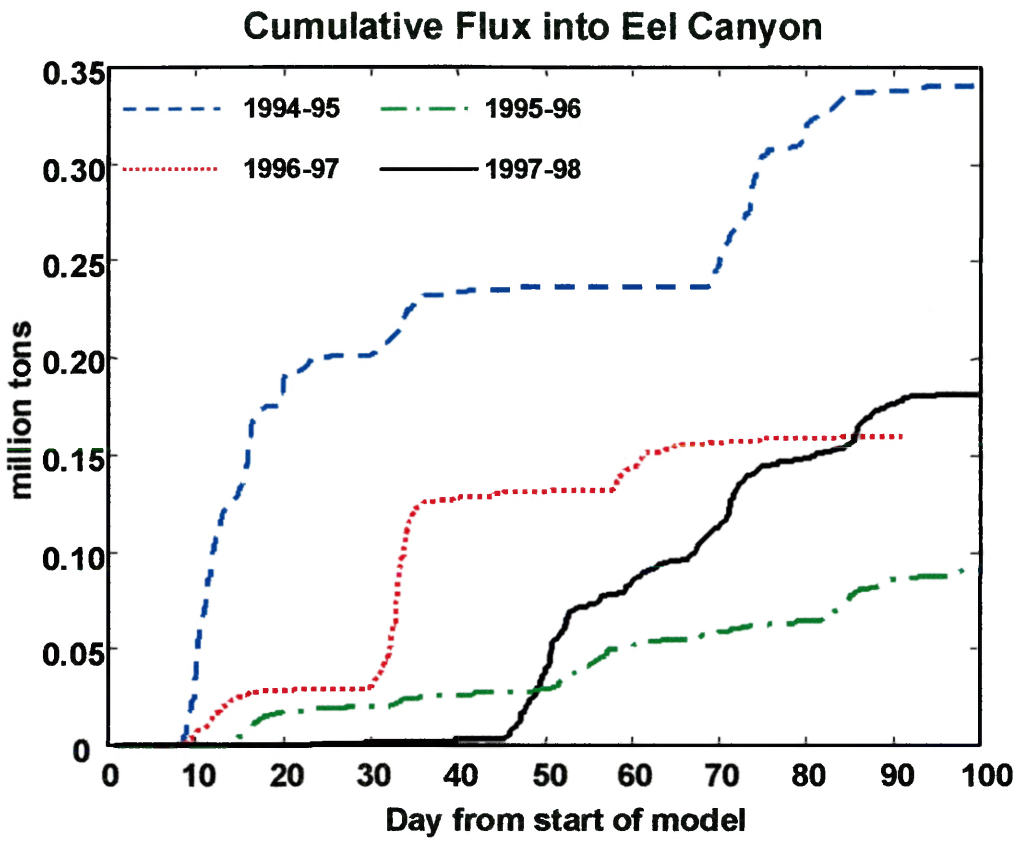

Figure 3-8 Time series of cumulative gravity-driven sediment flux into Eel Canyon for four flood seasons.

The results from Section 2 provide evidence that the bathymetry associated with the Eel River subaqueous delta inhibits deposition and favors gravity-driven sediment bypassing to the slope near the river mouth. While deposition predicted off the river mouth is significantly less than that predicted further to the north, the flux of sediment off-shelf is highest near the mouth (Figure 3-7c). While the in-shore sediment input is greatest in this region, the lack of deposition supports the concept of bathymetry controlled gravity-driven bypassing. Thus, the model results suggest that a significant fraction of the fine-grained sediment discharged from the Eel River may leave the shelf as gravity-driven flows.

3.3. MODEL SENSITIVITY

The ability of the model to reproduce the large-scale patterns of deposition that are consistent with observations collected from the margin provides some confidence that our approach is sensible. However, in order to implement the model, several important processes were either simplified or neglected to maintain simplicity. Numerous model runs were conducted to examine how these simplifications and the other processes included in the model affected the results.

3.3.1. Delivery of River Sediment

Clearly the inshore delivery of fine sediment from the Eel River will play a key role in where and when gravity-driven processes will occur. However, the analytical modeling results in Section 2 suggest that as long as sufficient sediment is delivered to critically stratify the wave boundary layer, the large-scale pattern of deposition will be controlled mainly by the bathymetry and wave energy. The results of the base model runs presented above provide additional support for this idea. Greater sediment deposition is predicted well north of the river mouth despite greatest sediment input close to the river mouth. To examine the impact of sediment delivery on model results, the model was run changing 1) the amount and 2) the along-shelf distribution of sediment input (Table 3-1).

3.3.1.1. Amount of Sediment Delivery

The amount of sediment delivered to the inner-shelf by the river plume is poorly constrained in our model. Uncertainty associated with the rating curve, as well as the possibility that sediment leaves the model domain without ever settling from the plume, could potentially influence the accuracy of the model results. Accordingly, model runs

were conducted in which the amount of sediment supplied to the inner-shelf by the river was varied. The impact of changing the amount of sediment delivered into the model varied significantly from year to year (Table 3-1). This is mainly the result of the relationship between sediment supply and wave energy. This can be illustrated most effectively by examining the changes in predicted deposition in 1996-97 versus 1997-98, when the supply of sediment input into the model was doubled.

In the 1996-97 base model run, the large input of sediment and low wave energy allowed the mid-shelf wave boundary layer to remain critically-stratified for significant periods of time (as seen by the constant value for C_d at S-60 in Figure 3-6b). Because for much of the time, the mid-shelf boundary layer was already carrying its maximum capacity, an increase in available sediment did not result in a proportional increase in mid-shelf deposition. Total mid-shelf deposition was predicted to increase by only 44% (Table 3-1), with the maximum predicted thickness for the 60-m depth increasing from roughly 6 to 8 cm. The majority of the additional sediment remained on the inner-shelf, where the predicted deposition increased by 150%. The low-energy wave boundary layer had low capacity and could not transport significantly more sediment to the mid-shelf.

In contrast, doubling the sediment input for 1997-98 had a much larger impact on the predicted mid-shelf deposition. Mid-shelf deposition increased by 250% and the maximum predicted deposition along the 60-m isobath increased by nearly a factor of five (Table 3-1). Interestingly, the increased sediment input resulted in a much more reasonable agreement between the predicted and observed deposition at K-60 (Figure 3-9). Assuming the increased sediment delivery, the model predicted the wave boundary layer at K-60 to remain critically-stratified during the large wave event beginning on JD-

1998 385 (marked with arrows in Figure 3-10d) when the most significant deposition was observed by Traykovski *et al.* (2000). As demonstrated in Figure 3-10, without increasing the sediment input, insufficient sediment was available to maintain critical stratification during this wave event and the model predicted erosion. While model results at K-60 agree more favorably with tripod observations when the sediment input is doubled, significantly greater deposition was also predicted over much of the mid-shelf for this case. Given the lack of evidence of flood layers observed in cores associated with this flood season, it is more likely that localized processes related to the delivery of sediment from the river plume may have resulted in higher sediment delivery to the K-transect.

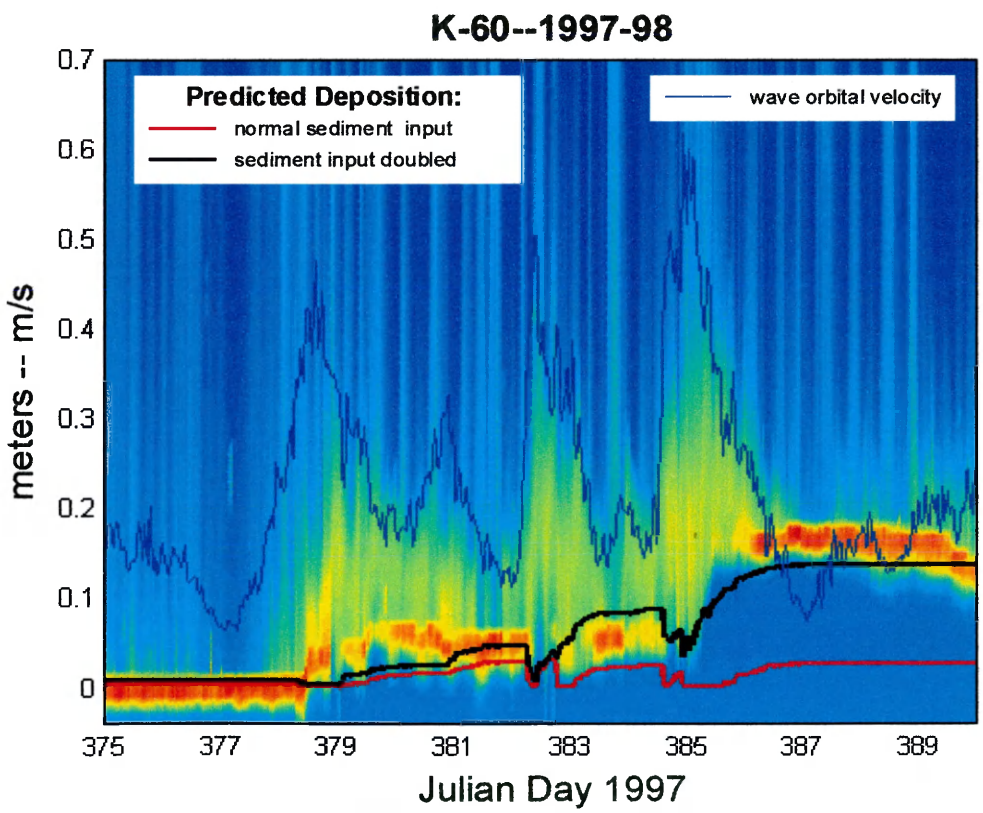

Figure 3-9 ABS image of bed elevation change and predicted deposition at K-60 in 1997-98 assuming normal sediment delivery (red line) and a 2-fold increase in sediment delivery (black line). Wave orbital velocities calculated from NDBC buoy 46022 are shown in blue.

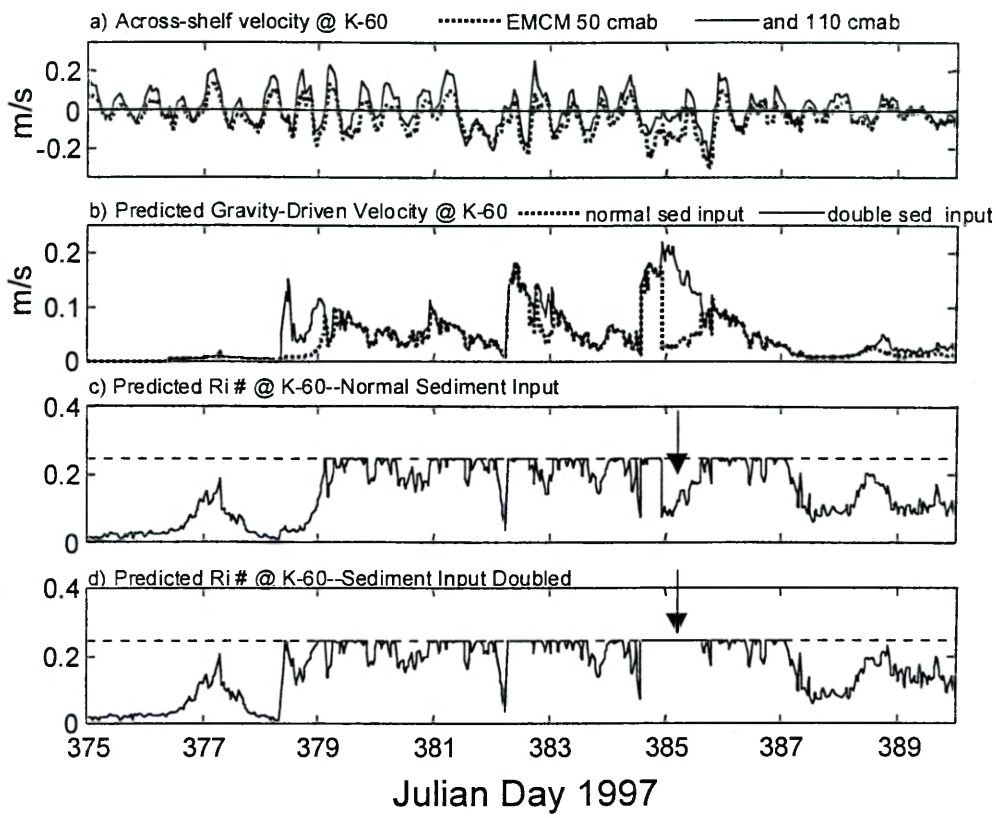

Figure 3-10 Observations and model predictions for K-60 during 1997-98. (a) Observed across-shelf velocity from EMCM 50 cmab (dashed line) and 110 cmab (solid line); (b) Predicted gravity-driven velocity at K-60 for normal sediment input (dashed line) and doubled sediment input (solid line). (c) Predicted Richardson number at K-60 for normal sediment input and (d) doubled sediment input.

The results presented above assume that all of the sediment from the Eel River was available for transport by gravity-driven processes. However, observations and modeling of sediment delivery from the Eel plume indicate that a fraction of unflocculated sediment may remain in the plume and be transported beyond our model domain (Harris *et al.,* 1999; Hill *et al.,* 2000). To account for the possibility that a significant amount of sediment is widely dispersed and not available for transport by gravity-driven flows, the model was run reducing the sediment input by 50%. The effect

of reduced sediment input had a similar effect on the predicted deposition for each year. The 50% reduction in sediment input resulted in a 57%, 46%, 32%, and 50% reduction in mid-shelf deposition for 1994-95, 1995-96, 1996-97, and 1997-98, respectively (Table 3-1). With the exception of 1996-97, the nearly proportional response of mid-shelf deposition to decreased sediment supply indicates that with 50% less sediment, the inner-shelf region was not critically-stratified for enough time to limit transport to the mid-shelf. The smaller reduction in predicted mid-shelf deposition during 1996-97 reflects the relatively low wave energy and high sediment input that resulted in long periods of critical stratification dominating the mid-shelf during this year, even given a large reduction in sediment supply.

3.3.1.2. Along-Shelf Distribution of Sediment

Model results obtained by using a uniform along-shelf distribution of sediment north of the river mouth highlight several important features of the Eel River depositional system. For all four years, mid-shelf gravity-driven mid-shelf deposition is still favored well north of the river mouth. However, the region of maximum deposition shifted to the north in all four years (Table 3-1). Additionally, the uniform sediment distribution slightly decreased predicted mid-shelf deposition for the 20-km region directly north of the river mouth (data not shown). The maximum predicted thickness also increased slightly when a uniform along-shelf distribution of sediment was used (Table 3-1).

The results presented in Section 2 suggest that given unlimited along-shelf sediment delivery, gravity-driven mid-shelf deposition should continue to increase northward from the river mouth. Decreasing mid-shelf deposition should begin where the northerly delivery of river sediment can no longer exceed the capacity of the

boundary for sufficient amounts of time to allow significant critically-stratified gravity-driven transport to occur. Using a uniform along-shelf distribution of sediment did effectively move the predicted region of maximum mid-shelf deposition to the north. However, greatest deposition was not observed at the northern limit of the model domain as expected based on the analytical results presented in Section 2. This decrease in predicted deposition towards the northern limit of the model domain while using a uniform distribution of sediment input suggests that factors not related to sediment delivery also contribute to decreased deposition along the northern region of the model. Potential explanations for this will be addressed later in the paper in the section discussing the influence of the along-shelf slope.

Changes to the along-shelf distribution of sediment also provide insight into the gravity-driven flux of sediment into Eel Canyon and past the shelf break. The model was run using a uniform along-shelf distribution of sediment where no sediment was supplied to the inshore region south of the river mouth. The model did not predict any sediment to enter the canyon under these conditions (Table 3-1). However, when sediment was distributed to the inshore region south of the river mouth, nearly all of it was predicted to enter the canyon. The increased wave energy associated with the flat, shallow region of the delta topset along with the increasing slopes offshore appeared to prohibit significant fine sediment accumulation. In all years except for 1996-97, the majority of the sediment input south of the river mouth was predicted to enter the canyon as a gravity flow. Model runs using the uniform along-shelf distribution of sediment also provide further support for enhanced sediment bypassing associated with the subaqueous delta. Similar to the

result shown in Figure 3-7c, higher gravity-driven flux off-shelf is predicted near the river mouth even when along-shelf sediment input remains constant (data not shown).

3.3.2. Along-shelf Currents

In the absence of gravity-driven processes, ambient currents will exert a dominant influence on the transport of suspended sediment. On the Eel shelf, observational and modeling studies indicate that across-shelf currents at the mid-shelf favor sediment accumulation due to flux convergence (Harris *et al.,* 1999; Wright *et al.,* 1999; Ogston *et al.,* 2000). While it is unlikely that this process could account for the rapid deposition observed at many locations on the mid-shelf, current interaction with near-bed gravity-driven flows could play an influential role on the timing and location of gravity-driven transport and deposition. In order to assess the importance of the relatively strong along-shelf currents observed on the Eel shelf, the model was run for periods when current data collected from tripods was available. These periods included the large flood in 1996-97 and several modest flood events in 1995-96 and 1997-98. No tripod data were collected during the 1994-95 flood season.

From the available data, the along-shelf current was linearly extrapolated down to the top of the wave boundary layer. The model was run adding the extrapolated along-shelf current to along-shelf component of the gravity-driven velocity assuming a uniform distribution of current across the shelf. Examination of ADCP data collected at G-60 and S-60 (roughly 25 km apart) in 1996-97 indicates that the 33-hour lowpass filtered along-shelf currents were generally correlated during the period of observation ($r = 0.79$). However, the across-shelf component of the currents was not correlated for the two locations ($r = -0.19$). Thus is seems reasonable to add a spatially uniform along-shelf

current, but not a spatially uniform across-shelf current. A linear extrapolation was used because of a logarithmic fit did a poor job for much of the data. The thickness of the wave boundary layer was estimated by $\delta_w = 0.08(u_{wave}/\omega)$ based on the observations of Traykovski *et al.* (2000). Adding the extrapolated along-shelf current to the along-shelf component of gravity-driven velocity probably represents the maximum influence that ambient currents could have had on gravity-driven flows because when high concentration near-bed layers are present, strong stratification at the top of the layer likely reduced the vertical exchange of momentum.

For the forty-two day period during 1995-96 when tripod data was available from S-60 (Wright *et al.,* 1999), along-shelf currents extrapolated to the top of the wave boundary layer were relatively weak with a mean magnitude of roughly 0.025 m/s. Tripod data was available for a considerably longer period of time during the 1997-98 flood season. Along-shelf currents at K-60 (Traykovski *et al.*, 2000) were relatively strong with a mean magnitude of 0.053 m/s extrapolated to the top of the wave boundary layer. The main impact of including the along-shelf currents in both 1995-96 and 1997-98 was the greater prediction of sediment flux into Eel canyon. Approximately 8% and 11% of the sediment input in 1995-96 and 1997-98 respectively, was predicted to enter Eel canyon without including the along-shelf current. However, the inclusion of the along-shelf current increased these percentages to 18% and 17%. The increase in flux into the canyon came mainly at the expense of mid-shelf deposition. Deposition at depths greater than 50 m was roughly 25% and 50% less when the along-shelf current was included. However, the along-shelf distribution of deposition remained relatively

unchanged, with the region of maximum deposition along the 60-m isobath shifted slightly to the north in 1995-96.

The influence of the along-shelf current appeared to have less of an impact on the predicted final fate of sediment in 1996-97. Predicted deposition on the inner- and mid-shelf, and fluxes off-shelf and into the canyon all changed by only 1% when along-shelf currents were included in the model. The along-shelf distribution and magnitude of mid-shelf deposition remained relatively unchanged despite the fact the strongest along-shelf currents were observed during 1996-97. Northward along-shelf currents in excess of 0.15 m/s at the top of the wave boundary layer occurred during the onset of gravity-driven transport and the mean current magnitude for the entire period was approximately 0.07 m/s.

These relatively strong along-shelf currents may have impacted the timing of gravity-driven transport. Field data collected during the 1996-97 flood season (Ogston *et al.,* 2000) indicates that high concentration layers arrive at the S-60 site ~30 km north of the river mouth prior to arriving at the G-60 site only ~4 km north of the river mouth. Ogston *et al.* (2000) proposed that the earlier arrival of sediment at the S-60 site could be explained by the greater off-shelf distance to the G-60 tripod if transport by gravity-driven flows were emanating from an inshore line source. This pattern was also reproduced by modeled gravity flows under specific forcing conditions. The model was run using a uniform along-shelf sediment distribution and no sediment delivery south of the river mouth. Without including along-shelf currents, the model predicted the arrival of sediment due to gravity-driven processes well before the inferred arrival from the G-60 and S-60 tripod data (Figure 3-11a). However, gravity-driven transport was predicted to

begin at S-60 prior to beginning at G-60. If the observed along-shelf current was included, the predicted arrival of sediment due to gravity-driven transport at G-60 agrees favorably with the on-set of high suspended sediment concentrations observed in the tripod data (Figure 3-11b).

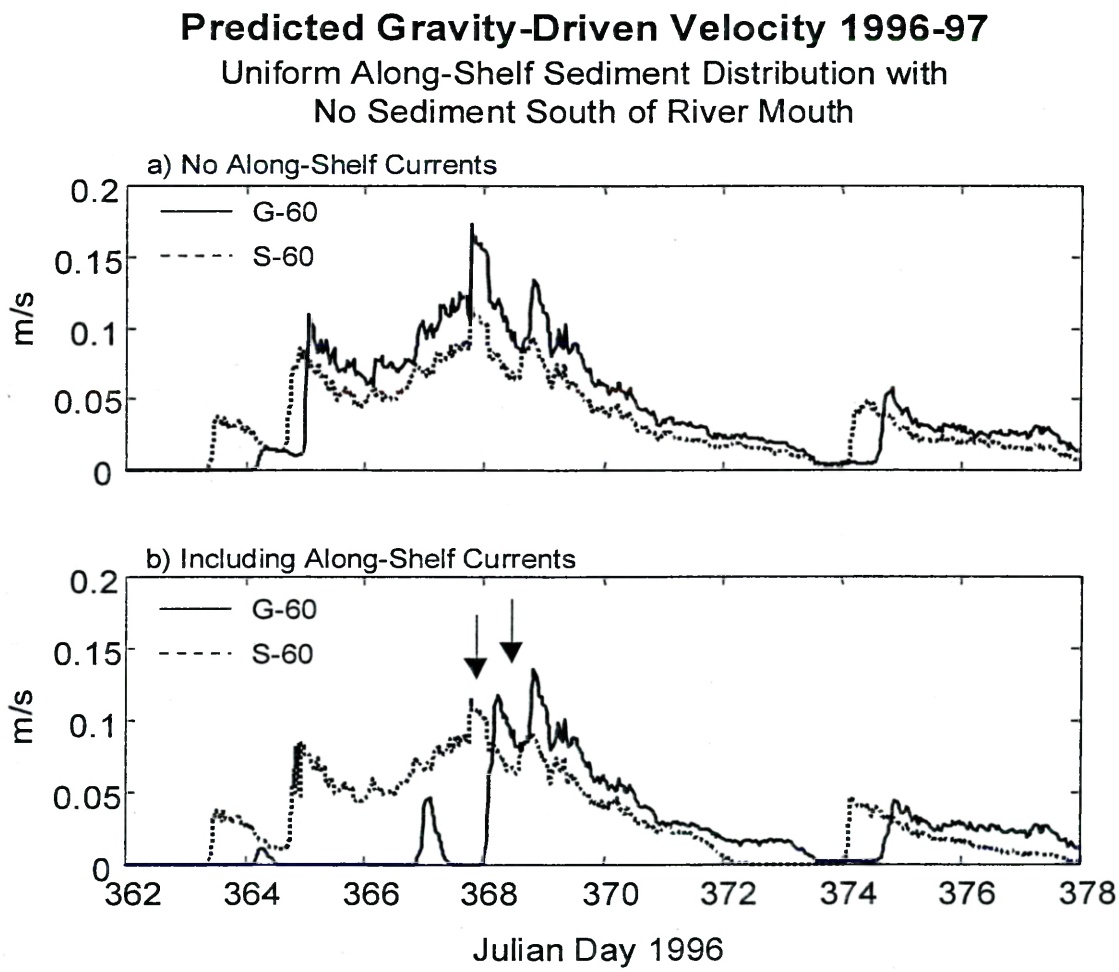

Figure 3-11 Predicted gravity-driven velocity at S-60 and G-60 for 1996-97 using uniform along-shelf sediment with no sediment input south of the river mouth (a) not including influence of observed along-shelf currents, and (b) including the influence of the observed along-shelf currents. Arrows indicate on-set of inferred gravity-driven transport from tripod observations @ G-60 and S-60.

The sustained period of high suspended sediment concentrations observed at G-60 is not consistent with wave resuspension and may have been the result of gravity-driven sediment delivery (Ogston *et al.,* 2000). However, there is little evidence of gravity-driven transport in current meter data at G-60. One possible explanation for the lack of current meter evidence for gravity-driven transport at G-60 is the relative strength of the observed along-shelf current. During periods of low wave energy or extremely high current velocity, the relative importance of the current shear velocity increases, suspending sediment out of the wave boundary and into the current boundary layer. This could reduce the near-bed negative buoyancy anomaly, halting gravity-driven transport. The increased importance of the current shear velocity with depth may play an important role in preventing significant amounts of sediment from leaving the shelf as gravity-driven flows, and cannot be accounted for in this model.

The along-shelf currents not only influence the transport direction of high-turbidity flows, but they also contribute to the generation of near-bed turbulence. However, for the sake of simplicity, the contribution of the along-shelf current (v_{curr}) to u_{max} was not included in the model runs discussed above. While it is relatively easy to infer bottom wave velocities for a large area from surface measurements of wave height and period based on regional wave buoys, making such inferences about near-bed currents without in situ tripods is significantly more difficult. Additionally, across-shelf gradients in the along-shelf current magnitude are likely to be much smaller than gradients in wave energy. As a result, one would not expect the contribution of the along-shelf current to contribute strongly to deposition by gravity-driven flows. This is supported by model runs in which the extrapolated along-shelf current velocity was

included in the calculation of u_{max} via Equations 2-4 and 2-11. As shown in Table 3-1, predicted deposition on the inner-shelf is slightly reduced due to the increase in carrying capacity associated with greater values of u_{max}. Mid-shelf deposition is either reduced or remains constant in all cases. By assuming the value v_{curr} was uniform across the slope, its contribution to u_{max} actually reduces the across-shelf gradient in carrying capacity resulting in less flux convergence on the mid-shelf due to gravity-driven flows. Although the gradient in the boundary layer capacity is reduced, the actual capacity is increased, so greater amounts of sediment were predicted to leave the shelf.

3.3.3. Resuspension/Erosion

The resuspension of recently deposited fine sediment plays an important role in the model. When wave orbital velocity exceeds the threshold value, unconsolidated sediment is resuspended until the capacity of the boundary layer is met. This is clearly a simplification of a very complex problem and neglects the importance of wave-current interaction, increasing bed strength due to consolidation, and potential bed armoring. However, our model is intended to represent an extreme case where resuspension of sediment is controlled almost entirely by near-bed stratification. As long as the observed orbital velocity exceeds the threshold for erosion sediment will be resuspended into the boundary layer until the capacity is limited by sediment-induced stratification. If advection from neighboring grid points already provides the maximum capacity possible, no erosion will occur. This is consistent with observations at K-60 (Traykovski *et al.*, 2000) that show significant deposition during large wave events when the boundary layer is inferred to be critically-stratified and erosion associated with significantly lower wave energy when insufficient sediment is presumably available for critical stratification.

However, choosing a value for the resuspension threshold is not straightforward, especially when dealing with cohesive fine sediment. The observations of Traykovski *et al.* (2000) document a decrease in bed elevation of approximately 8 cm, beginning with wave orbital velocities of roughly 0.20-0.25 m/s, suggesting an approximate threshold for erosion and resuspension for recently deposited fine sediment. However, approximately two weeks after deposition, no change in bed elevation was observed despite orbital velocities of nearly 0.70 m/s, presumably because significant consolidation had occurred. Work conducted on the Washington shelf reports resuspension of fine sediment at mid-shelf depths occurring when wave orbital velocities exceed 0.35 m/s (Sternberg and Larsen, 1976). Clearly processes associated with time-dependent consolidation will make selecting one representative value difficult.

The model was run using several different resuspension threshold values over relatively wide but realistic range of values, to assess the impact on the model results. Table 3-1 displays the results of these runs. In general, lower threshold values support greater sediment transport off-shelf, with less inner-shelf deposition. Clearly if sediment is relatively easy to erode, the initiation of gravity-driven transport will be favored and little sediment will remain on the inner-shelf. Changes to the resuspension threshold had less of an impact on predicted flux into the canyon. These results suggest that the intensification of wave energy around the relatively flat and shallow Eel River subaqueous delta prevents significant near-shore deposition after floods, except for cases with very low associated wave energy.

The effect of erosion and resuspension on model predictions of mid-shelf deposition appears to be slightly more complex. While lower threshold values promote

the initiation of gravity-flows and transport to the mid-shelf, low threshold values also can lead to significant erosion at mid-shelf depths. In 1997-98 low threshold values allowed erosion to remove nearly all mid-shelf deposition. As the threshold was increased, predicted mid-shelf deposition in 1997-98 consistently increased. However, high threshold values also can prevent the initiation of gravity-driven transport. In 1996-97, predicted deposition increased slightly and then generally decreased as the critical erosive threshold was increased toward higher values. Given high threshold values, the low wave energy in 1996-97 prevented the initiation of inshore gravity-driven flows reducing mid-shelf deposition. Although, the erosion and resuspension of sediment in the model is clearly a simplification of a complex process, at first order a threshold value of 0.35 m/s appeared to do a reasonable job representing and explaining the observed patterns of deposition.

3.3.4. Consolidation

The resuspension of fine sediment is closely related to the processes that govern sediment consolidation. Without consolidation on an energetic shelf such as off northern California, long-term preservation of fine sediment at mid-shelf depths would be unlikely. The tripod observations from K-60 suggest that consolidation on the Eel shelf occurs relatively rapidly. These observations are consistent with recent work in estuaries suggesting that significant consolidation of mud deposits occurs within 7-14 days of deposition (Metha and McAnally, 2001). The Eel Shelf model was run using consolidation times ranging from one day to two weeks. With the exception of 1997-98, predicted mid-shelf deposition appeared relatively insensitive to changes in the consolidation time. This appears to be the case because wave orbital velocities in excess

of 0.35 m/s were relatively rare at mid-shelf depths during all of the seasons that were modeled except 1997-98. In 1997-98, wave orbital velocities exceeded this value at mid-shelf depths on numerous occasions. As a result, the model predicted significant erosion and little sediment was preserved in a mid-shelf deposit unless consolidation times were sufficiently rapid. However, given the lack of evidence of fine-grained layers in cores collected after the 1997-98 flood season, extremely rapid consolidation is probably unrealistic. During the less energetic years, orbital velocities only periodically exceeded the threshold at mid-shelf depths and only minor erosion was predicted. Longer consolidation times allowed greater opportunity for the initiation of gravity flows, favoring enhanced deposition on the mid-shelf. In general, these minor increases in deposition at the mid-shelf associated with longer consolidation time appear to be offset by minor erosion during the few times when the resuspension criteria is exceeded at mid-shelf depths.

Inner-shelf deposition and off-shelf flux were much more sensitive to consolidation time. Longer consolidation times allowed more fine sediment to be eroded from the inner-shelf and greater amounts of sediment to leave the shelf as gravity flows. In all but the low wave year of 1996-97, a long consolidation time resulted in very little predicted inner-shelf deposition. While slight increases in mid-shelf sedimentation were observed, longer consolidation times tended to greatly increase the predicted flux off-shelf. Significantly less sediment was predicted to leave the shelf as a gravity flow when shorter consolidation times were used. However, in the high wave energy case of 1997-98, a significant percent of sediment was still predicted to leave the shelf even when complete consolidation was assumed to occur in one day. Model runs using the shortest

consolidation time (1 day) represent a more conservative estimate for the role of gravity-driven transport in the Eel River sediment budget. These runs limit gravity-driven processes to a relatively short period of time associated only with high river discharge.

3.3.5. Along-shelf Slope

As discussed above, a uniform distribution of inshore sediment input did not result in a continued increase in predicted mid-shelf deposition moving away from the river mouth, as predicted by the analytical results. One potential explanation for this is the increasing along-shelf slope in the northern third of the model domain. Near the northern edge of the model, the coastline trends slightly more to the north-northwest approaching Trinidad Head. With the depth contours roughly paralleling the coastline, the bed slope in this region has a stronger southerly component. To assess the importance of the along-shelf component of the bed slope, the model was run using only the across-shelf component of the bed slope, ignoring all transport induced by the along-shelf slope. These model runs used the exponentially decaying along-shelf distribution of sediment depicted in Figure 3-1. As seen in Figure 3-12, the along-shelf component of the slope clearly increased the predicted deposition in the region from 10 to 35 km north of the river mouth, while decreasing deposition at the northern and southern ends of the model domain. Maximum deposition along the 60-m isobath was increased by 47% and 18% for 1994-95 and 1996-97, respectively. This increase in deposition comes at the expense of deposition along the northern and southern regions of the model. So, not only is the across-shelf bathymetry associated with the Eel River subaqueous delta unfavorable to gravity-driven deposition, but the northerly directed slopes associated with delta appear to preferentially steer gravity-driven transport away from this region. The

along-shelf slope tends to enhance gravity-driven deposition near the observed region of the flood depo-center. The southerly directed slopes near Eel Canyon do not appear to divert significant sediment into Eel Canyon. In fact, the flux into Eel Canyon remains relatively unchanged. Along the northern portion of the model, the southerly-directed slopes associated with Trinidad Head divert gravity-driven transport to the south, explaining why deposition is not predicted to continually increase to the north.

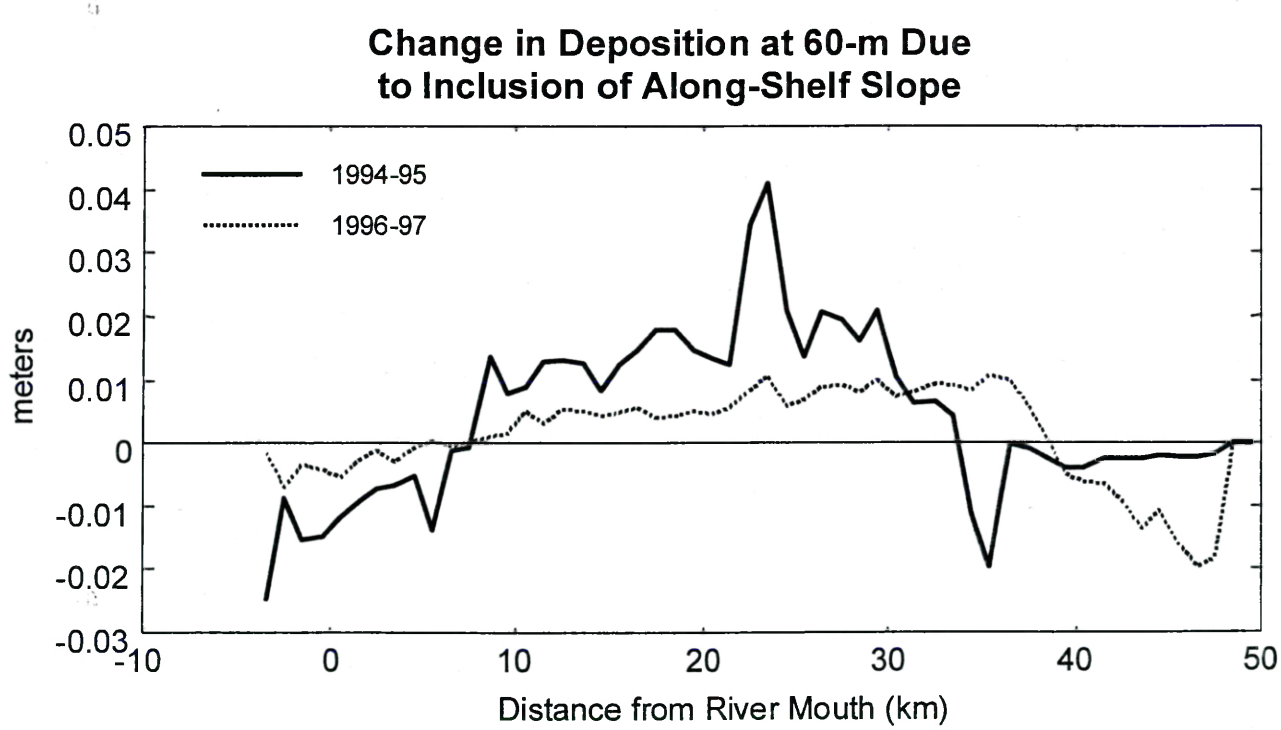

Figure 3-12 Change in predicted deposition along 60-m isobath due to including effect of along-shelf slope for 1994-95 (solid line) and 1996-97 (dashed line). The predicted deposition along the 60-m isobath without including the influence of the along-shelf slope was subtracted from the predicted deposition including the influence of the along-shelf slope.

Model runs using a uniform along-shelf distribution of sediment without including the along-shelf component of slope provide further insight into the patterns of predicted deposition. The results from the 1996-97 flood season with uniform along-shelf input were very similar to the analytical results showing a continued increase in mid-shelf deposition moving northward away from the river mouth. However, this trend in increasing deposition was not observed in the other three years (Figure 3-13). This unexpected result is also related to the mid-shelf bathymetry. The far northern and far southern regions of the model both have relatively high mid-shelf bed slopes. High slopes lead to greater gradients in wave energy that favor gravity-driven deposition. However, higher slopes also result in a greater boundary layer capacity. This greater boundary layer capacity allows greater amounts of sediment to be removed from the bed when the critical resuspension threshold is exceeded. So, in the absence of critical stratification, when mid-shelf orbital velocities exceed the resuspension threshold, unconsolidated sediment will be preferentially removed from regions with higher slopes. In 1996-97, sufficient sediment was supplied so that on the few occasions when the resuspension threshold was exceeded at mid-shelf depths, the boundary layer was critically-stratified and preferential erosion could not remove sediment from regions of higher slope. However, the other three years had greater wave energy and the resuspension threshold was exceeded on a number of occasions at the mid-shelf.

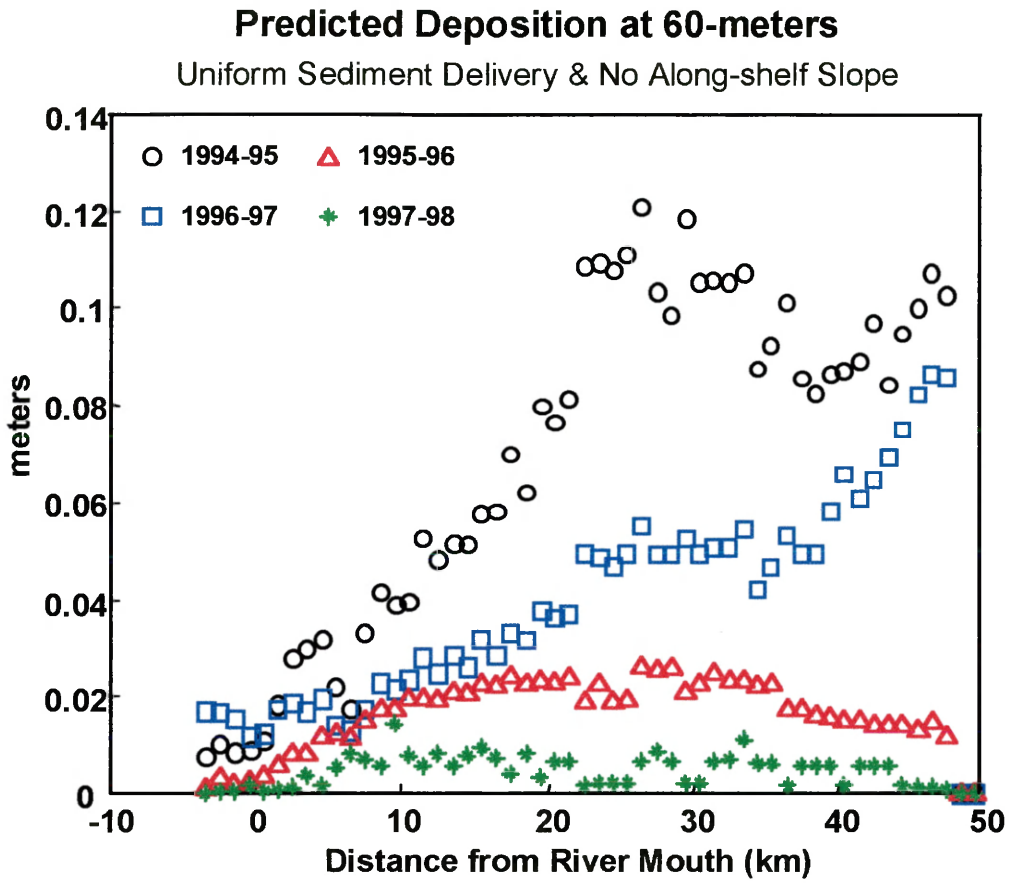

Figure 3-13 Predicted deposition along the 60-m isobath for model run using uniform along-shelf sediment delivery and neglecting the effect of the along-shelf slope for the four years modeled.

3.3.6. Richardson Number & Drag Coefficient

Previous work has established that the drag coefficient and Richardson number are closely related. The flume experiments of van Kessel and Kranenburg (1996) found that values for C_d were of the order 0.003 for critically-stratified turbidity currents O(10 cm) in thickness. Based on fits of Equation 2-3 to field observations from both the wave and current boundary layers, Wright *et al.* (2001) found generally similar values and reported an inverse relationship between Ri and C_d upon which the model was based. To explore model sensitivity the present model was run using several variations on this

relationship, including runs where C_d and Ri remain constant. Using constant values of Ri ≈ 0.25 and $C_d \approx 0.003$ only slightly changed the predicted model results. In general, using the constant values slightly decreased inner and mid-shelf deposition while increasing off-shelf flux. Because the drag coefficient did not increase during times when critical stratification was absent, greater gravity-driven flux was allowed when the boundary layer was not carrying its maximum capacity. This would lead to less flux convergence and explain the lower predicted inner and mid-shelf deposition. The inverse relationship between Ri and C_d delayed the onset of gravity-driven transport in many cases. When the boundary layer was not critically-stratified, the higher predicted drag prevented significant down-slope transport. However, in the absence of any dispersive process, sufficient additional sediment was soon added to achieve critical stratification and down-slope transport was only delayed slightly.

Model results were relatively sensitive to the values of C_d and Ri selected to represent critical stratification. Specifically, the ratio of Ri to C_d for $C_d \approx 0.003$ and Ri ≈ 0.25 is close to the maximum values allowable in the model. Increases to this ratio would bring the value of β in Equation 2-10 close to its limiting value of one for many locations on the Eel shelf. As the value of β approaches 1, the predicted gravity-driven velocity will increase rapidly. This asymptote represents the transition to auto-suspension where the velocity of the gravity current generates sufficient turbulence to sustain the flow. This model is not intended to represent such a situation.

The model was run using a constant value of $C_d = 0.006$ (with Ri = 0.25), as well as a constant value of Ri = 0.15 (with $C_d = 0.003$). As expected, the increased drag coefficient increased predicted deposition on the inner-shelf in all years but 1997-98,

when energetic waves prevented any significant deposition on the inner-shelf (Table 3-1). However, in all years but 1996-97, the increased drag also resulted in greater mid-shelf deposition. This result can be explained as follows: increased drag effectively reduces the carrying capacity of the boundary layer through its influence in Equation 2-12. Therefore, given the same amount of sediment, the model will predict that the mid-shelf boundary layer will be critically-stratified for longer periods of time when a larger drag coefficient is used. When the boundary layer at the mid-shelf is carrying its maximum capacity for longer periods, greater flux convergence will occur leading to greater deposition. In years with extremely large sediment supply such as 1996-97, enough sediment is supplied to critically stratify the boundary layer for very long periods already, so the increase in drag will not significantly change the duration of predicted critical stratification, and less deposition will be predicted because of the reduced flux capacity.

Decreasing Ri had a similar effect on model results. Like an increase in C_d, a decrease in the value of Ri also effectively reduces the amount of sediment that can be maintained in suspension, allowing for longer periods of critical stratification, but decreasing deposition during periods of critical stratification. This is consistent with the analytical model presented in Section 2 that reports both sediment flux and deposition are proportional to the ratio of Ri^2_{cr}/C_d. Reducing Ri decreased this ratio by more than the increase in C_d. As a result, in 1996-97 when prolonged periods of critical stratification occurred, mid-shelf deposition was reduced by a greater amount by decreasing Ri than by increasing C_d.

4. CONCLUSIONS

4.1. CONCLUSIONS FROM ANALYTICAL MODEL

The analytical model presented in this paper provides several important insights into the transport, deposition and dispersion of sediment on the Eel River continental margin. By assuming that a negative feedback maintains the near-bed Richardson number at its critical value, the model reasonably reproduces observed time-series of down-slope velocity and bed elevation change, knowing only the surface wave forcing and shelf bathymetry. Application of the model is limited to periods when a sufficient supply of easily suspended sediment is available to critically stratify the wave boundary layer. This appears to occur when the volume of sediment supplied to the inner-shelf by river floods exceeds the down-slope flux capacity of the gravity flow. In the absence of critical stratification, wave orbitals on an energetic shelf will increase drag and retard down-slope transport and limit gravity-driven deposition.

Model results indicate that the thickness of gravity-driven mid-shelf deposition during large floods is controlled primarily by the magnitude of wave energy and not the magnitude of river discharge. Higher wave energy increases the capacity of critically-stratified gravity flows to transport sediment down-slope and results in greater gradients in flux and hence deposition. This provides an explanation for why the largest flood during the STRATAFORM program did not produce the thickest observed mid-shelf flood layer. In fact, the largest flood layer observed in cores was produced by the flood with the largest associated wave energy. The magnitude of wave energy also will play a key role in determining the ultimate fate of river-derived sediment. Following large floods with relatively weak wave energy, the model predicts the capacity of the wave

boundary layer to be exceeded closer to shore, resulting in significant gravity-driven deposition on the inner-shelf. This could account for some of the fine sediment discharged from the Eel River that is not accounted for in the mid-shelf mud deposit. Conversely, during moderate to large floods with high associated wave energy, gravity-driven transport is an effective mechanism for moving sediment across-shelf and may allow large amounts of flood-derived material to escape to the continental slope or enter Eel Canyon.

The bathymetry of the Eel margin plays a critical role in gravity-driven transport and deposition. In the mid-shelf region near the Eel River mouth, the increasing off-shelf slope allows the gravity-driven velocity to increase rapidly enough to prevent flux convergence due to the off-shelf decay in orbital velocity. As a result, no deposition is predicted on the mid-shelf within several kilometers of the river mouth and sediment can travel past the shelf break or into Eel Canyon as a gravity-driven flow. Given the preferential settling of sediment near the river mouth, gravity-driven sediment bypassing across the shelf and into Eel Canyon also may account for a significant fraction of the sediment not accounted for in the mid-shelf flood deposit.

In contrast to region near the river mouth, the region 15-25 km north of the river mouth is characterized by much flatter and even slightly concave upward mid-shelf profiles. The decrease in off-shelf slope in this region in conjunction with the off-shelf decay of wave orbital velocity favors gravity driven deposition. The consistency of historic deposition in this region provides strong support for gravity-driven emplacement of the Eel River flood deposit. The model predicts gravity-driven deposition to cease in the vicinity of the 90-m isobath. The increase in slope again allows the contribution of

the gravity flow velocity to prevent significant flux convergence, limiting the off-shelf extent of gravity-driven deposition.

Farther from the river mouth, the supply of sediment eventually is reduced to the point where gravity-driven transport and deposition are no longer possible. Estimates of sediment delivery by the river plume relative to down-slope flux by gravity flows predict the northern limit of the flood deposit should occur where critically-stratified gravity-driven transport can no longer be maintained. As a result, larger floods are capable of gravity-driven transport and deposition much further from the river mouth than smaller floods.

Our modeling efforts provide further evidence for the importance of gravity-driven processes in forming a mid-shelf mud deposit. The ability and simplicity of our formulation in not only capturing the large scale patterns of deposition, but in reproducing time-series observations of near-bed velocity and bed elevation change, shows great promise for future efforts to model the long-term formation of continental strata.

4.2. CONCLUSIONS FROM NUMERICAL MODEL

The numerical model presented in this paper simulates gravity-driven deposition of the fine sediment derived from floods of the Eel River on the adjacent continental shelf. Using observed sets of forcing parameters, the model reproduces the magnitude and location of observed flood deposition on the mid-shelf. The thickest mid-shelf deposits are predicted to coincide with large floods that have the highest associated wave energy. Following large floods, gravity-driven mid-shelf deposition is predicted to account for roughly 25-30% of the estimated input of river sediment. This is consistent

with independent analysis of cores obtained from the mid-shelf. Significant inner-shelf deposition of mud is predicted when floods are large or are associated with relatively low wave energy. For example, the 1996-97 flood season had the largest flood event modeled and the lowest associated wave energy and nearly 55% of the sediment input was predicted to remain inshore of the 50-m isobath. When the wave energy is high or floods are small, significant amounts of sediment are predicted to escape across the shelf or enter Eel Canyon as gravity-driven flows. During the 1997-98 flood season for example, conservative estimates indicate that nearly 50% of the sediment active in gravity-driven processes traversed the shelf to the continental slope as a gravity-driven flow. An additional 10% of the sediment was predicted to enter Eel Canyon.

With the exception of extremely large floods, sensitivity analysis indicates that the input of sediment to the model is important. A 50% reduction in sediment input caused the model to under-predict observed mid-shelf deposition for all four winters considered. This suggests that if our estimates based on the rating curve are accurate, much of the fine sediment discharged from the river must be available for gravity-driven transport. This also suggests that on margins with bathymetry and accumulation rates comparable to the Eel shelf, but adjacent to rivers with a significantly smaller sediment load, gravity-driven processes may not play a dominant role in the transport and deposition of sediment on the mid-shelf during floods. Doubling the sediment supply did not significantly increase mid-shelf deposition during very large floods, however, indicating that gravity-driven deposition does place an upper limit on the amount of sediment that can be placed on the mid-shelf during large events.

Bathymetric controls caused model results to be relatively insensitive to the along-shelf distribution of sediment. Greatest mid-shelf deposition was consistently predicted to occur in the region 10- 35 km north of the river mouth. This is the net result of three aspects of the shelf bathymetry: (1) Relatively constant to slightly concave upward across-shelf bathymetric profiles favor greater across-shelf gravity-driven flux convergence; (2) Northerly-directed slopes associated with the Eel River subaqueous delta combined with southerly-directed slopes approaching Trinidad Head favor along-shelf flux convergence; and (3) Steeper slopes and greater associated boundary layer capacity in regions away from the depo-center favor preferential erosion of sediment. However, increased sediment delivery to the inshore region near the river mouth did shift the location of the predicted depo-center slightly to the south from the bathymetrically-favored region.

Model results suggest that the mid-shelf bathymetry also plays a key role in gravity-driven flux off-shelf and into Eel Canyon. Despite the greatest sediment input near the river mouth, the model predicted little deposition and significant sediment bypassing in this region due the concave downward mid-shelf bathymetry. In all four winters, the majority of the sediment input south of the river mouth was predicted to enter Eel Canyon. Without the influence of along-shelf currents, no sediment input north of the river mouth was predicted to enter the canyon as a gravity-driven flow. However, model runs including the observed along-shelf currents suggest that southerly along-shelf flows can effectively steer gravity-driven flows into Eel Canyon. In fact, accounting for the along-shelf current significantly increased the predicted flux into the canyon for years with low river discharge, when strong gravity-driven transport occurred only

episodically. During the 1996-97 winter, when strong gravity-driven transport was predicted for relatively long periods of time, the inclusion of the along-shelf current had no appreciable impact on the predicted model results. In all years with available tripod date, the inclusion of the along-shelf current had little impact on the predicted along-shelf location of maximum mid-shelf deposition, providing further evidence that gravity-driven deposition on the Eel shelf is bathymetrically controlled.

Model results were relatively unaffected when the along-shelf current magnitude was included in calculations of the wave boundary layer capacity. The minor impact attributed to the ambient currents, particularly in years with strong and sustained gravity-driven transport, allows the model to be implemented using only the inputs of river discharge, surface wave data, and the regional bathymetry. However, neglecting wave-current interaction in the model may result in an over-prediction of gravity-driven off-shelf flux. At deeper locations on the shelf, where wave energy has significantly decayed, the increased importance of the current shear velocity may be capable of suspending sediment out of the wave boundary layer. This process could effectively reduce the negative buoyancy force in the wave boundary layer and halt near-bed gravity-driven transport. Without including wave-current interaction, the estimates of off-shelf flux presented in this paper probably represent maximum possible values.

The model included sediment resuspension and consolidation in a relatively crude, but effective manner. Clearly more accurate accounting for these processes will be extremely import to future modeling efforts in muddy environments such as the continental shelf off northern California. Model results obtained using a resuspension threshold of 0.35 m/s and consolidation time of 7 days gave reasonable predictions for

mid-shelf deposition and are consistent with previously published values for these parameters. Consistent with observations, deposition rather than erosion was predicted when the boundary layer was carrying its maximum capacity, despite highly energetic waves. The presence of sediment induced stratification will greatly impact the resuspension of fine sediment and should continue to be a focus for ongoing research. The values for the drag coefficient and the critical Richardson number appear to influence model results through their control over the boundary layer capacity. The value for these parameters used in the model are consistent with those reported in the literature. However, the values of Ri# and C_d used may respectively represent maximum and minimum values appropriate to gravity-driven transport.

LITERATURE CITED

Allan, J.C., and Komar, P.D., 2000. Are ocean wave heights increasing in the eastern north Pacific? EOS, Transactions, American Geophysical Union, 81 (No. 47, pp. 561).

Borgeld, J.C., Hughes Clark, J.E., Goff, J.A., Mayer, L.A., and Curtis, J.A., 1999. Acoustic backscatter of the 1995 flood deposit on the Eel shelf. Marine Geology 154, 197-210.

Borgeld, J.C., and O'Shea, D., 2000. Eos. Trans. AGU, 81 (48), Fall Meet., Suppl., Abstract OS62A-29.

Brown, W.M. and Ritter, J.R., 1971. Sediment transport and turbidity in the Eel River basin, California: U.S. Geological Survey Water-Supply Paper, 70p.

Crockett, J.S., Nittrouer, C.A., and Driscoll, N.W., 2000. Eos. Trans. AGU, 81 (48), Fall Meet., Suppl., Abstract OS62A-21.

Drake, D. A., 1999. Temporal and spatial variability of the sediment grain-size distribution on the Eel shelf: the flood layer of 1995. Marine Geology 154, 169-182.

Drake, D.E., Wheatcroft, R.A., Borgeld, J.C, and Ogston, A.S., 2000. Eos. Trans. AGU, 80 (49), Fall Meet., Suppl., Abstract OS61A-10.

Eisma, D. and Kalf, J., 1984. Dispersal of Zaire River suspended matter in the estuary and the Angola Basin. Netherlands Journal of Sea Research 17, 385-411.

Ellison, T.H. and Turner, J.S., 1959. Turbulent entrainment in stratified flows. Journal of Fluid Mechanics 6, 423-448.

Foster, G. and L. Carter, 1997. Mud sedimentation on the continental shelf at an accretionary margin: Poverty Bay, New Zealand. New Zealand Journal of Geology and Geophysics 40, 157-173.

Friedrichs, C.T., Wright, L.D., Hepworth, D.A. and Kim, S.C., 2000. Bottom boundary layer processes associated with fine sediment accumulation in coastal seas and bays. Continental Shelf Research 20, 807-841.

Geyer, W.R., Hill, P.S., Milligan, T., and Traykovski, P., 2000. The structure of the Eel River plume during floods. Continental Shelf Research 20, 2067-2093.

Harris, C.K., Geyer, W.R., and Signell, R.P. 1999. Eos. Trans. AGU, 80 (49), Ocean Sci. Meet., Suppl., Abstract OS42K-06.

Harris, C.K., and Wiber, P.L. Feedbacks between sediment resuspension and seabed texture. Journal of Geophysical Research, in press.

Hill, P.S., Milligan, T.G., and Geyer, W.R., 2000. Controls on effective settling velocity of suspended sediment in the Eel River flood plume. Continental Shelf Research 20, 2095-2112.

Huang, X, and Garcia, M.H., 1999. Modeling of non-hydroplaning mudflows on continental slopes. Marine Geology 154, 131-142.

Kineke, G.C., Sternberg, R.W., Trowbridge, J.H. and Geyer, W.R. 1996. Fluid mud processes on the Amazon continental shelf. Continental Shelf Research 16, 667-696.

Komar, P.D., 1977. Computer simulation of turbidity current flow and the study of deep-sea channels and fan sedimentation. In: Goldberg, E.D.., McCave, I.N., O'Brian, J.J. and Steele, J.H. (Eds.), Marine Modeling (The Sea, vol. 6), John Wiley, New York, pp. 603-621.

Kundu, P.K., 1981. Self-similarity in stress-driven entrainment experiments. Journal of Geophysical Research 86, 1979-1988.

Lopez-Galindo, A., Rodero, J., and Maldonado, A. 1999. Surface facies and sediment dispersal patterns: southeastern Gulf of Cadiz, Spanish continental margin. Marine Geology 155, 83-98.

Mathew, J. and Baba, M. 1995. Mudbanks of the southwest coast of India, II: wave-mud interactions. Journal of Coastal Research 11, 179-187.

McCave, I.N., 1972. Transport and escape of fine-grained sediment from shelf areas. In: Swift, D.J.P., and Duane, D.B., Pilkey, O.H. (Eds.), Shelf sediment transport: Process and pattern. Dowden, Huttnison and Ross, Stroudsberg, PA, pp 225-248.

Metha, A. J. and McAnally, W. H., 2001. Fine-grained sediment transport. Ch. 4, In: M. Garcia (Ed.), Sedimentation Engineering (2nd ed.), ASCE, Reston, VA (in press).

Milliman, J.D., and Syvitski, J.P.M., 1992. Geomorphic/tectonic control of sediment discharge to the ocean: The importance of small mountainous rivers. Journal of Geology 100, 525-544.

Mulder, T., and Syvitski, J.P.M., 1995. Turbidity currents generated at river mouths during exceptional discharges to the ocean: the importance of small mountainous rivers. Journal of Geology 100, 525-544.

Mulder, T., Syvitski, J.P.M., and Skene, K.I., 1998. Modeling of erosion and deposition by turbidity currents generated at river mouths. Journal of Sedimentary Research 68, 124-137.

Mullenbach, B.L., and Nittrouer, C.A., 2000. Rapid deposition of fluvial sediment in the Eel Canyon, northern California. Continental Shelf Research 20, 2191-2212.

Nittrouer, C.A., and R.W. Sternberg, 1981. The formation of sedimentary strata in an allochthonous shelf environment: the Washington continental shelf. Marine Geology 42, 201-232.

Nittrouer, C.A., 1999. STRATAFORM: Overview of its design and synthesis of its results. Marine Geology 154, 3-12.

Ogston, A.S. and Sternberg, R.W., 1999. Sediment transport events on the northern California shelf. Marine Geology 154, 69-82.

Ogston, A.S., Cacchione, D.A., Sternberg, R.W. and Kineke, G.C., 2000. Observations of storm and river flood-driven sediment transport on the northern California continental shelf. Continental Shelf Research 20, 2141-2162.

Parker, G., Fukushima, Y., and Pantin, H.M., 1986. Self-accelerating turbidity currents. Journal of Fluid Mechanics 171, 145-181.

Price, J.F., 1979. On the scaling of stress-driven entrainment experiments. Journal of Fluid Mechanics 90, 509-529.

Reed, C.W., Niedoroda, A.W., and Swift, D.J.P., 1999. Modeling sediment entrainment and transport processes limited by bed armoring. Marine Geology 154, 143-154.

Sherwood, C.R., Butman, B., Cacchione, D.A., Drake, D.E., Gross, T.F., Sternberg, R.W., Wiberg, P.L., and Williams, A.J., 1994. Sediment-transport events on the northern California continental shelf during the 1990-1991 STRESS experiment. Continental Shelf Research 14, 1063-1099.

Sommerfield, C.K. and Nittrouer, C.A., 1999. Modern accumulation rates and a sediment budget for the Eel shelf: a flood-dominated depositional environment. Marine Geology 154, 227-242.

Sommerfield, C.K., Drake, D.E., and Wheatcroft, R.A., 2000. Marine record of fluvial distribution, north-coastal California. (Abstr.) EOS, Transactions, American Geophysical Union, 81 (No. 48, Suppl.), pp. F631.

Sternberg, R.W., and Larsen, L.H., 1976. Frequency of sediment movement on the Washington continental shelf: a note. Marine Geology 21, M37-M47.

Syvitski, J.P. and Morehead, M.D., 1999. Estimating river-sediment discharge to the ocean: application to the Eel margin, northern California. Marine Geology 154, 13-28.

Thompson, R.O.R.Y., 1979. A reinterpretation of the entrainment process in some laboratory experiments. Dynamics of Atmospheres and Oceans 4, 45-55.

Traykovski, P., Geyer, W.R., Irish, J.D. and Lynch, J.F., 2000. The role of wave-induced density-driven fluid mud flows for cross-shelf transport on the Eel River continental shelf. Continental Shelf Research 20, 2113-2140.

Trowbridge, J.H. and Kineke, G.C., 1994. Structure and dynamics of fluid muds on the Amazon continental shelf. Journal of Geophysical Research 99, 865-874.

van Kessel, T. and Kranenburg, C., 1996. Gravity current of fluid mud on sloping bed. Journal of Hydraulic Engineering 122, 710-717.

Ward, M.N. and Hoskins, B.J., 1996. Near-surface wind over the global ocean 1949-1988. Journal of Climate 9, 1877-1895.

Wheatcroft, R.A., J.C. Borgeld, R.S. Born, D.E. Drake, E.L. Leithold, C.A. Nittrouer, and C.K. Sommerfield, 1996. The anatomy of an oceanic flood deposit. Oceanography 9, 158-162.

Wheatcroft, R.A., Sommerfield, C.K., Drake, D.E., Borgeld, J.C and Nittrouer, C.A. 1997. Rapid and widespread dispersal of flood sediment on the northern California margin. Geology 25, 163-166.

Wheatcroft, R.A., 2000. Oceanic flood sedimentation: a new perspective. Continental Shelf Research 20, 2059-2066.

Wheatcroft, R.A., and Borgeld, J.C., 2000. Oceanic flood deposits on the northern California shelf: large-scale distribution and small-scale physical properties. Continental Shelf Research 20, 2163-2190.

Wright, L.D., W.J. Wiseman, D.B. Prior, J.N. Suhayda, G.H. Keller, Z.-S. Yang, and Y.B. Fan, 1988. Marine dispersal and deposition of Yellow River silts by gravity-driven underflows. Nature 332, 629-632.

Wright, L.D., W.J. Wiseman, Z.-S. Yang, B.D. Bornhold, G.H. Keller, D.B. Prior, and J.M. Suhayda, 1990. Processes of marine dispersal and deposition of suspended silts off the modern mouth of the Huanghe (Yellow River). Continental Shelf Research 10, 1-40.

Wright, L. D., Kim, S.-C. and Friedrichs, C.T., 1999. Across-shelf Variations in Bed Roughness, Bed Stress and Sediment Transport on the Northern California Shelf. Marine Geology 154, 99-115.

Wright, L. D., Friedrichs, C.T., Kim, S.-C. and Scully, M.E., 2001. The effects of ambient currents and waves on the behavior of turbid hyperpycnal plumes on continental shelves. Marine Geology 175, 25-45.

Zang, Y., Swift, D.J.P., Fan, S., Niedoroda, A.W., and Reed, C.W., 1999. Two-dimensional numerical modeling of storm deposition on the northern California shelf. Marine Geology 154, 155-168.

VITA

MALCOLM ELLIS SCULLY

Born August 24, 1971 in Athens, Greece. Graduated in 1989 from the University of Virginia with a B.A. in Environmental Science. Lived in Ocracoke, NC, Washington, DC, and San Francisco, CA in between trips to Central America before entering the masters program at the College of William and Mary, School of Marine Science in August 1998.